Reaction Monitoring Using Real-time Methods

by

Yang Wu
B. Eng., Central South University, 2014

A Thesis Submitted in Partial Fulfillment
of the Requirements for the Degree of

MASTER OF SCIENCE

in the Department of Chemistry

Supervisory Committee

Reaction Monitoring Using Real-time Methods

by

Yang Wu
B.Eng., Central South University, 2014

Supervisory Committee

Dr. J. Scott McIndoe, Department of Chemistry
Supervisor

Dr. David Harrington, Department of Chemistry
Departmental Member

Abstract

Supervisory Committee
Dr. J. Scott McIndoe, Department of Chemistry
Supervisor
Dr. David Harrington, Department of Chemistry
Departmental Member

Electrospray ionization mass spectrometry (ESI-MS) is a powerful method to monitor organometallic reactions. It is fast at generating spectrum, soft to fragile organometallic compounds and sensitive to intermediates in low concentration. When coupled with the pressurized sample infusion (PSI) that helps to continuously inject reacting solution to the MS, both an inert-gas atmosphere and real-time reaction monitoring can be achieved. Also collision induced dissociation (CID) of MS can be used to probe the relative binding affinities of phosphine ligands in ruthenium complexes.

PSI ESI-MS can be coupled with Fourier transform infrared spectroscopy (FTIR) to monitor the rhodium-catalyzed hydroacylation simultaneously. This technique expands the dynamic range to 5 magnitudes.

The effect of mass-transfer in heterogeneous hydrogenation of charge-tagged alkyne was also studied by PSI ESI-MS. In this study cross area, stirring effect, catalyst loading and hydrogen concentration were considered and tested. Also in the study an interesting finding reveals in heterogeneity of the solution.

Relative binding affinities of different phosphine ligands were attained from comparing the relative intensities of fragmentation products from MS/MS. And the phosphine ligand substitution reaction was monitored by the ESI-MS in a real-time manner. A competitive

dissociative substitution mechanism was proposed and confirmed by the simulation and modeling of COPASI.

Contents

List of Tables

List of Figures

List of Schemes

List of Equations

List of Abbreviations

Ar	aryl
ATOFMS	aerosol time-of-flight mass spectrometry
$[BAr^{F}{}_{4}]^{-}$	tetrakis[3,5-bis9trifluoromethyl)phenyl]borate
^{n}Bu	neobutyl
1,2-DCE	1,2-dichloroethane
CID	collision-induced dissociation
COD	cyclooctadiene
DART-MS	direct analysis in real time mass spectrometry
DCM	dichloromethane
DIOP	2,3-O-isopropylidene-2,3-dihydroxy-1,4-bis(diphenylphosphino)butane
DMF	dimethylformamide
dppb	1,4-bis(diphenylphosphino)butane
dppe	1,2-bis(diphenylphosphino)ethane
ESI	electrospray ionization
FPh	fluorobenzene
FTIR	Fourier transform infrared spectroscopy
HPLC	high pressure liquid chromatography
IMS	ion-mobility mass spectrometry
m/z	mass-to -charge ratio
MALDI	matrix-assisted laser desorption
MCP	microchannel plate
Me	methyl
MS	mass spectrometer/mass spectrometry/mass spectrum
MS/MS	tandem mass spectrometry
NCPh	benzonitrile
NMR	nuclear magnetic resonance spectroscopy
$P^{c}Pr_{3}$	triscyclopropylphosphine
PCR	polymerase chain reaction
PEEK	polyetheretherketone
Ph	phenyl
PSI	pressurized sample infusion
PTFE	polytetrafluoroethylene
R	alkyl
rt	room temperature
SPS	solvent purification system
TIC	total ion current
TDC	time signal converter

TOF	time of flight

Acknowledgments

At first I would like to thank Dr. J. Scott McIndoe for having me in his group to explore such a great opportunity in chemistry. In the last two years of my master degree, it won't go so smoothly without his mentor and confidence in me.

Robin, thanks for her kindness and effort to teach me almost everything from the very beginning. She is a great teacher. Rhonda, thank you for being a helpful lab associate. Jane, joining the group with me at the same time and being someone wise to talk to.

Adrian, as a landlord thank you for treating me like your son. Mike, thank you for being such a nice and supportive man as you always are.

All of these won't be complete without mentioning my father and his unconditional support and belief in me. He is always the role model of fortitude and wisdom that will accompany me through all difficulties in the future.

Dedication

To those of great wisdom but still remain naïve and simple:

I remember, I remember,

Where I was used to swing,

And thought the air must rush as fresh

To swallows on the wing;

My spirit flew in feathers then,

That is too heavy now,

And summer pools could hardly cool

The fever on my brow!

I remember, I remember,

The fir trees dark and high;

I used to think their slender tops

Were close against the sky;

It was a childish ignorance,

But now ‘tis little joy

To know I’m farther off from heaven

Than when I was a boy.

Thomas Hood

1 Overview of Orthogonal Real Time Monitoring of Organometallic Catalysis by ESI-MS and FTIR

1.1 Organometallic Catalysts

By adding KCl solution to a refluxing ethanol mixture of $PtCl_2$ and $PtCl_4$, the first organometallic complex was successfully synthesized in 1827[1]. Later in 1890, the first metal carbonyl compound, tetracarbonylnickel, was made by Carl Langer, Ludwig Mond and Friedrich Quinke[2].

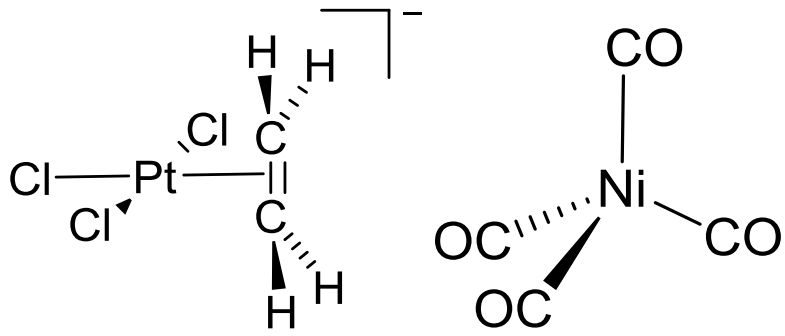

Figure 1.1. Anion of Zeise's Compound (left) and tetracarbonylnickel (right)

In the 20th century chemists witnessed a boom in the study of organometallic chemistry, driven primarily by the application of organometallic compounds in catalysis[3]. At the beginning of 20th century, a French chemist, Victor Grignard, found that the addition of magnesium to organic halide led to alkylation of carbonyl derivatives. This seminal finding gave him 1912's Nobel Chemistry Prize. Also interestingly, the driving force of organometallic catalysis was not from academia but from industry. After the first successful implantation of Fischer-Tropsch process in 1925, producing linear alkane and alkene from CO and H_2 by heterogeneous catalysis, Roelen reported the oxo process in 1938, which uses $Co_2(CO)_8$ to catalyze the hydroformylation of alkenes[4]. Soon after

Reppe reported a variety of discoveries in homogeneous catalysis with organometallic compounds, like the tetramerization of cyclo-octatetraene in 1948[5].

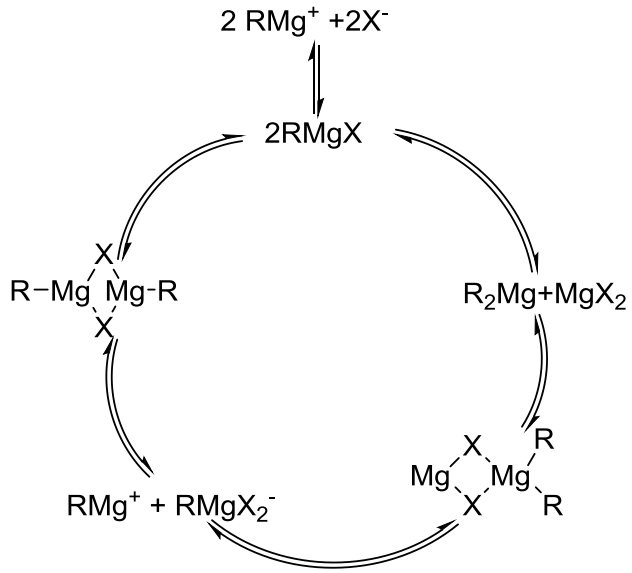

Scheme 1.1. Grignard reagent in reactions

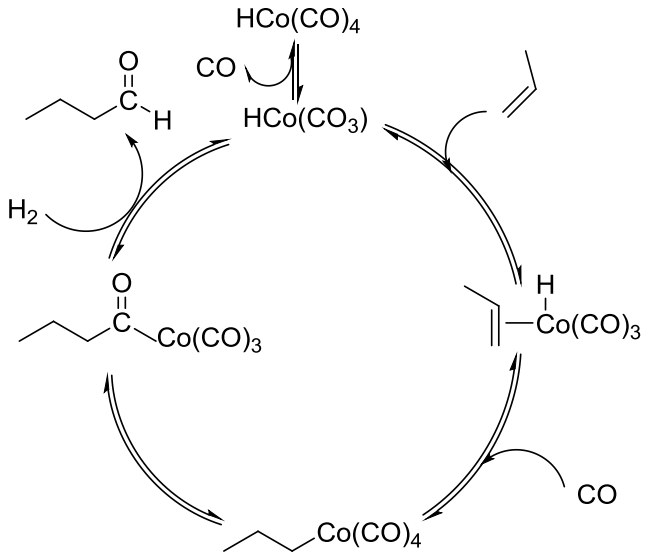

Scheme 1.2. Oxo process mechanism

Coming into the late 20th century, this golden age of organometallic synthesis included the first total synthesis of B_{12} coenzyme by Robert B. Woodward in 1961[6] and this

brought him a Nobel medal in 1965. Among the same time, Wilkinson, Ziegler, E. O. Fisher, Richard R. Schrock and many other organometallic chemists made tremendous contributions to catalyst design. Coming into the 21st century, there are already 9 chemists who have been awarded Nobel prizes for their contributions to organometallic chemistry. They are William S. Knowles, Ryoji Noyori, K. Barry Sharpless in 2001 for the development of catalytic asymmetric synthesis[7]. And Yves Chauvin, Robert H. Grubbs and Richard R. Shrock shared the Nobel chemistry prize in 2005 for fundamental studies on metathesis mechanism[8]. The latest organometallics-related Nobel Prize came to Richard F. Heck, Ei-ichi Negishi and Akira Suzuki for palladium-catalysed cross-coupling in organic synthesis[9].

Because of the prominent ideas of "green chemistry", the application of organometallic complexes as homogeneous catalysts is sure to enjoy increasing attention[10]. In the 12 principles of green chemistry[11], the authors clearly state that catalysis (as selective as possible) help achieve greener chemical process in numerous ways.

1.2 Mass Spectrometry of Organometallic Compounds

A mass spectrometer is an instrument in which the gaseous ions are produced and separated according to their mass/charge ratio. It consists of three main sections: the source for ionizing the sample, the mass analyzer and the detector.

Mass spectrometer is a powerful instrument for organometallic chemistry, especially those employ soft ionization techniques like ESI (Electrospray Ionization) and MALDI (Matrix Assisted Laser Desorption Ionization) which can avoid unwanted fragmentation[12]. Mass spectrometry enjoys high dynamic range, sensitivity and speed. These mean that the samples for MS do not need to be concentrated (actually high

concentration will result in undesirable saturation and suppression effects). Unlike other techniques, MS does not require the sample to be pure as the overlap of signals within a narrow region seldom happens. As for the extremely high sensitivity of mass spectrometer, one study shows that DART-MS (Direct Analysis in Real Time Mass Spectrometry) can even detect the target analyte by opening the volatile dopant at the opposite end of the lab for less than a second[13]. However, despite all these merits of MS, its capability to provide direct structural information and distinguish stereo-isomers is limited. Recent developments in ion-mobility mass spectrometry (IMS) coupled with MS has enabled separation of ions with the same mass/charge ratio duo to the differences in collision cross section of isomer ions colliding with a neutral gas in the drift region [14]. Even for those interested analytes that are not charged, Scott's group uses long alkylated bisphosphines doped into the neutral complexes to provide extra charges[15], which is called charge tagging.

1.2.1 Ionization Method: Electrospray Ionization

One of the main differences of mass spectrometers is the ionization technique they are using. The ionization techniques can be roughly classified into the hard, like electron ionization which results in extensive fragmentation, and the soft, like ESI that can provide intact molecular ions.

The electrospray ionization process depends on the creation of charged hyperfine droplets under high electric field, which was first found by Dole[16] and improved by Fenn and Yamashita[17].

When the liquid sample is injected through a 2-5 kV charged-capillary into a chamber at atmospheric pressure, it undergoes nebulisation, in which a cone of highly charged fine droplets are produced.

The fine droplets containing the ions of interest are further desolvated by counter-flow of hot nitrogen gas. Therefore, the size of the droplets will get smaller and the charge density will increase. When the latter increases to the order close or the same as the surface tension, the droplets may split into many smaller daughter droplets in a series of "Coulomb explosion". At the same time, another process under which the ions "evaporate" from the droplet can also happen[18]. Overall, these processes are very soft and no or little fragmentation will occur.

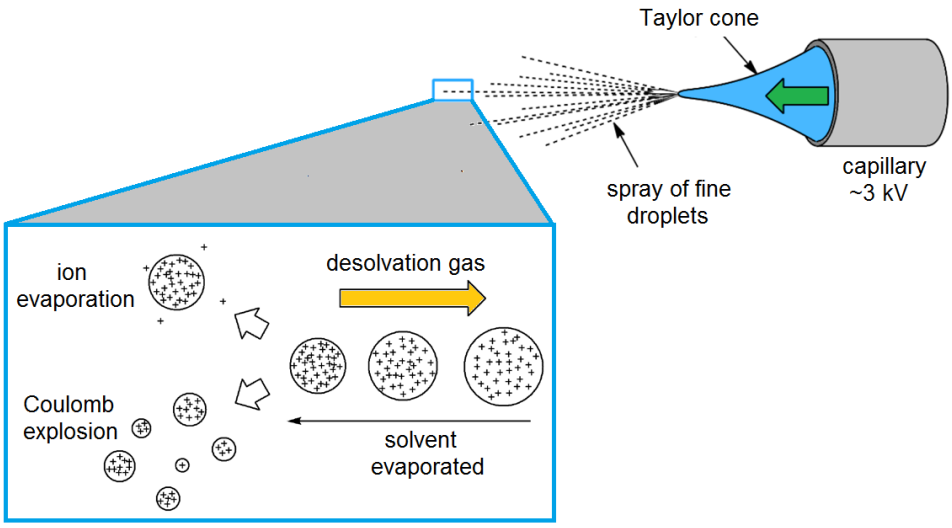

Figure 1.2. The desolvation process in the source

Overall, ESI as an ionization technique enjoys low chemical background and extraordinary detection limits thanks to its soft nature, avoiding uncontrolled fragmentation. Also ESI is good for a large number of analytes as long as they are charged, polar or basic.

1.2.2 Mass Analyser: Time of Flight[19]

The job of mass analyser is separating the ions entering the MS according to their mass/charge ratio (m/z). And the one used in our lab, TOF (time of flight), can be regarded as the most direct and easiest method of analysis. Also thanks to the development of electronic timing technology, the performance of the TOF improved a lot.

Firstly discussed half century ago, the theory behind the TOF is quite easy to understand[20]. Firstly, the ions produced in the source enter the TOF after being accelerated by an electric field. The energy input by the electric field is so large that the other energies the ion has before entering the field can be ignored. Thus this electric field is supposed to impart the same kinetic energy to all the ions entering into it:

$$KE = zeV$$

where z is the charge of the ion, e is the charge of an electron in coulombs, and V is the strength of the electric field in volts.

Also, according to the other equation about kinetic energy we know:

$$KE = \frac{1}{2}mv^2$$

so:

$$v = \sqrt{\frac{2zeV}{m}}$$

or:

$$\frac{m}{z} = \frac{2eV}{v^2} = 2eV\frac{\Delta t^2}{\Delta x^2}$$

Where m is the mass of the ion in kilograms, Δt is the flight time recorded by the TOF in seconds, and Δx is the flight path length in meres.

Here from the last equation we can see that the mass/charge ratio of the ion flying through the TOF can be determined by the time of its flight, given the flight path length is certain. And the heavier the ion is, the more flight time it will need.

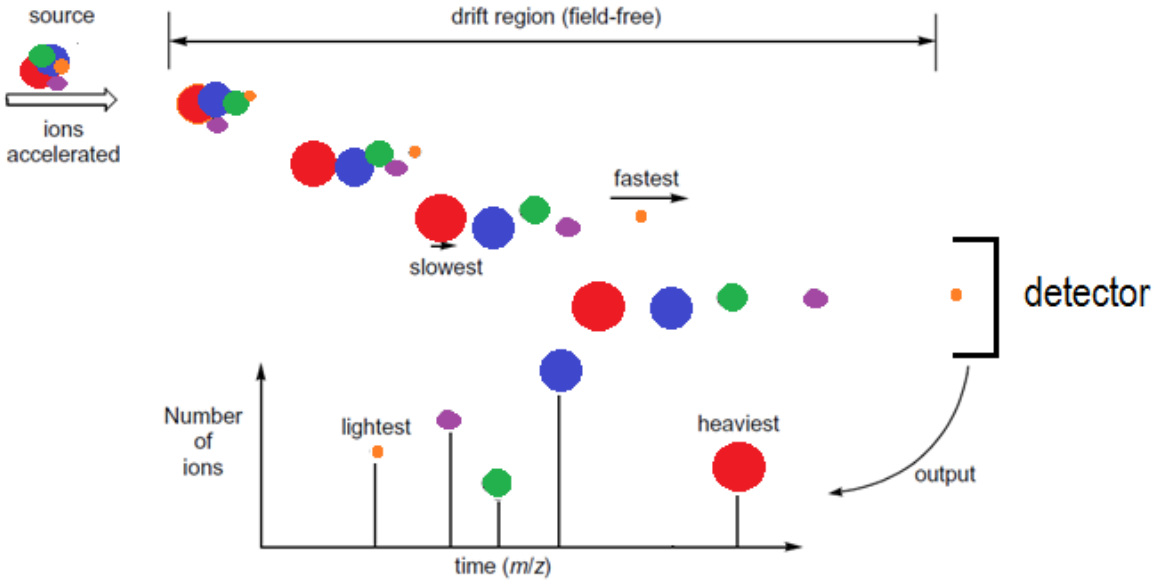

Figure 1.3. Ion path in the TOF

To achieve for high resolution, the TOF asks for high vacuum to avoid collision of ions in their flight time. This means that always an expensive turbomolecular pump is required, making the TOF-MS less attractive than the others from this perspective.

Also the precision of the TOF depends on the assumption that all ions leave the source at the same time, which is hard to achieve. Nor do the ions with the same mass/charge ration have the exact same kinetic energy, even though the energy provided by the electric field overshadows the energy the ions originally have. Thus, to compensate the discrepancy of starting time and kinetic energy, a reflectron is used to improve the TOF's performance. See as figure 1.4:

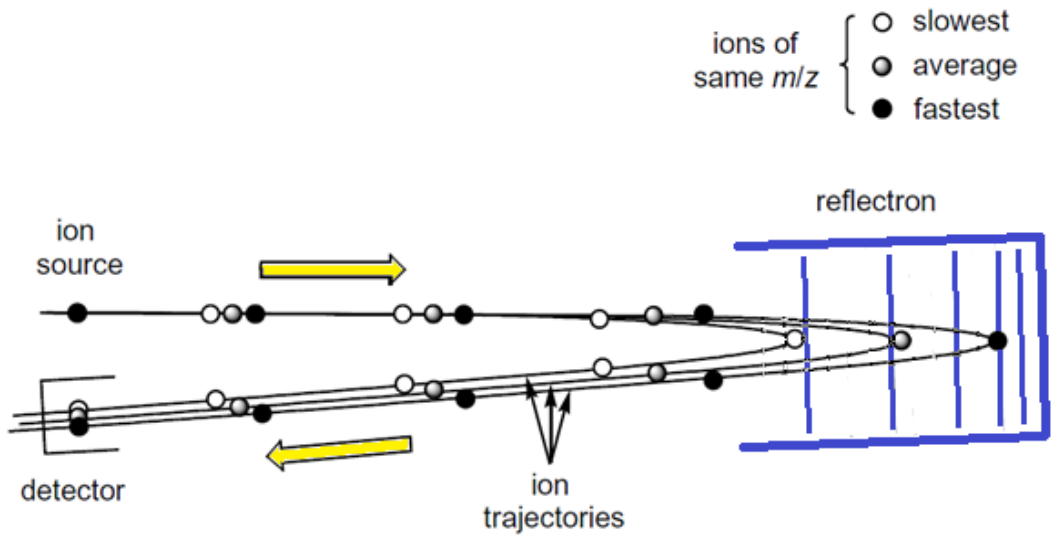

Figure 1.4. Schematic of reflectron

Reflectron, designed by Russian scientist S. G. Alikhanov[21], is mainly a ion mirror that can reverse the direction of the ions entering it. As shown from the graph above, the ion with higher kinetic energy is flying faster and penetrating into the reflectron further. By letting the ions with higher energy stay in the reflectron longer, the discrepancy of kinetic energy can be diminished and ultimately the ions with the same mass/charge ratio can reach to the detector at the same time.

1.2.3 Detector: Microchannel Plate

To avoid any ions being left undetected, the microchannel plate (MCP) consists of a large amount of tightly bunched 'microchannels', each of which is a tiny electron multiplier tube. When an ion hits any of these microchannel, a blizzard of electrons are formed to give a detectable signal. After that, the signal is sent to a time-to-digital converter (TDC). The TDC is so precise that is can distinguish the arriving time signal intervals even less

than a nanosecond. However, the TDC can record the arriving time signal precisely but not the intensity. That is to say when two ions attack the MCP at the same time, still only one signal is produced and recorded. Even though the probability of this is very low, concentrated sample should still be avoided in case of suppression.

1.2.4 Collision-Induced Dissociation (CID)

Collision-induced dissociation, also known as collision-activated decomposition (CAD), happens when ions collide with the residual gas (nitrogen or inert gases) and the transitional energy is converted into internal energy[22]. To stabilize itself, the ion redistribute the energy to all over its structure through vibration soon after the collision. If this energy is above the binding affinity of the ligand or functional group of the analyte ion, fragmentation happens. Because fragmentation happens in a predictable way, with the weakest bonds breaking first, we can speculate about the likely structure of the analyte ion.

The controlled fragmentation led by CID occurs at a separated space called collision cell, which is usually a quadrupole or hexapole. Firstly, the analyte ions will transit to MS-1, which acts as an ion selector only allowing the ions with the desired mass/charge ratio to pass through. Then the ions are accelerated into immobile target gas, causing fragmentation. At last all the product ions will be analyzed by the second mass analyzer, MS-2.

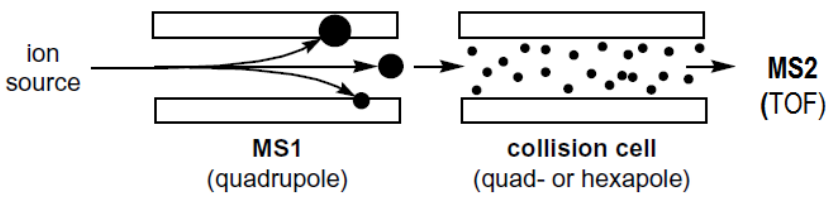

Figure 1.5. Ion path in the collision cell

1.3 Fourier Transform Infrared Spectroscopy (FTIR)[23]

Infrared spectroscopy is a technique that measures the absorption of infrared light by the sample. Fourier transform is a mathematical method to convert the actual signal into a spectrum. Different from the conventional dispersive IR which measures the absorption at a single wavelength of light individually at a time, FTIR can produce signals from a whole range of desired frequencies simultaneously. With this advantage, the sampling time of FTIR is a lot less than conventional IR (usually a few seconds as opposed to several minutes).

To achieve this, the FTIR has to employ a special but simple device named interferometer first developed by Michelson[24], which is always equipped with a beam splitter. The interferometer is made of one stationary mirror and one moving flat mirror at its diagonal position. At first the beam of light will be split into two (50% vs. 50%) beams at the beam splitter, one of which travels toward the stationary mirror and the other toward the moving mirror. After reflection, these two beams of light will join again at the beam splitter and pass through the sample. By adjusting the position of the moving mirror, the interferometer can produce constructive or destructive interference at certain wave length in the newly joined beam of light. The spectrum made from this kind of light beam is called interferogram. An interferogram can be regarded as a function of the positon of the moving mirror and can be added up to the signal that has information of all the infrared wavelength.

The major advantages of FTIR are as below[25]:

1) **Speed**: as all the frequencies in the infrared region are measured at the same time, thus most measurements can be done in a manner of seconds instead of minutes.

2) **Mechanical simplicity**: the only motional part is the moving mirror, which highly increase the stability of the equipment and avoiding the possibility of mechanical breakdown.

3) **Internally calibrated:** by employing the HeNe as an inner wavelength calibration standard, the other calibrations by the use can be avoided.

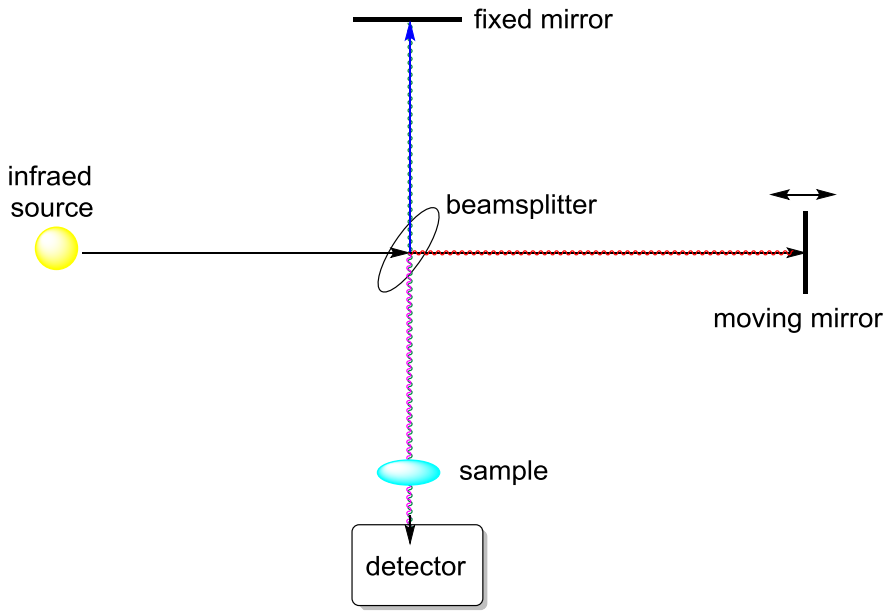

Figure 1.6. Schematic of FTIR

1.4 Air/Moisture Sensitive Sample Handling and PSI-ESI-MS

Most organometallic catalysts used in our lab are air[26] or moisture sensitive[27]. To avoid decomposition of these catalysts, most preparations were either done in an inert atmosphere glove box or using a Schlenk line. When running the mass spectrometer, to steadily inject the liquid sample into the source and keep the sample under an inert gas atmosphere, we are using the custom technique developed in our group called pressurized sample infusion (PSI). A designed glass connector is used to link the argon tank and the flask as the picture below.

Also to avoid clogging in the capillary of the MS, cotton filter is needed. A small piece of cotton is wrapped around one end of the PEEK tubing with polytetrafluoroethylene (PTFE) seal tape.

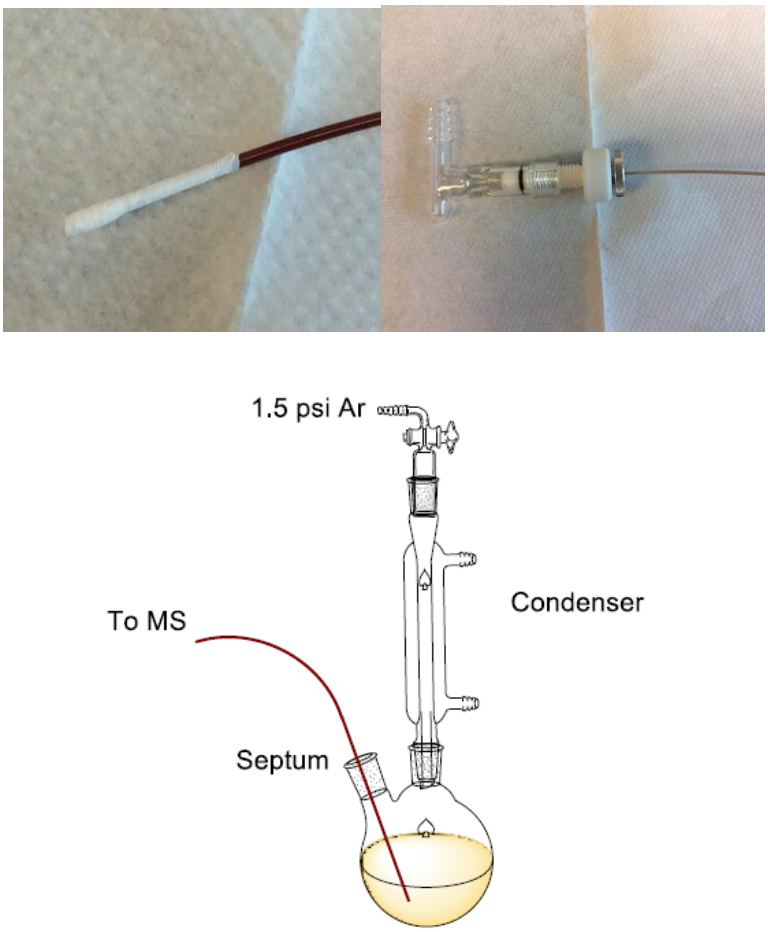

Figure 1.7. The connector (up right), the cotton filter (up left) and the set-up (bottom)

1.5 Coupling of IR and MS on Real-time Reaction Monitoring

The first real-time reaction monitoring was achieved by Thomas Covey using tandem mass spectrometer in 1989[28]. This idea was tested on a series of reaction by measuring the appearance of the products or the disappearance of the reactants. The two examples are as below:

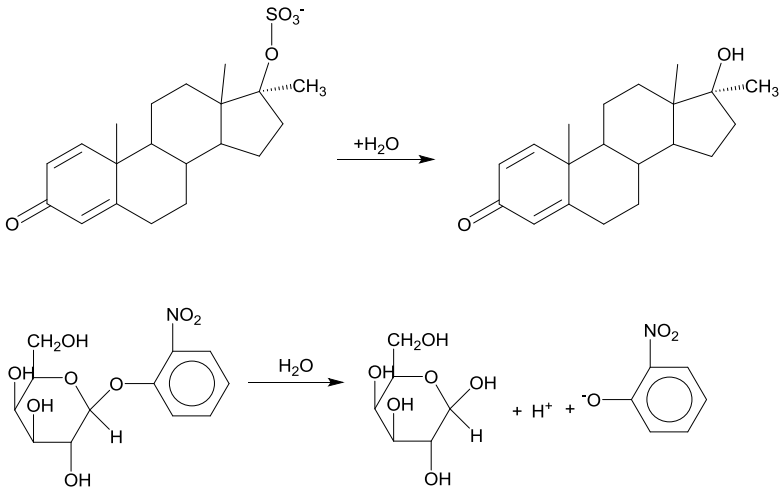

Scheme 1.3. The first two examples of real-time reaction monitoring done by Thomas Covey in 1989, simply measuring the disappearance of the charged reactant or appearance of the charged product.

Later on a boom of cases were reported on this topic. They can be mainly divided into 2 types, biochemical reaction monitoring and organic reaction monitoring.

For biochemical reactions, microfluidic electrochemical sensors[29] and polymerase chain reaction (PCR)[30] are always used. The time resolution can be made close to 1 minute which is good enough to the comparatively long reaction time for biochemical reactions.

For the organic reaction then the FTIR[31] and various kinds of mass spectrometers like direct analysis in real time (DART)[32] and aerosol time-of-flight mass spectrometer (ATOFMS)[33] were used. These two techniques are suitable for real-time reaction monitoring because of their high speed at generating single spectrum, usually one per second.

Even though ESI-MS enjoys many advantages as mentioned above (in chapter 1.2), such as being soft, quick and sensitive, the usage of the MS is limited by the concentration of the sample. In the other word, the MS has an upper concentration

limit, which is around 10^{-5} Molar[34], due to the saturation and suppression. When the analyte concentration is above the upper limit, the response of ESI to the concentration will level off[35]. However, when using the MS alone, we are always restricted to use the concentration region nearly below the upper concentration limit because of practical limitations. So the potential of detecting charged species at much lower abundance region is being restricted. In the coupling of IR and MS, however, the IR can monitor the behavior of the uncharged reagents and products at the abundance across the upper limit region. Then the MS can fully focus on those charged species at lower concentration region, fully exploiting the potential of the MS's dynamic range. Through this coupling, the dynamic range of the MS can be increased by several magnitudes.

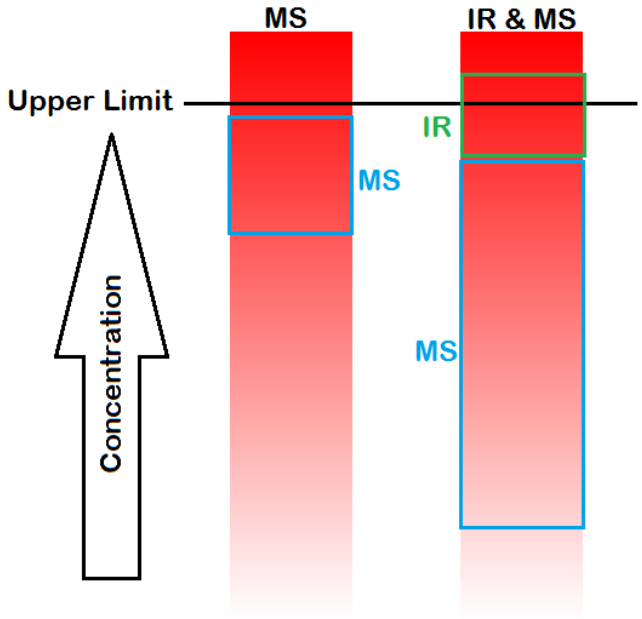

Figure 1.8. When using the MS alone, the dynamic range is narrowed nearly below the upper concentration limit (left). When IR and MS are detecting the reaction simultaneously, the dynamic range of MS is enhanced.

2 Simultaneous Orthogonal Methods for the Real-Time Analysis of Catalytic Reactions

The powerful coupling of infrared spectroscopy (IR) and mass spectrometry (MS), letting IR monitor the reactant and product while MS focus on the charged catalytically reactive species at much lower concentration, greatly exploits the potential of MS and deepens the mechanic insight into catalytic reaction with the dynamic range of 5 magnitudes. To test the utility of this methodology, a hydroacylation reaction using cationic rhodium complex as catalyst is studied. And through such a deep probing the behavior of precatalysts, intermediates, catalyst impurities and decomposition products is revealed. Also simple guides to distinguish different types of species in catalytic cycle are provided.

2.1 Brief Introduction on Hydroacylation[36]

Hydroacylation is the atom-economic addition of a formyl C-H to an unsaturated C-C bond. This C-H bond activation can be facilitated by a variety of transition metals. Through decades of development, hydroacylation can be classified into 4 types, depending on whether they are intra- or intermolecular and of alkenes or alkynes.

The first reported hydroacylation was accomplished by Sakai's group in 1972[37]. It is an intramolecular alkene hydroacylation, taking stoichiometric amount of Wilkinson's catalyst to transform a series of 4-enals into cyclopentanone up to 34% with the by-product from decarbonylation cyclopropane around 30% yield. Thanks for this phenomenal start, a lot of works have been done to decrease the catalyst loading and to prepare a larger range of ring sizes. The intramolecular alkene hydroacylation has been the best studied.

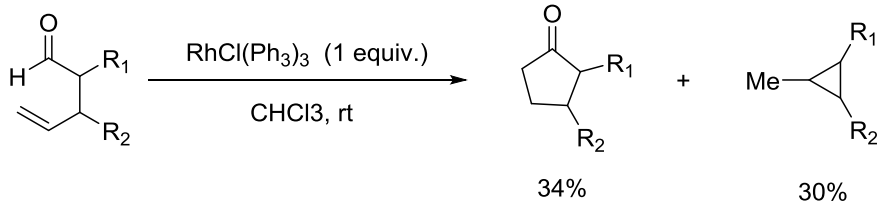

Equation 2.1.

According to our study, we are going to focus on the intermolecular hydroacylation enabled by the rhodium catalyst. The first intermolecular hydroacylation was found by Miller in his intramolecular studies[38]. He found that when switching the catalyst from Wilkinson's catalyst to $Rh(acac)(C_2H_4)_2$ it made the reagent react in a intermolecular manner. Later Vora proved that the double bond in the aldehyde helps to increase the activity by letting the alkene coordinate with catalyst at first[39].

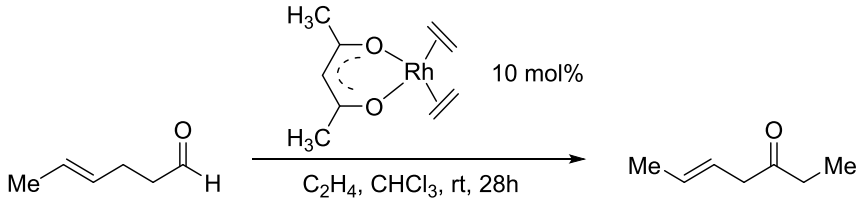

Equation 2.2.

To expand the utility of the intermolecular hydroacylation Marder and Millstein catalyzed a range of aromatic aldehydes with the indenyl rhodium complex $[Rh(\eta^5\text{-}C_9H_7)(C_2H_4)_2]$[40].

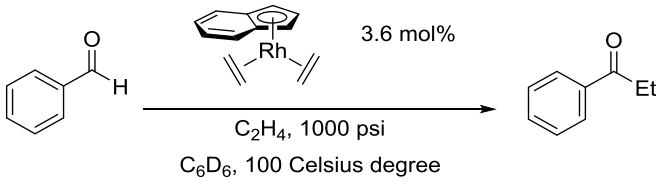

Equation 2.3.

As mentioned above, the success of the initial intermolecular hydroacylation was accounted on the catalyst stabilization by coordinating the alkene motif of the aldehyde to the Rh catalyst. This belief was soon be corrected by a number of findings using the heteroatom of the aldehyde chelate to the rhodium and stabilize the catalyst. For example, Suggs managed to hydroacylate quinolone-8-carboxaldehyde with Wilkinson's catalyst and isolate the intermediate[41]. Another example is reported by Jun, employing the phosphine group of the benzaldehyde to stabilize the Wilkinson's catalyst[42].

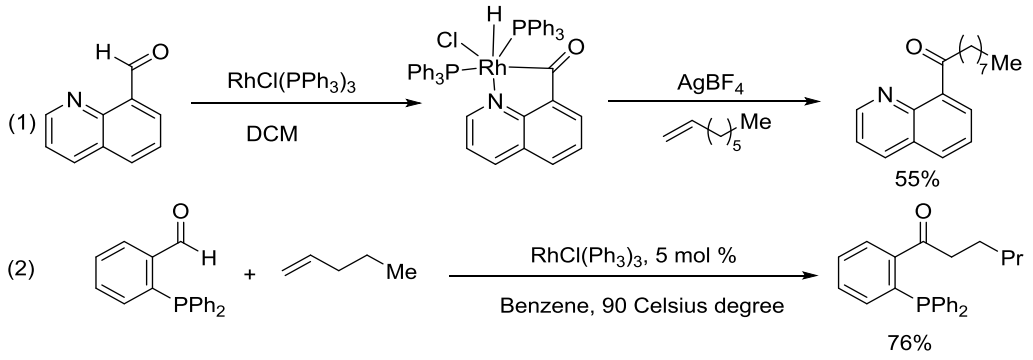

Scheme 2.1. Suggs' finding (above): treating the intermediate with $AgBF_4$ and octene results in a considerable yield. Jun's finding (below): o-diphenylphosphino benzaldehyde reacted with neutral alkenes with low catalyst loading of Wilkinson's catalyst

Besides the two methods mentioned above to use quinoline- or phosphine-substituted aldehyde to stabilize the rhodium catalyst, recently the Willis group found a bunch of examples to use S-chelation to increase the intermolecular hydroacylation. Like the first reaction below, the author proposed a five-membered S-chelating structure to explain the observed activity. And the application of $[Rh(dppe)]ClO_4$ allows this intermolecular hydroacylation run under a mild situation[43].

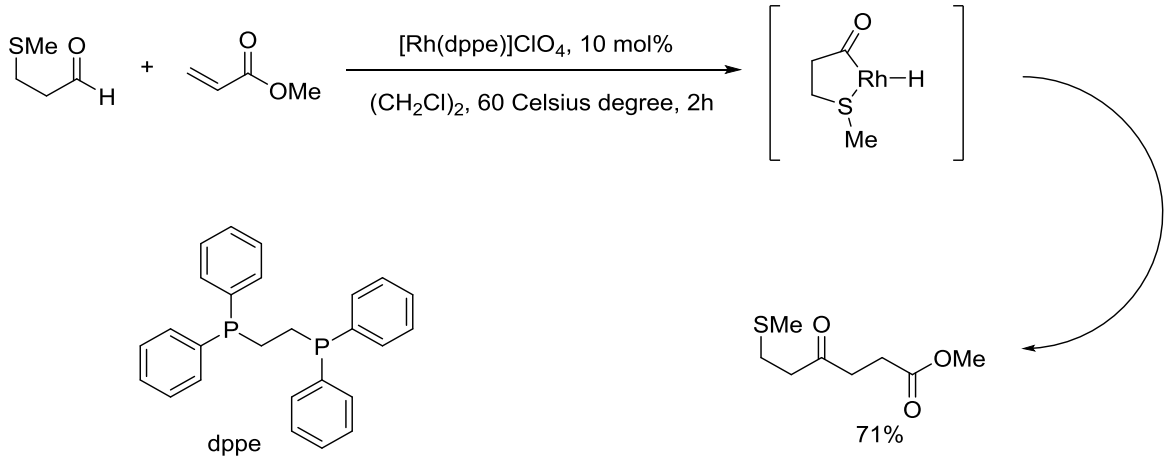

Scheme 2.2. β-Methylsulfide-propanal hydroacylated with electron-poor alkene by $[Rh(dppe)]ClO_4$

Moreover, Weller and Willis successfully hydroacylated the β-methylsulfide-propanal and the poorly reactive neutral hexene[44]. The active catalysts were made from $[Rh(COD)Cl]_2$, DPEphos and $Ag(ClO_4)$. It is the flexible DPEphos ligand that has various coordination modes and geometries makes the catalyst longer-lived.

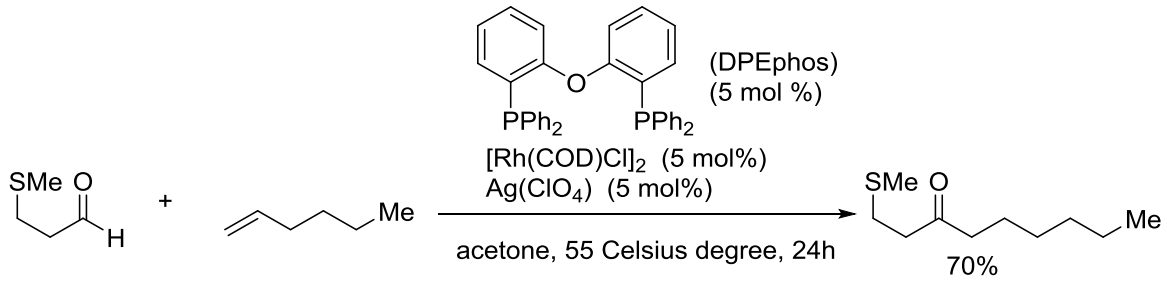

Equation 2.4.

Almost all the preceding examples ask for stabilization of the rhodium catalyst by chelation from the aldehyde. The Tanaka group stabilized the rhodium catalyst with the bidentate alkene[45]. The *N*,*N*-dialkyl acrylamide, as the alkene component, can stabilize the active intermediate and accommodate a wider range of aldehydes. In this case, cationic rhodium catalyst with bidentate phosphine ligand was used again. But this time

1,4-bis(diphenylphosphino)butane (dppb) was used instead of the commonly used 1,2-bis(diphenylphosphino)ethane (dppe).

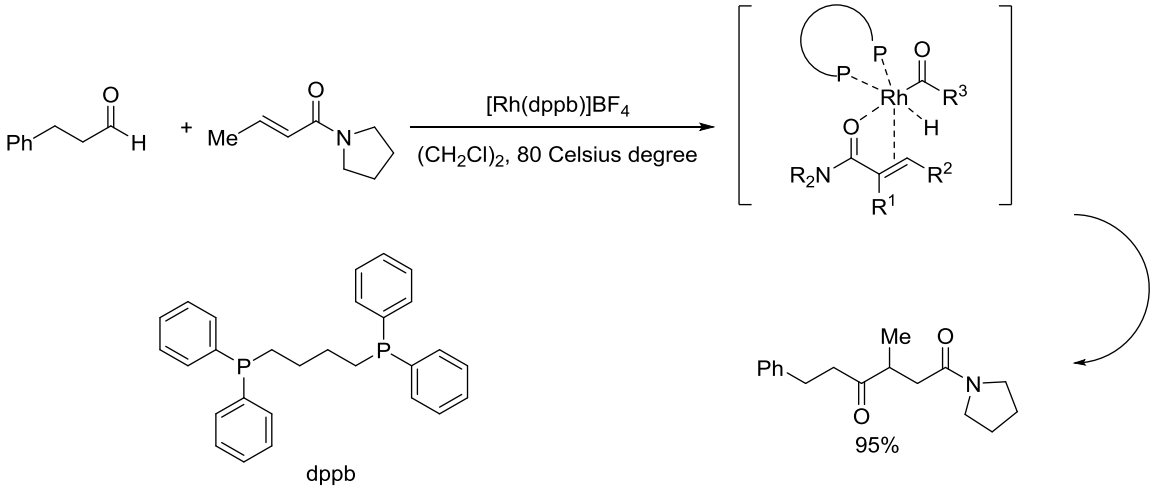

Scheme 2.3.

Also Brookhart discovered rhodium(I)bis-olefin as an effective intermolecular hydroacylation catalysts, though the application is limited to the use of vinylsilanes as stabilizing ligands[46]. And the strong electron-withdrawing group CF_3 is believed to make the catalyst more effective than its penta-methyl counterpart.

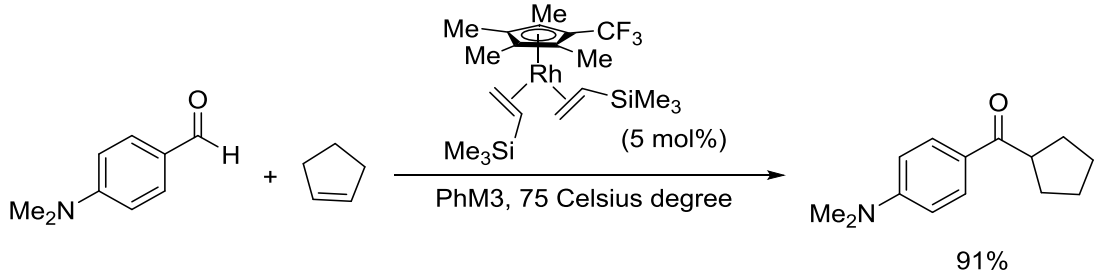

Equation 2.5.

All the examples discussed above ask for one of the reagent containing stabilizing constituent to stabilize the catalyst and this limits the scope of the available substrates to

choose from. The Jun's group later demonstrated the addition of amine to the reaction system can help to stabilize the catalyst thus the range of applicable substrates is widened[47].

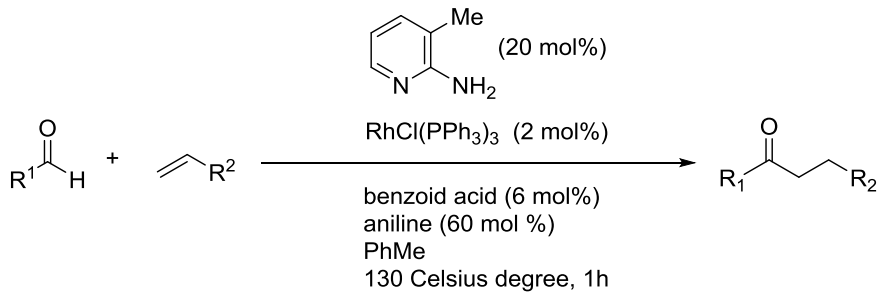

Entry[a]	R^1	R^2	Yield(%)
1	Ph	Bu	98
2	Ph	Pr	83
3	Ph	Hex	99
4	Ph	*t*Bu	84
5	Ph	$SiMe_3$	95
6	Ph	C_6F_5	98
7	Ph	$PhOCH_3$	95
8	4-MeO-C_6H_4	Bu	79
9	4-CF_3-OC_6H_4	Bu	71
10	4-Me_2N-C_6H_4	Bu	60
11	4-Ph-C_6H_4	Bu	95

[a] 5 equivalents of alkene used.

Equation 2.6.

Moreover, this reaction can be further simplified by utilizing alcohol as the aldehyde precursor. The simple alcohol was first catalysed by the rhodium complexes with one equivalent of alkene as the oxidant. Then the aldehyde went through hydroacylation catalysed by the same rhodium complexes[48]. The most efficient catalyst was discovered to be $RhCl_3•H_2O$ (only 3.3 mol %). And the catalysts were used in combination with triphenylphosphine and stoichiometric amount of 2-amino-4-picoline. Further modifications were made on this reaction to allow amines to be employed and let methanol to form formaldehyde and undergo double hydroacylation[49].

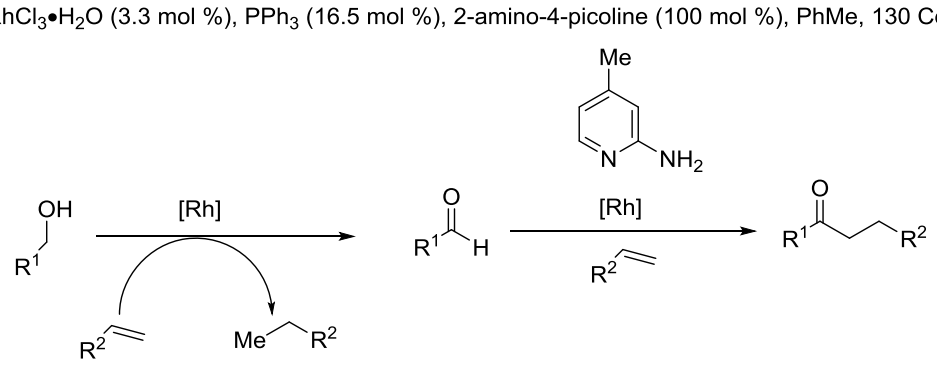

Equation 2.7.

A number of mechanic studies on hydroacylation have been done. For intermolecular alkyne/alkene hydroacylation, the key step involves the oxidative addition of aldehyde on the rhodium catalyst. Then the unsaturated carbon bond associated to the rhodium center and underwent 1,2-insertion. At last the product is removed from the rhodium through reductive elimination. Competitively, the complex can undergo reductive decarbonylation, a major problem in the hydroacylation reaction.

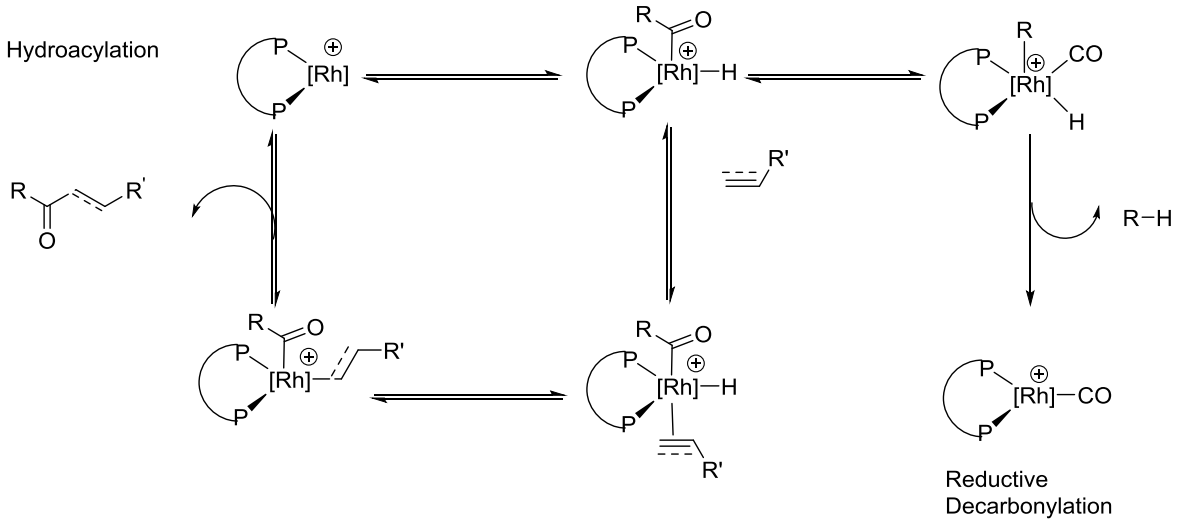

Scheme 2.4. General mechanism for hydroacylation

2.2 Results and Discussion

In this study, we especially focused on the intermolecular hydroacylation between 2-(methylthio)benzaldehyde and 1-octyne catalyzed by $[Rh(PNP^{i}Pr_2)_2]^{+}[BAr_4^{F}]^{-}$ in 1,2-dichloroethane(DCE) at room temperature (Equation 2.8).

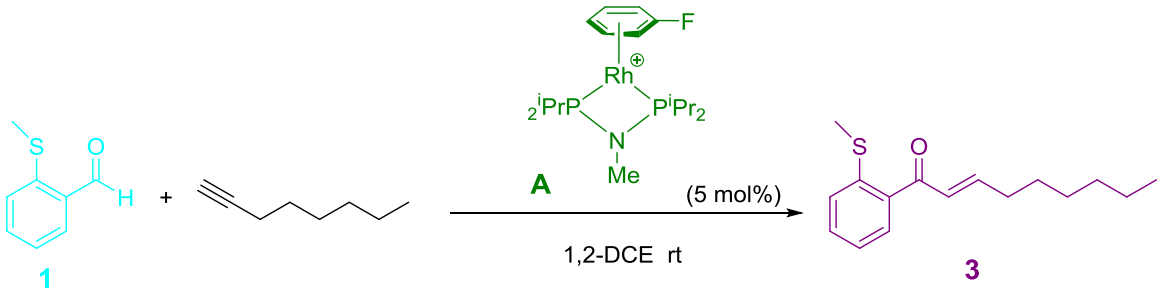

Equation 2.8. Hydroacylation between methylthiobenzaldehyde and 1-octyne in DCE at room temperature.

Firstly from the FTIR the behavior of the reagent methylthiobenzaldehyde and the product ketone were recorded. From the exponential manner in which the ketone increased and the aldehyde decreased, we know that it is a first-order reaction. To test this, we graphed the relationship between natural log of intensity of aldehyde and the

time. And the linearity fits well with the R^2 equals to 0.99726. According to the Donna G. Blackmond's study on reaction kinetics, as the complex **D** (product bound rhodium complex) is the predominant catalytic species at resting state, the catalysis should be at first order to both catalyst and aldehyde[50]. And the slowest step is the one in which the product dissociate from the rhodium complex. In the Figure 2.2, the linear relationship between the reaction rate constant with catalyst loading reveals the reaction is indeed at the first order to the catalyst loading. The reason why this line dose not start from the original point is that there is always a certain amount of the catalyst gets poisoned and thus not active during the catalysis.

Also the relatively large error of the average concentration of ketone and aldehyde at the first few minutes of the reaction is believed to be caused by the slow reaction at the beginning. The slow reaction at the beginning shows that there is an introduction period in which the precatalyst needs to go through some process (usually dissociation of a ligand) to become the active catalyst. Thus before all the precatalyst was converted to catalyst and the catalysis reached to steady state, the concentration of catalyst was low and reaction rate was slow.

(The experimental data here mainly comes from Robin Theron, a former M.Sc. student in our group).

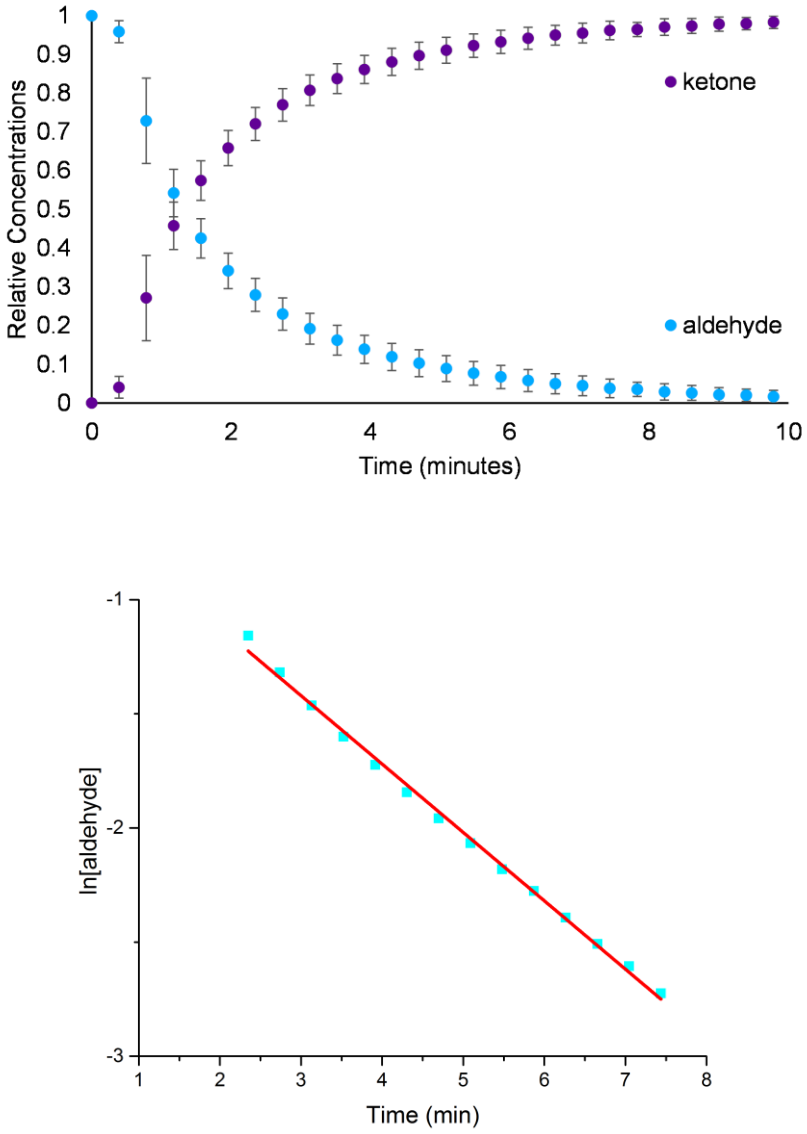

Figure 2.1. The increase of the product and the decrease of the reagent were monitored by the FTIR. It is the average of the 10 replicates of the reactions (up). Relationship between natural log of the intensity of aldehyde and time (down).

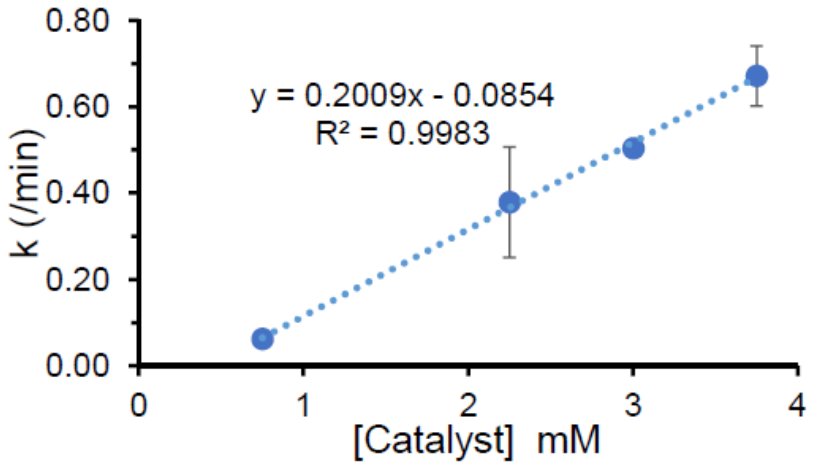

Figure 2.2. The linear relationship between the reaction rate constant and catalyst loading, which reveals the whole catalysis is at first order to the catalyst.

The ESI-MS was responsible for detection of the charged species. The figure provided below is the average of seven replicates. As the catalyst loading is 5 mole percent, the highest concentration of the precatalyst should be one twentieth of that of aldehyde. Thus the graph below shows the behavior of charged active species with intensity zoomed in 20 times.

The complex **A** is the precatalyst we added to the solution and the **D** is the product bound with the rhodium catalyst. The exponential decreasing manner of the **A** and its assignment reveal its role as precatalyst in the system which will soon convert into the active catalyst in the introduction period.

As for the magenta line of **D**, the product bound rhodium complex, it reached to the steady state after introduction period as the main catalytic complex in the system. As mentioned earlier the slowest step is the dissociation of product from **D**, the abundance of **D** will build up until it reaches equilibrium.

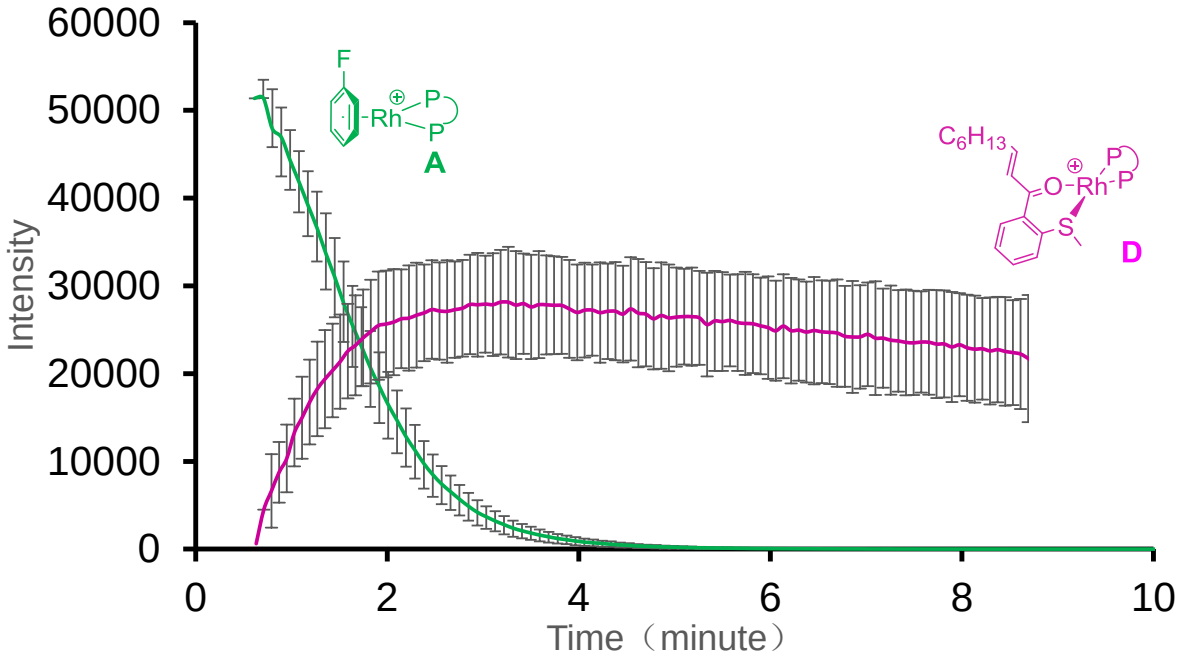

Figure 2.3. The most two prominent species detected by the MS, with the intensity one twentieth of that of the aldehyde.

When zoomed in eight thousand times, a number of impurities were detected. There are six impurities in total and they are been labeled separately as **I**, **E**, **J**, **K**, **O** and **L**. According to their isotope pattern and MS/MS fragmentation, all the six impurities were assigned. Their sudden appearance at the moment of adding the catalyst and the steady trend all reveal they are the catalyst impurities. Also these impurities are believed to originate from the catalyst synthesis and solvent stabilizer.

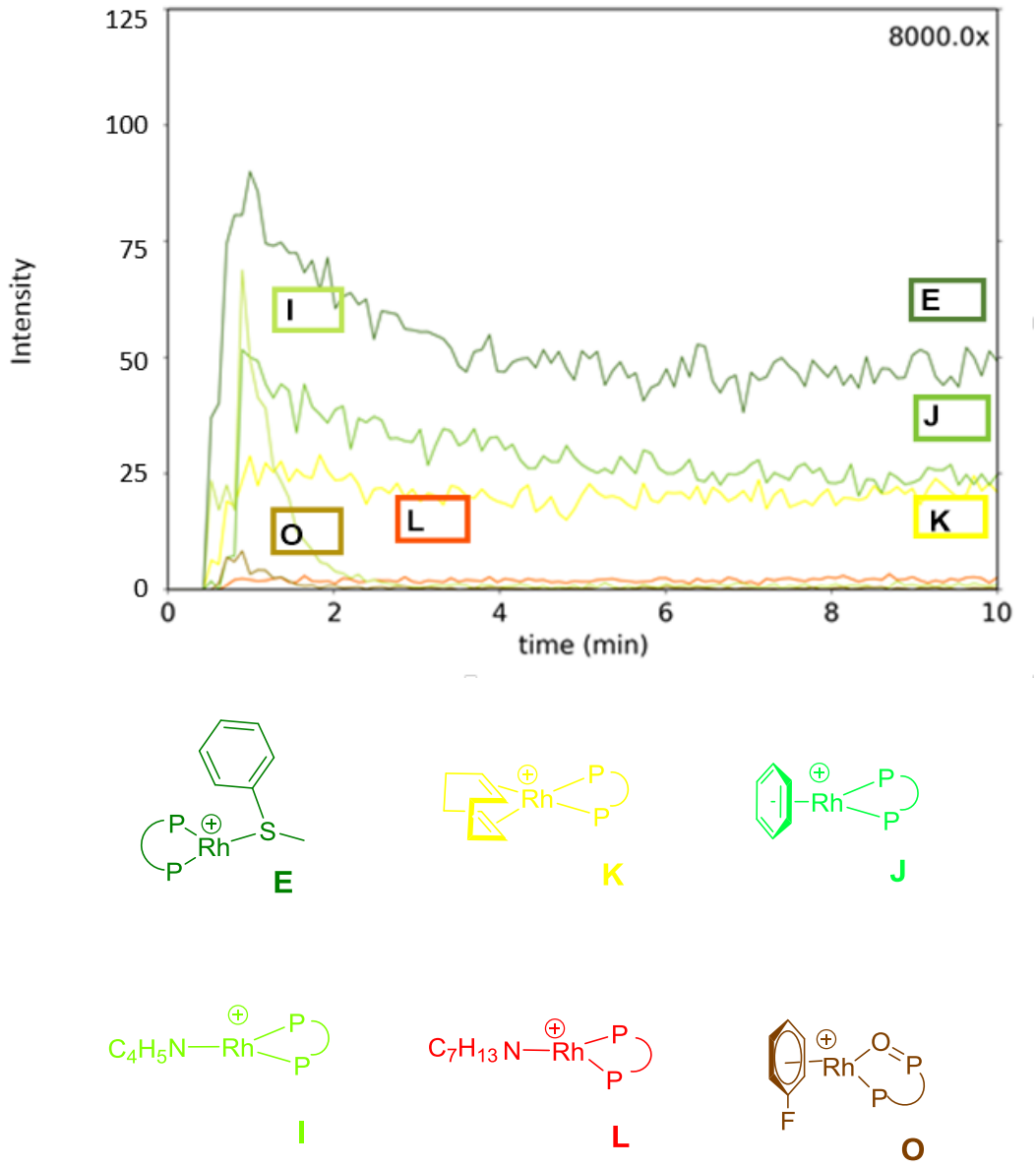

Figure2.4. Drilling the mass spectrum deeper in 8,000 times, six impurities were found and assigned.

Continue to zoom in 50,000 times, the intermediate **B** was found. The kinetics of **B** tells us it is joining the fastest step of the reaction and soon be removed rapidly. Because **B** was not present originally in the catalyst, it must be an intermediate.

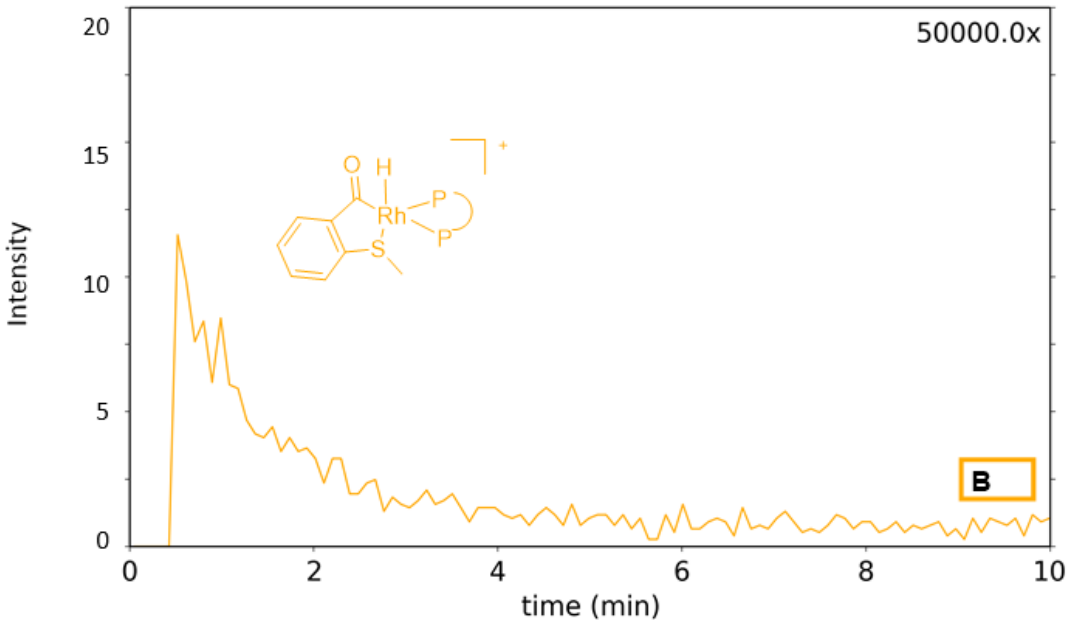

Figure 2.5. Zoomed in 50,000 time, the intermediate B is found.

At last, we delved the detection into a one hundred thousandth of the concentration. The linear increase of these three species unveils that they are the catalyst decomposition or poisoned products. Because usually only a small portion of the reagents can be poisoned, the change of the concentration of them can be ignored. Thus the poisonous reaction is at pseudo zeroth order and the decomposition product will increase linearly throughout the time.

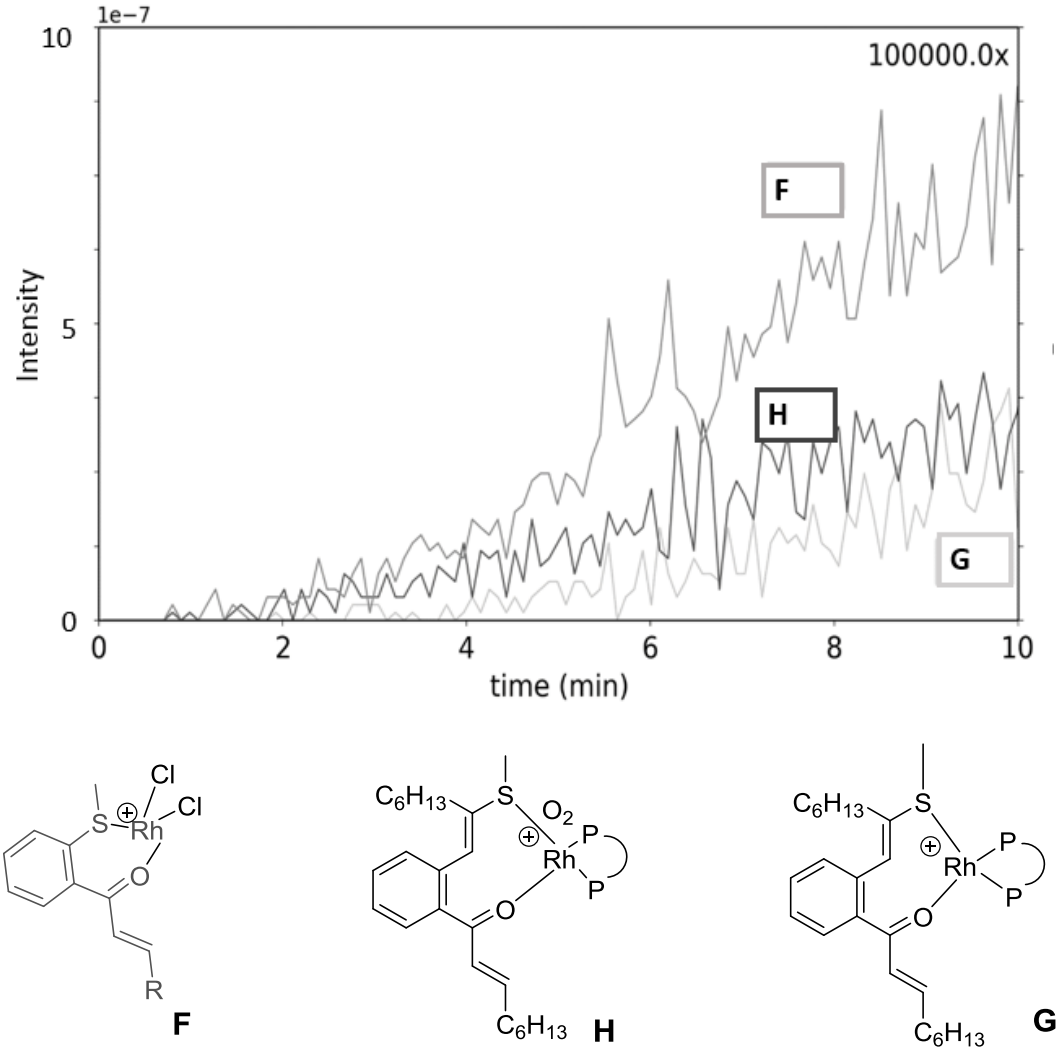

Figure 2.6. Three catalyst decomposition products were found when the MS spectrum was zoomed in 100,000 times.

2.3 Conclusion

There is no example like this coupling of IR and MS that can explore a reaction with all active species covering 5 magnitudes of abundance. Not only were the reagent and product which are neutral and in abundant taken care of by the FTIR, but the charged and catalytic species in extremely low abundance were monitored simultaneously by the ESI-MS.

The role of each species in the catalysis can be easily assigned according to their patterned kinetic behavior. These behaviors can mainly be classified by the following 4 questions:

1) Is this species in high or low abundance?

2) Dose this species decrease or increase?

3) Dose it change in a linear or exponential manner?

4) Does the change happen before or after the starting point of the reaction?

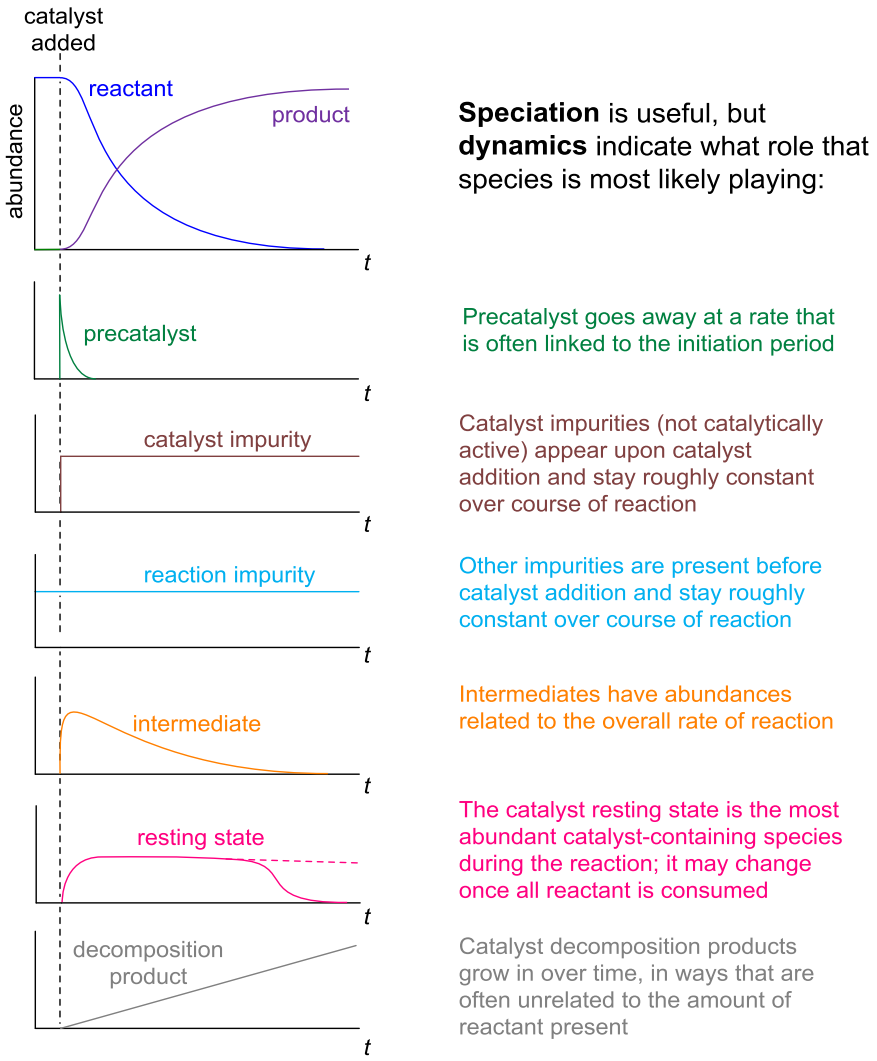

Firgure2.7. A simple guidance help to classify different species' role in the catalytic reaction based on their patterned behavior.

After gathering all the information like the chemical structure and the role it plays in the system of each specie, the mechanism can be easily figured out by placing them in the appropriate spot.

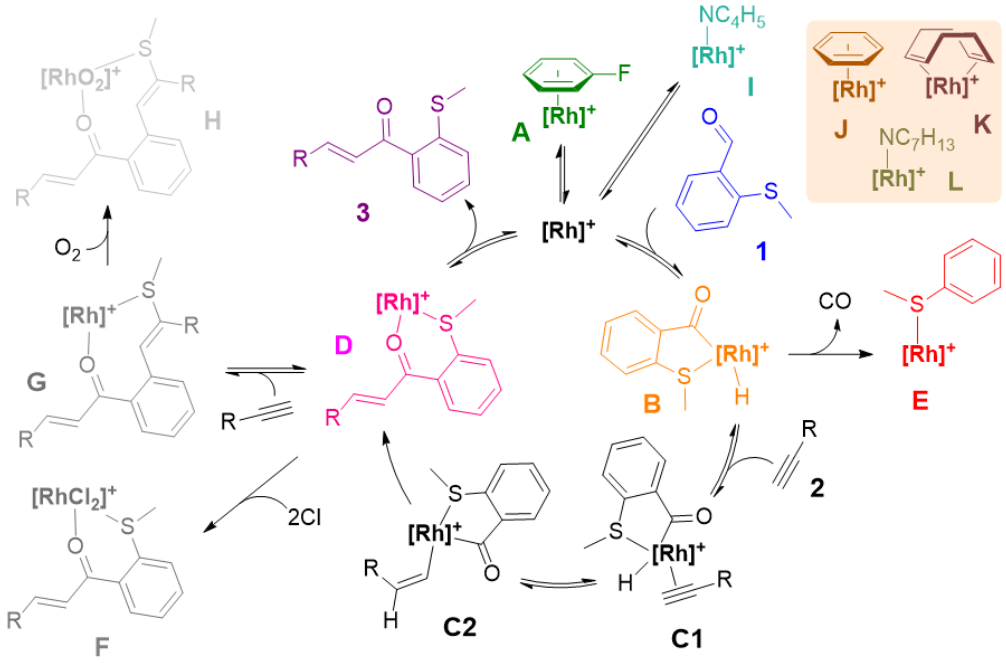

Figure 2.8. Proposed mechanism for the intermolecular alkyne hydroacylation.

2.4 Experimental

General

Solvents were obtained from MBraun solvent purification system in HPLC grade. 1,2-DCE was obtained from Caledon Labs, redistilled and stored over 4 Å molecular sieves overnight before use. 2-(methylthio)benzaldehyde was synthesized and kept in glove box. 1-octyne was gained from Sigma Aldrich, redistilled and dried over calcium hydride before use.

Prior to detection, both MS and FTIR were rinsed with the solvent, 1,2-DCE, to remove impurities and produce IR background spectrum for data processing. Then a solution of

2-(methylthio)benzaldehyde (90 mmol/L, 0.225 mmol) and 1-octyne (135 mmol/L, 0.338 mmol) in 1,2-dichloroethane (2.5ml) was added to the argon filled Schlenk flask and linked like the graph below. And the reaction was started by injecting a solution of $[Rh(L)(FPh)]^{+}$ $[BAr^{F}{}_{4}]^{-}$ in 1,2-dichloroethane (0.5 ml, 22.5 mmol/L, 0.0113 mmol). The reactions were well stirred.

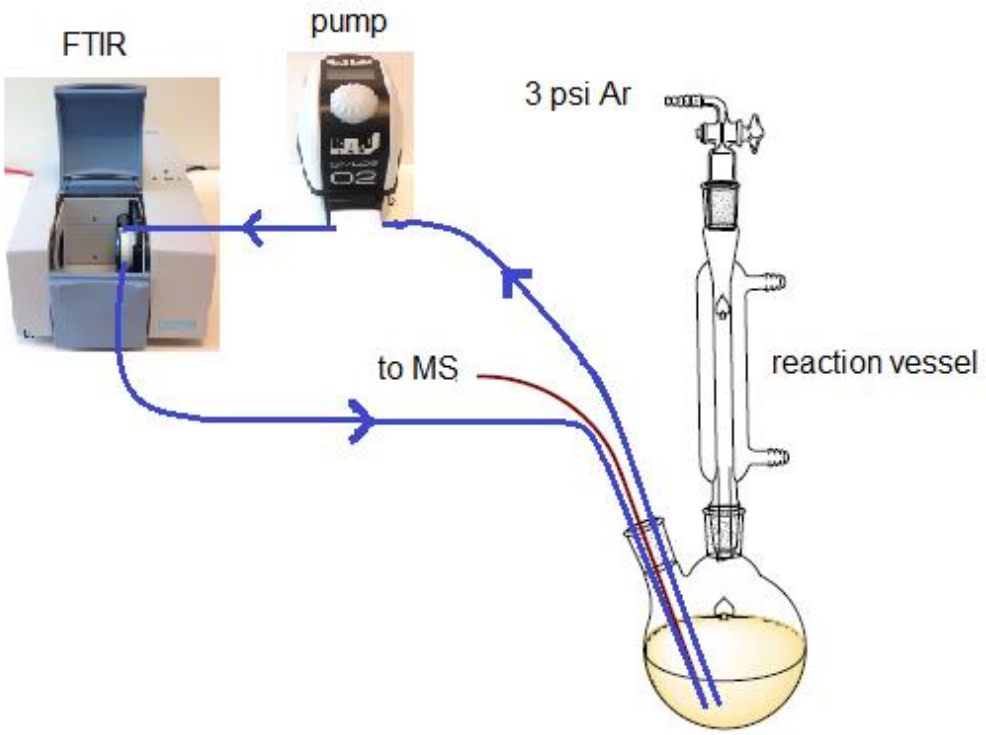

Figure 2.9. Equipment set-up for the coupling of IR and MS. The reaction vessel was slightly over-pressurized by the gas Ar to push the reacting solution through the 125 μm inner diameter PEEK tubing (red) to the MS. At the same time the dosage pump would pump the reaction solution through the 250 μm inner diameter PEEK tubing (blue) to the FTIR and recycle it back to the reaction vessel.

Synthesis of 2-(methylthio)benzaldehyde

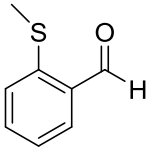

A solution of methanethiol sodium salt (17.7 mL, 3.0 M in water, 53.1 mmol) was added dropwise to a solution of 2-fluorobenzaldehyde (5.09 mL, 48.3 mmol)) in DMF (60 mL) at room temperature. The reaction was stirred for 16 hours after which water (40 mL) was added to the mixture. The product was extracted with Et_2O (3´ 20 mL). The organic layers were washed with water (20 mL) and brine (3 ´ 10 mL) then dried over $MgSO_4$ and concentrated under reduced pressure. The crude oil was purified by flash column chromatography on silica (20% EtOAc/Hexanes) to obtain aldehyde as a yellow oil (5.5 g, 75%).

Monitoring by IR. IR measurements were done on a Bruker Alpha FT-IR fitted with a Harrick demountable transmission flowcell with BaF_2 windows, a 100 μm pathlength, and a 5 μL cell volume. The reaction solution was circulated through the flow cell via tubing of 250 μm inner diameter using a Simdos 02 Pump at a flow rate of 2.5 mL/min. A background of 1,2-dichloroethane was collected before each experiment, after which the pump was purged with argon before introducing reaction solution.

Monitoring by ESI-MS. ESI-MS measurements were done on a Micromass Q-Tof *micro* mass spectrometer in positive ion mode using pneumatically assisted electrospray ionization: capillary voltage 2900 V; sample cone voltage 15 V; extraction voltage 0.5 V; source temperature 84°C; desolvation temperature 184°C; cone gas flow 100 L/h; desolvation gas flow 200 L/h; collision voltage 2 V; MCP voltage 2400 V. Reaction solution was continually fed from the reaction flask into the mass spectrometer via 125 μm inner diameter PEEK tubing. Spectral assignment was aided by the free tools available at chemcalc.org.[28] Abundance vs. time traces in the paper were assembled from

averages of multiple runs, and no smoothing or other manipulation of the data was performed.

3 Mass Transfer and Convection Effects in Small-Scale Catalysis

3.1 Introduction

Catalytic reactions involving a gaseous reactant always complicate mechanistic studies as the mass transfer, mainly diffusion, may become turn-over limiting, affecting the reaction rate and deviating the species of interest from their normal behavior when studied by real-time monitoring. Especially when using modern spectroscopic methods, reacting samples are usually in small and narrow reaction vials (e.g. NMR tubes) and monitored under relatively low pressure. In both cases the influence of mass transfer becomes an increasingly important concern. In this study, the hydrogenation of a charge-tagged alkyne was monitored by mass spectrometer under systematically altered situations like varied contact area (4 specially designed vials with doubling cross section from V1 to V4), stirring or not stirring, different hydrogen partial pressures (1 eq. vs 2 eq.) and catalyst loading to examine the mass transfer effect. During the study it was found that under extreme circumstances, convection effects result in complex and erratic discrepancies from the expected behavior, which shows the sampling method examines a single point in the reacting solution instead of the average of the whole and thus can reveal heterogeneities in solution composition.

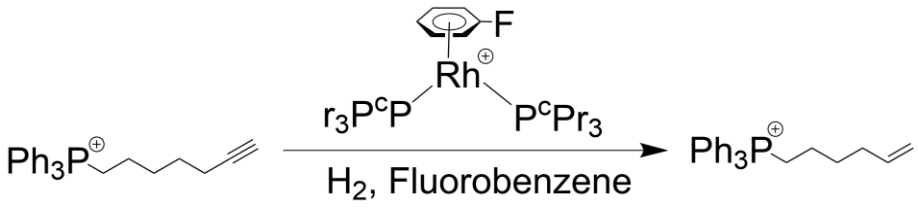

Equation 3.1.

3.1.1 Homogeneous Hydrogenation with Rhodium Catalyst[51]

Hydrogenation is the addition of molecular hydrogen to an unsaturated compound. It always involves the presence of either a homogeneous catalyst or a heterogeneous catalyst. This process is mostly used to partially saturate a carbon-carbon multiple bond in organic synthesis[52].

In this case, we focused on partial hydrogenation of charge-tagged alkynes using cationic rhodium complexes as homogeneous catalysts.

The term "homogeneous hydrogenation" was first mentioned in 1938 by Melvin Calvin[53]. In his case, Melvin used rhodium ammine complexes in aqueous solution to reduce p-benzoquinone. Then in the 1960s, Wilkinson, Bennett and Coffey made the complex $Rh(PPh_3)_3Cl$ ("Wilkinson's catalyst")[54]. And they found this complex can hydrogenate alkenes in a reliable, selective and efficient manner[55]. Later on Halpern studied the mechanisms of the hydrogenation using Wilkinson's catalyst[56].

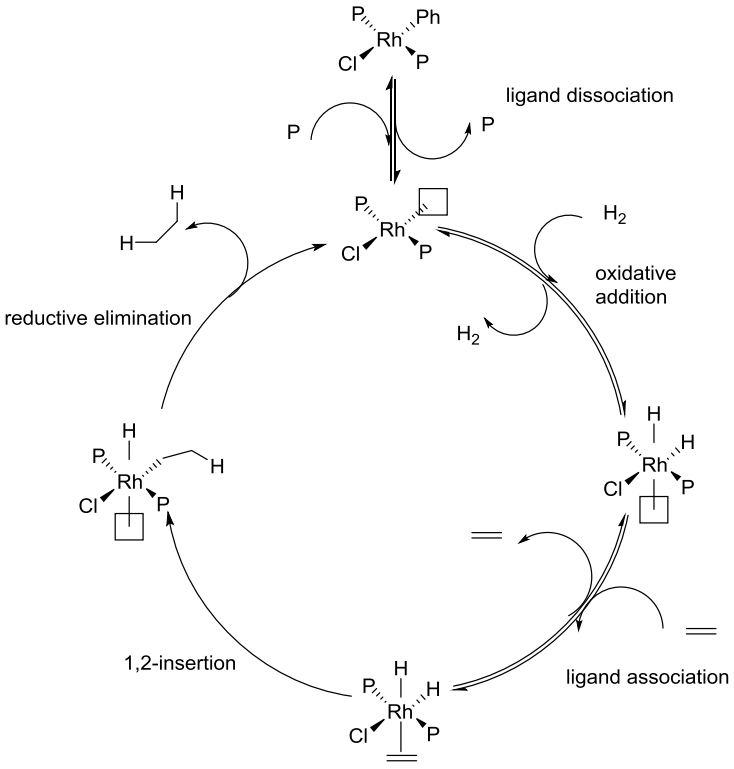

Scheme 3.1. Mechanism of Hydrogenation using Wilkinson's catalyst

Soon after the discovery of Wilkinson's catalyst, chemists' attention has been focused on the controlling the diastereoselectivity and enantioselectivity of homogeneous hydrogenation catalysis. Horner[57] and Knowles[58] both published chiral rhodium catalysts with monophosphines that had three different substituents bound to the phosphorus. Phosphine ligands like this are called P-chiral ligands. In research aimed at increasing the stereoselectivity of the reaction, Kegan had the three following findings[59]:

1) Rhodium complexes with bisphosphine ligands have higher enantioselectivity than those with monophosphines. That is because the chelation of the bisphosphines to the rhodium increases the ligand's rigidity and decreases its order of freedom.
2) Ligands showing C_2 symmetry have less isomers formed by the coordination of the prochiral olefin, which thus reduces the number of species reacting with competing enantioselectivity. Even though this was later disproved by Inoguchi[60], this rule were still followed by chemists like Knowles.
3) The center of chirality does not need to be the phosphorus atom. Ligands like DIOP, 2,3-O-isopropylidene-2,3-dihydroxy-1,4-bis(diphenylphosphino)butane, having the ligand backbone as the stereocenter, actually have substantial or even higher enantioselectivity. It is because the stereochemistry of the backbone results in preferred conformations of substituents bound to the phosphorus atom. And this conformational preference can be transferred to the binding site of the transition metal.

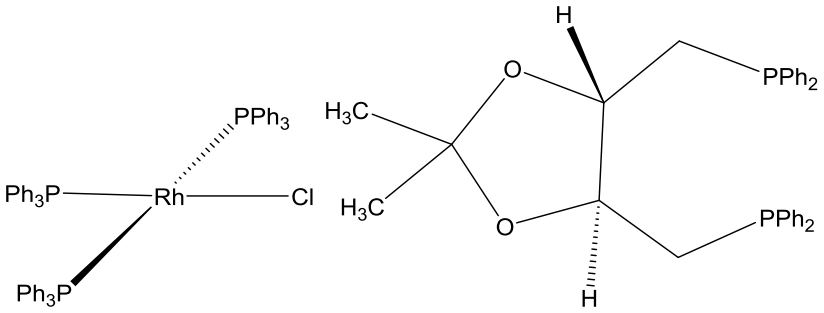

Figure 3.1. Wilkinson's catalyst (left) and DIOP (right)

3.1.1.1. Neutral Rhodium Catalyst

Wilkinson's catalyst is the most important neutral rhodium catalyst. This complex is mildly air/moisture sensitive. When contact with oxygen, some triphenylphosphine will convert to triphenylphosphine oxide. Also the Wilkinson's catalyst is better freshly prepared before using as the "aged" complex, the dimer $[Rh(PPh_3)_3Cl]_2$ with bridging chloride, will result in poor performance in reaction rate and regio/stereoselectivity.

The synthesis of Wilkinson's catalyst is simple and easy. Rhodium (III) chloride is heated with PP h_3 in ethanol. The main impurity is the phosphine oxide, which can either comes from the oxidation of triphenylphosphine or the hydrolysis of the resulting Ph_3PCl_2.

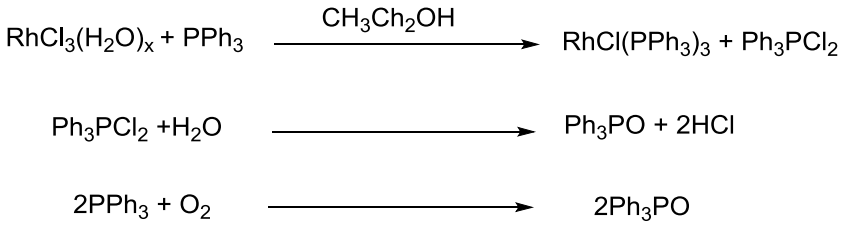

Scheme 3.2. Oxidation of phosphines

The mechanism of hydrogenation employing neutral rhodium catalysts is often called the "hydrogen-first" mechanism[61]

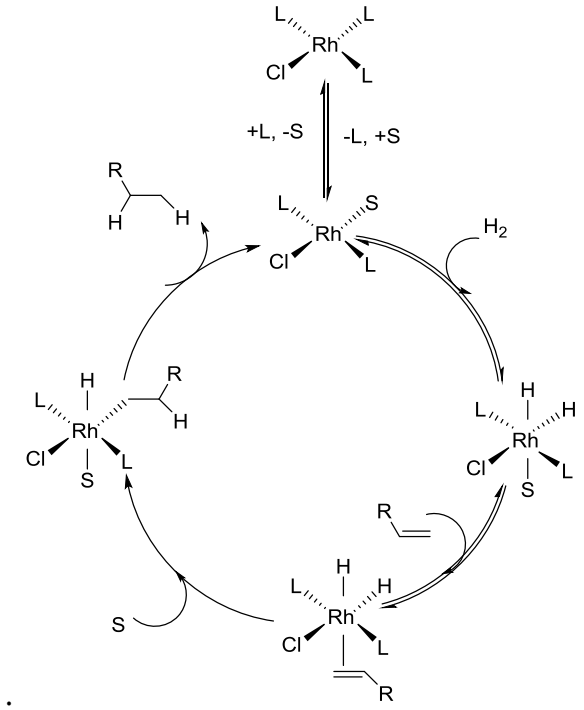

Scheme 3.3. “Hydrogen-first” mechanism in hydrogenation with neutral rhodium catalysts

3.1.1.2. Cationic Rhodium Catalyst

Cationic rhodium catalysts are comparatively more catalytically reactive and regio/stereoselective than their neutral counterparts and now more popular. They share the general formula $[RhL_2(S)_2]^+$, where the S stands for polar solvent and the L_2 represents two tertiary phosphines or a chelating bisphosphine. Osborn and Schrock showed that the stronger electron-donating the ligands are, the more reactive is the cationic rhodium complex[62].

Also according to Osborn’s studies on these catalysts[63], firstly, the activation of the catalyst involves the hydrogenation of the coordinated alkene from$[Rh(alkene)L_2]^+$. Secondly, the reactive complexes $[Rh(S)_2L_2]^+$ react with hydrogen to form the cationic dihydride complexes $[Rh(H)_2L_2]^+$. Thirdly, the hydrides are acidic and the presence of

basic group or trialkylamine results in neutralization of the catalyst and the same mechanism as Wilkinson's catalysts.

The mechanism[64] of hydrogenation employing cationic rhodium catalysts depends on the phosphine ligands. If the cationic rhodium catalyst contains aromatic phosphines, then the mechanism is followed is the "alkene-first" mechanism.

The reasons behind it are, firstly, it is less thermodynamically favored oxidation of hydrogen to the cationic rhodium catalysts and this step is slower. Secondly, the alkene can more easily substitute the solvent that is more weakly bound to the cationic complex than the third phosphine ligand. In most cases, the cationic catalysts are used for the hydrogenation of alkenes that can chelate the rhodium with the double bond and the electron-donating functional group. Like in Scheme 3.4, the "alkene-first" mechanism occurs by the initial substitution of the solvent with the alkene, followed by the oxidative addition of H_2. Later the rearrangement involves the 1,2-insertion of the olefin onto the monohydride, leading to the final release of the product and restoration of the catalyst.

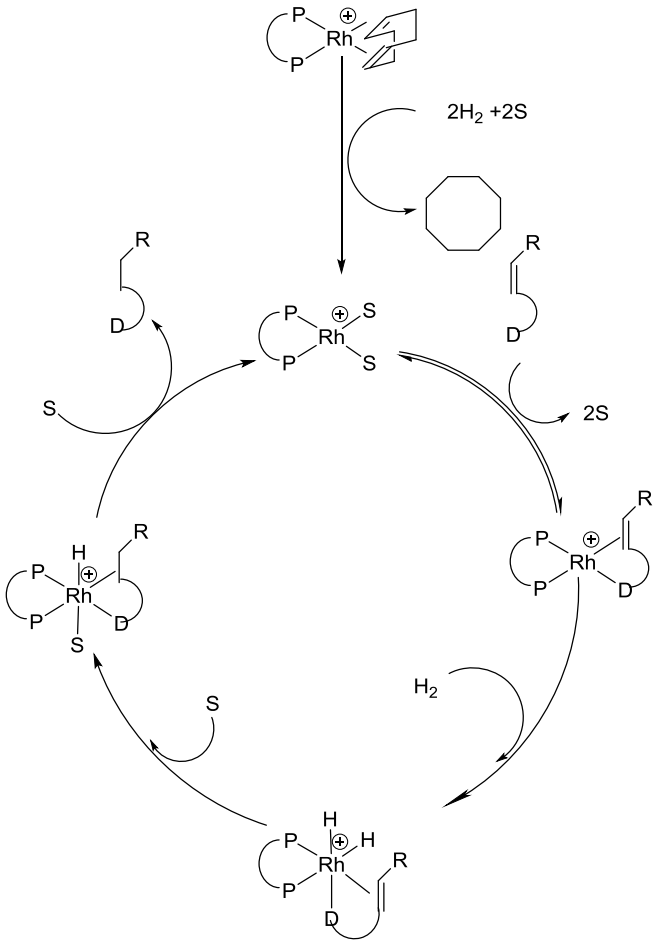

Scheme 3.4. “Alkene-first” mechanism in hydrogenation with cationic rhodium catalysts containing aromatic phosphines

If the cationic rhodium catalyst contains alkylphosphine ligand, the mechanism of hydrogenation appears to be “hydrogen-first” rather than the “alkene-first”. It is because that these alkylphosphine ligands are electron rich enough, despite of being cationic, to increase the rate of oxidative addition of the hydrogen on the rhodium, the turnover-limiting step in the mechanism[65].

3.1.1.3. Rhodium Monohydride Catalysts[66]

A special class of rhodium catalysts for hydrogenation is those with only one hydrogen bound to the metal, monohydride catalysts. The most common one is the $Rh(H)(PPh_3)_3(CO)$. This catalyst can hydrogenize terminal olefins under mild conditions (25 °C and less than 1 atm H_2). As for internal olefins, this catalyst can only speed up the isomerization instead of the hydrogenation.

What is interesting about this catalyst is that it can also been used for hydroformylation of olefins, when the olefin insert into the carbon monoxide instead of the hydride ligand.

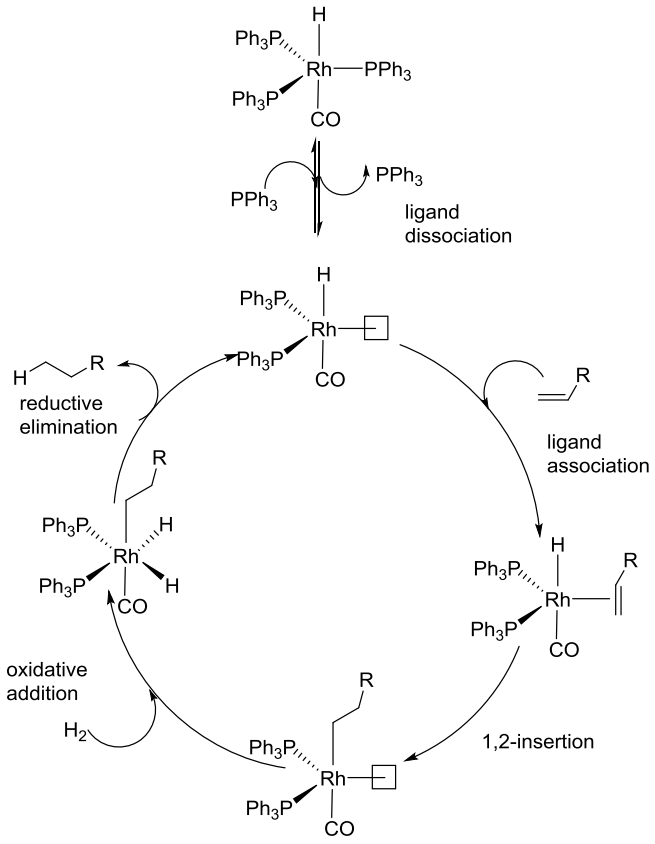

Scheme 3.5. Monohydride mechanism

3.1.1.4 Ligands Used for Asymmetric Hydrogenation

An important finding in homogeneous hydrogenation is that through careful ligand and catalyst design it is possible to achieve high regio/stereoselectivity. As discussed at the beginning of this chapter, the first enantioselective hydrogenation was made though P-chiral bisphosphine ligands. But it is the discovery of aromatic bisphosphines with axial chiral backbones that actually broadened the number and application of asymmetric hydrogenation.

2,2'-bis(diphenylphosphino)-1,1'-binaphthyl (BINAP) is the forerunner of this kind of phosphine ligands first made by Noyori[67].

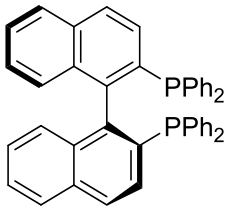

Figure 3.2. (S)-BINAP

The great success of BINAP at imparting high selectivity provoked inorganic chemists to synthesize similar ligands containing the axial backbone. Even though these ligands were made to circumvent the patents of BINAP, many of them were still very successful and exhibited better turnover numbers, reaction rate and selectivity. By comparing these ligands' performance in hydrogenation, scientists derived the following rules:

1) The dihedral angel of the backbone can affect the enantioselectivity. The smaller the dihedral angle, the higher the enantioselectivity[68].
2) Substituents on the aryl groups bound to the phosphorus, especially in the meta- positions, can improve the enantioselectivity by decreasing the degrees of freedom[69].

3) The electronic properties of the backbone can also influence the enantioselectivity. Bisphosphine ligand with more electron-donating backbone (hydrogenated for example) can contribute higher enantiomeric excess (ee) in catalysis[70].

Besides those aromatic bisphosphines containing chiral backbone, there are also aliphatic bisphosphines that are used in enantioselective hydrogenation. The discovery of aliphatic bisphosphines with the phosphonane unit is the main breakthrough after the finding of BINAP. These catalysts in general are highly enantioselective[71].

3.1.2 Mass Transfer: Diffusion and Convection[72]

Mass transfer means the net movement of one mass from one location to another. This phrase is usually used in chemical engineering for physical processes in which chemicals transfer through diffusion or convection. Mass transfer is an important field of study in engineering as this is often the slowest step, the rate-determining step, in a reaction. Now, if the reaction being monitored involves a heterogeneous reagent and the reaction situation is not good for the mass transfer, such as small contact area or poor mixing, the mass transfer will be an issue distorting our picture of the reaction.

Diffusion is the transfer of mass from one phase to the other due to concentration differences between those phases. Diffusion can be mainly classified into two types: molecular diffusion and eddy or turbulent diffusion. The former is merely dependent on the random movement of individual molecule. The latter is assisted by mechanical agitation to cause a turbulent motion.

According to Fick's first law of diffusion[73], the rate of diffusion is mostly dependent on the concentration gradient, as described in the equation below:

$$J_A = -D_{AB}\left(\frac{\partial C_A}{\partial Z}\right)$$

in which the $J_A$is the molar flux in $mol \cdot m^{-2} \cdot s^{-1}$, and D_{AB} is the diffusion coefficient in $m^2 \cdot s^{-1}$ and $\frac{\partial C_A}{\partial Z}$ is the concentration gradient.

Convection, on the other hand, is the collective movement of a number of molecules within the fluids (gas or liquid). Convection can occur in a diffusion manner and mostly in an advection manner, in which the mass is transported in a much larger scale motion of current in the fluid[74].

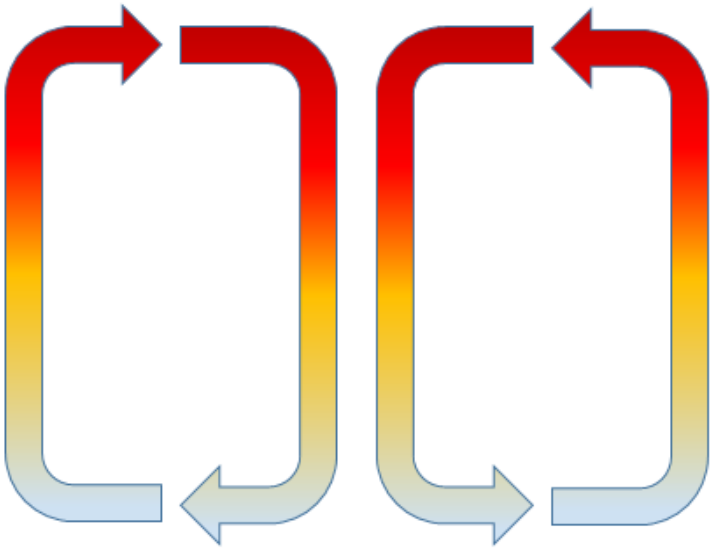

Figure 3.3. Convection

3.1.3 Charge-tagging

Even though ESI-MS is a powerful technique at monitoring organometallic reactions due to the advantages we discussed in the first chapter. However, there are many species and reactions that are not charged and therefore cannot be easily detected by the ESI-MS. To make them visible, there are various ionization pathways available. The first is protonation to form $[M + H]^+$or various cationizations such as $[M + Na]^+$, $[M + K]^+$

and $[M + NH_4]^+$ depends [75]. Transition metal halide complexes can become positively charged by losing the halide to form $[L_nMX_{m-1}]^+$. It is a popular and simple ionization pathway for halide complexes[76]. Complexes with acidic protons can also lose the proton to generate the anion $[M - H]^-$ to be detected in the negative mode of MS[77]. These ionization techniques, except the protonation, require certain electronic or composition properties, which limit their application for comprehensive usage. Inspired by the protonation, Henderson brought up the idea to use "electrospray friendly" phosphine ligands like P(p-$C_6H_4OMe)_3$ and P(p-$C_6H_4NMe)_3$ bind to the transition metals to increase the probability of protonation[78]. Our group has used the charged ligands to tag the catalysts[79]. The theory behind it is quite simple as below:

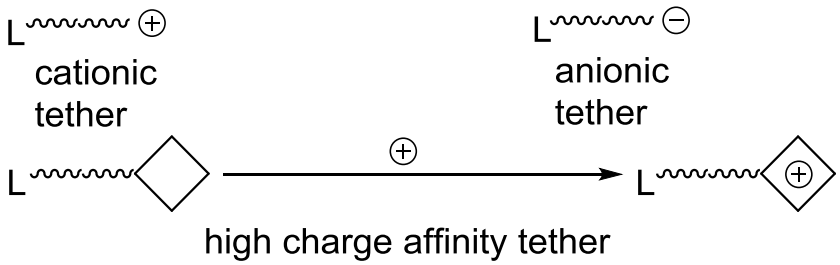

Scheme 3.6. Charge-tagging theory

To make the cationic tether, appending the charged groups like ammonium or phosphonium is challenging but plausible. The model is like $L - ER_3^+$ $(E = N\ or\ P, R = H, alkyl\ or\ aryl)$. The ligand is always phosphine ligand due to its innocence in catalysis. And the anionic tether is mostly made by direct sulfonation to provide $L - SO_3^+Na^-$. The last and most interesting strategy is to link the ligand with groups like crown ether, proton sponge or polyether. They are not charged themselves but have affinity and selectivity to charged species like alkali metal ions or proton.[80]

3.2 Results and Discussion

In the study, we systematically alternate the reaction situation of the hydrogenation of the charge-tagged alkyne.

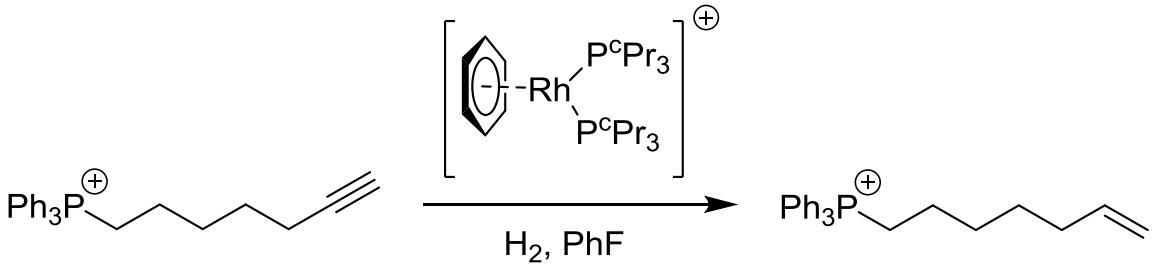

Firstly is the contact area. We specially designed 4 glass vials with doubling cross section from V1 to V4, in which V1 = 1.3 cm^2, V2 = 2.8 cm^2, V3 = 5.3 cm^2 and V4 = 10.8 cm^2. We choose these values because they matched standard glass tubing sizes. Secondly, we considered the stirring effect on the reaction rate. We set the stir rate at 240 rounds per minute as this is enough to stir efficiently but won't disturb the surface (usually reactions are stirred at over 500 rpm). Thirdly, the catalyst percent loading was increased from 10% to 20%. At last, the hydrogen partial pressure was also increased from 1.eq to 2.eq of H_2.

Table 3.1. Design information of the 4 vials

Vial#	V(ml)	S(cm^2)	D(cm)	L(cm)
1	20	1.3	1.3	17.0
2	20	2.8	1.9	7.5
3	20	5.3	2.6	3.8
4	20	10.8	3.7	1.9

The exact interfacial area was adjusted for the curved surface of the meniscus with the consideration of PEEK tubing's influence. The data below is from Dr. David Harrington.

Table 3.2. Interfacial area of the 4 vials

Vial #	Interfacial area/ cm^{-2}	Ratio
1	1.58	1.00
2	3.17	2.00
3	6.04	3.82
4	11.82	7.48

3.2.1 Contact Area Effect

When the reaction was under 10% catalyst loading, 1 equivalent of hydrogen and 240 rpm stir rate, the hydrogenation reaction rate in 4 vials was monitored separately. The results are shown in Figure 3.4. From V1 to V3, the reaction rate was obviously enhanced with the increasing contact area. While the contact area reached to V4, the reaction rate remained almost the same as that of V3. It is because when the contact area is below a certain value (between V3 to V4), the contact area is the main limiting factor, which explains why the reaction rate increases with the contact area. And when it reaches above that threshold contact area, then the reaction rate is merely controlled by the kinetics of the reaction itself. Therefore in the graph below the lines representing V3 and V4 overlap.

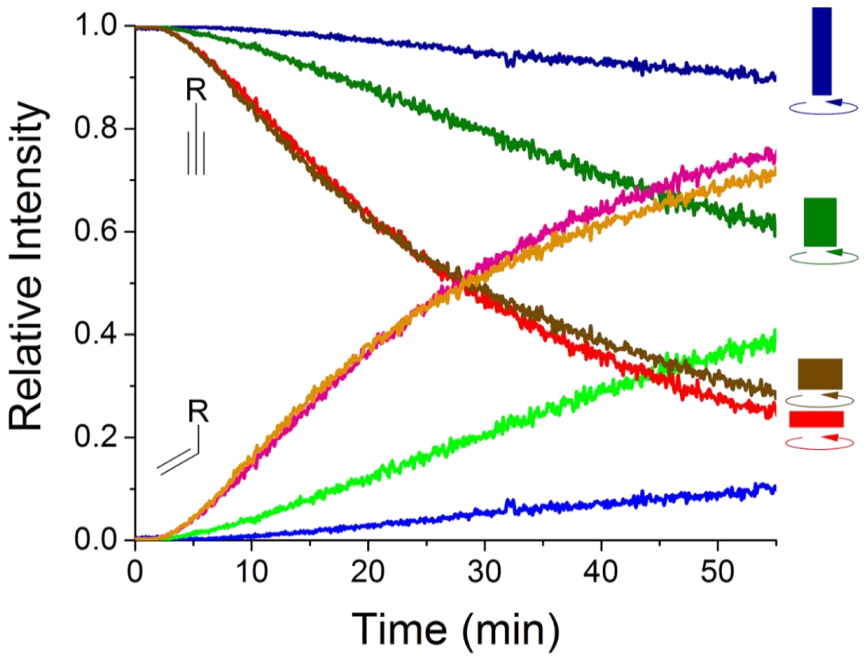

Figure 3.4. 10 % catalyst loading, 1.eq of H_2 and under stirring rate of 240 rounds per minute.

To find out the exact value of interfacial area above which the hydrogenation rate is transferred from under mass transfer control to under reaction kinetics control, the mechanism of the whole process needs to the considered as below:

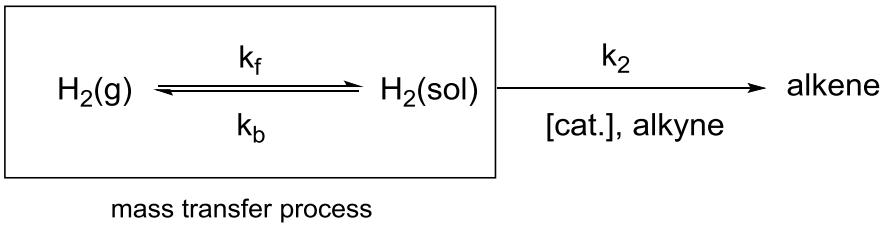

Figure 3.5. Mechanism involving the mass transfer as a reversible reaction at the beginning of reaction

According to the paper, the hydrogenation we were studying is at the first order to both the catalyst and hydrogen in the solution[81]. The rate law of the whole process can be inferred as below:

$$Rate = \frac{d[alkyne]}{dt} = k_2[cat.][H_{2(sol)}]$$

In steady state:

$$\frac{d[H_{2(sol)}]}{dt} = k_f[H_{2(g)}] - k_2[cat.][H_{2(sol)}] - k_b[H_{2(sol)}] = 0$$

Thus: $$[H_{2(sol)}] = \frac{k_f[H_{2(g)}]}{k_b + k_2[cat.]}$$

$$Rate = \frac{k_2[cat.]k_f[H_{2(g)}]}{k_b + k_2[cat.]}$$

When the reaction was under control of mass transfer, $k_2[cat.] \gg k_b$

$$Rate = k_f[H_{2(g)}]$$

In the mass-transfer process which is dependent on the interface area, the apparent rate constant k'_f and k'_b was used:

$K_f = k'_f A/V_g$

$K_b = k'_b A/V_l$

Where A is the interface area, V_g is the gaseous volume and V_l is the liquid volume.

In conclusion:

$$Rate = k'_f A/V_g [H_2(g)]$$

Based on this conclusion when the hydrogenation was run under mass transfer's control, the reaction rate should be linearly proportionally to the contact area until the process was transferred to under control of the reaction kinetics.

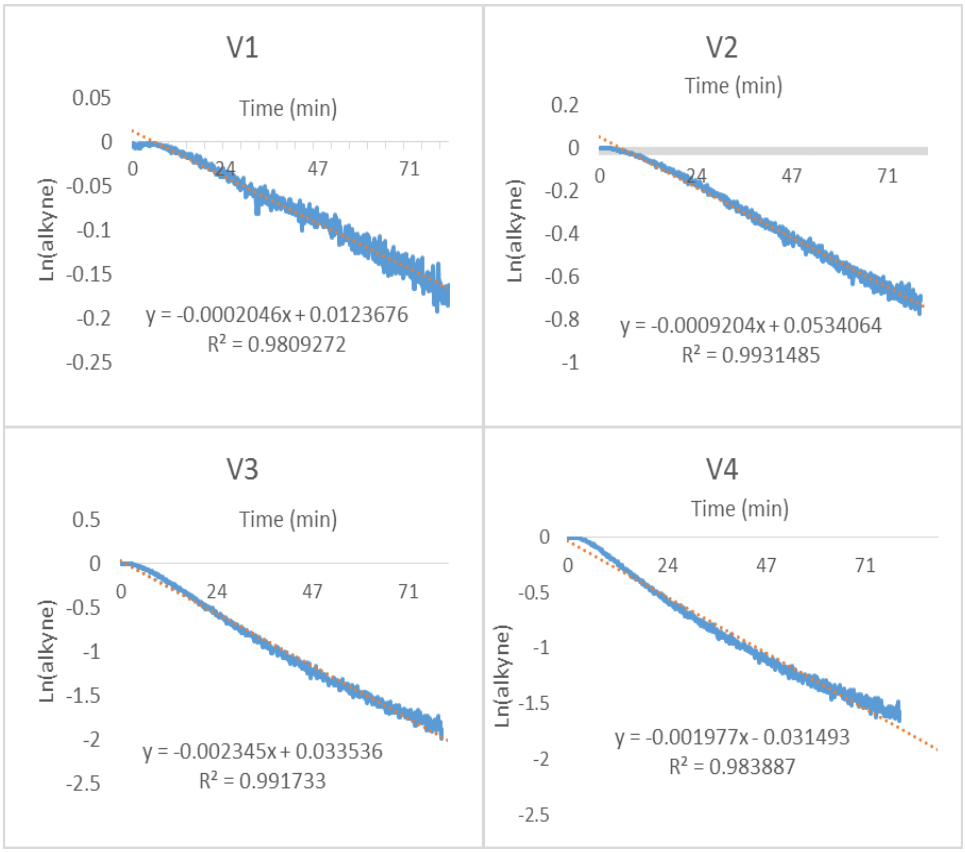

Figure 3.6. Reaction rate constants of the 4 hydrogenation in the 4 vials

The overlapping of V3 and V4 means that they were no longer under the control of the mass transfer. Thus the max overall reaction rate should be the average of the reaction rate of V3 and V4: k= (0.002345+0.001977)/2=0.002161 min^{-1}. The linear relationship between the reaction rate and the interfacial area is proved below:

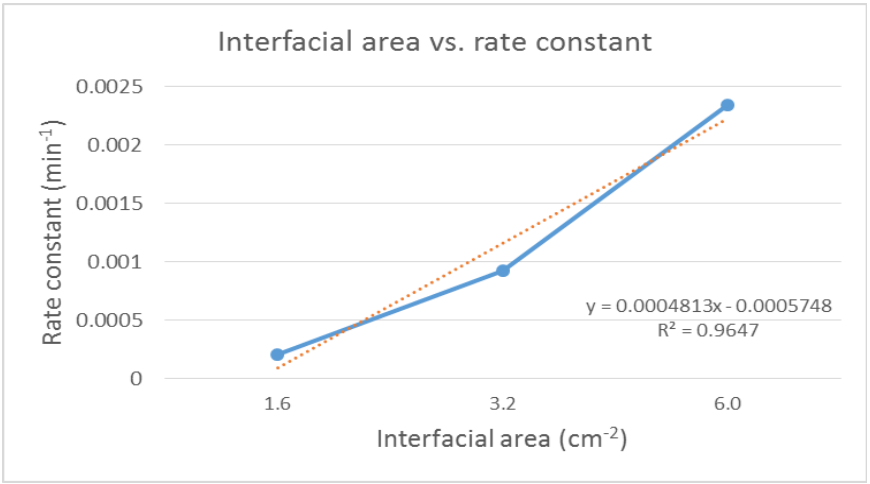

Figure 3.7. Linear relationship between interfacial area and reaction rate constant

When the reaction rate constant reaches to the 0.002161 min^{-1}, it is no longer under the control of the mass transfer, and the critical interfacial area is 5.68 cm^{-2}.

It is a different story when the reactions are run under the same circumstances but not stirred. When the contact area is below a certain number (somewhere between V2 and V3), stirring (or not) is the determining factor of mass transfer instead of the contact area. Therefore the reaction rate is mostly the same for V1 and V2. It was not until the contact area increased to V3 did contact area start taking over as the diffusion-limiting factor.

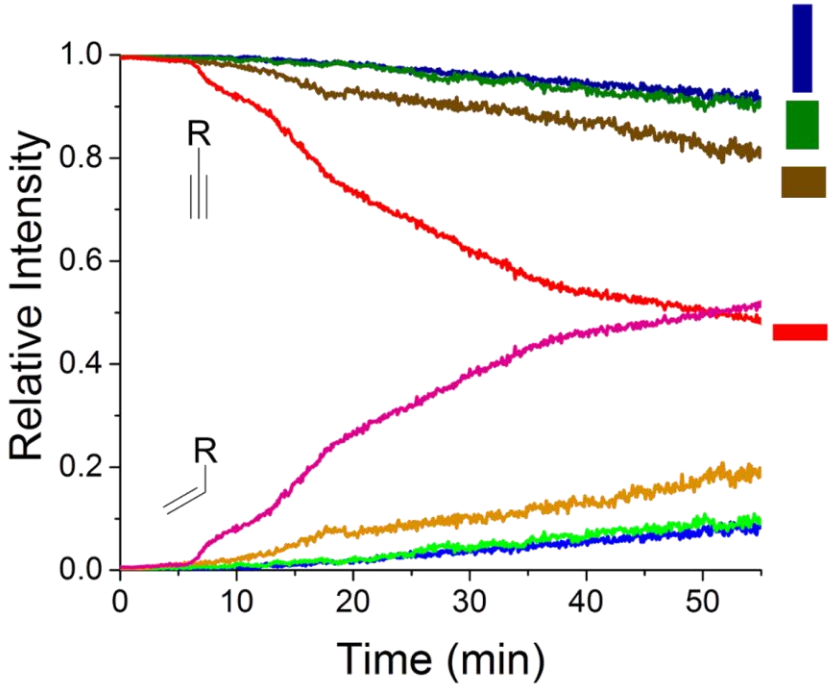

Figure 3.8. 10 % catalyst loading, 1.eq of H_2 and under stirring rate of 0 round per minute.

3.2.2 Stirring Effect

When the reactions were run under 10% catalyst loading and 1 eq. of hydrogen and the contact area was below a certain number of V2, the contact area is the turnover-limiting factor. So the hydrogenation rate of alkyne was almost the same in vial 1. Then from V2

to V3, the stirring effect starts acting as the limiting factor therefore the reaction rate was increased obviously by stirring. When the contact area being enlarged to V4, the limiting-factor is changed into the kinetics of the reaction itself, thus the stirring makes mostly no changes again on reaction rate.

Like the second graph below (Figure 3.10), we measured the reaction rate still under 10% catalyst loading but 2eq. of hydrogen in both stirring and non-stirring circumstances. We observed the same behavior as above. However, when the reacting solution was not mixed, we saw obvious disturbance from ideal behavior. And these unexpected phenomena were convection and will be explained in detail in the latter section.

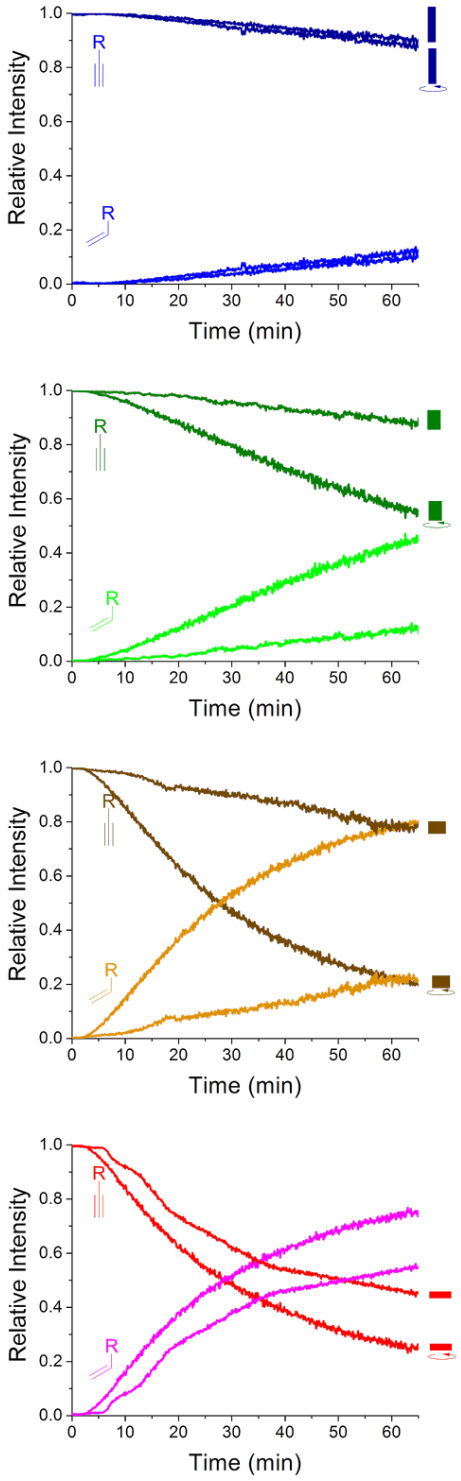

Figure 3.9. 10 % catalyst loading, 1.eq of H_2. Comparing reaction rate run under stirring or not in each vial.

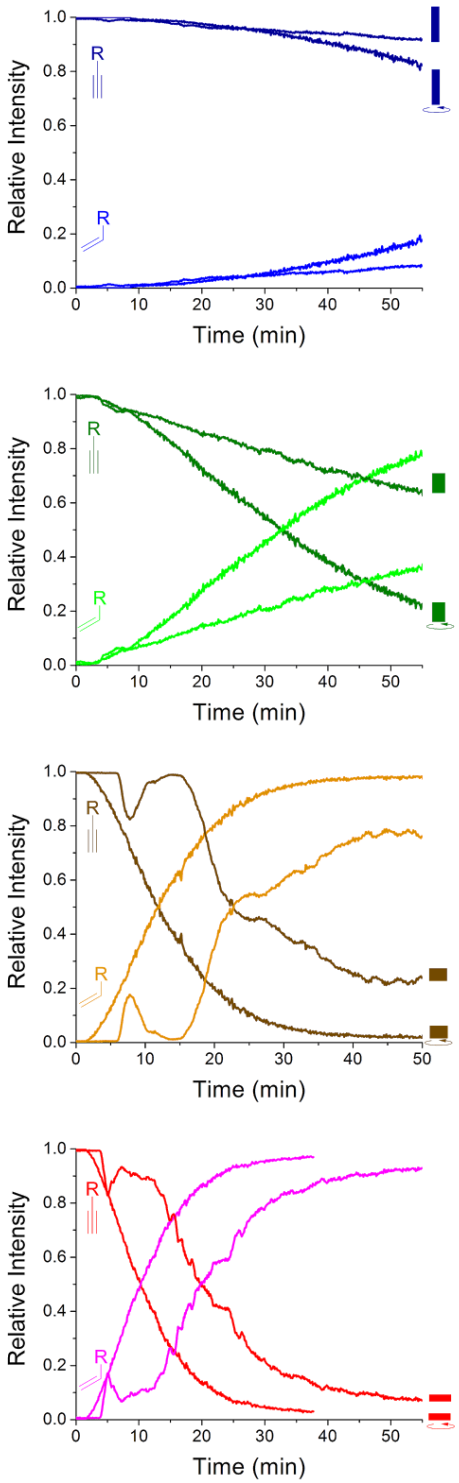

Figure 3.10. 10 % catalyst loading, 2.eq of H_2. Comparing reaction rate run under stirring or not in each vial.

3.2.3 Catalyst Loading Effect

When we increased the catalyst loading to 20%, the doubling of catalyst concentration failed to double the reaction rate until the contact area increased to V4. It is because when the contact area is below a certain value, somewhere around V3, the reaction rate is mainly controlled by the mass transfer. According to our calculation the threshold contact area is 5.68 cm^{-2} which is slightly below that of V3. Thus it may still be partially influenced by the mass transfer. And the reaction rate started being increased by the catalyst loading when the contact area enlarged to V4 under which the reaction kinetics started to take control.

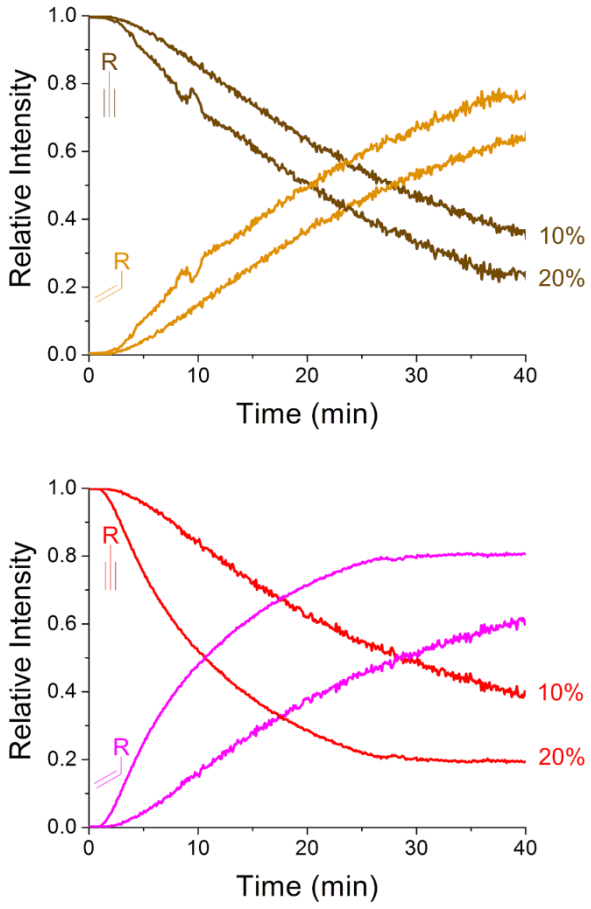

Figure 3.11. 10% vs. 20 % catalyst loading, 1.eq of H_2 in vial 3 and vial 4

3.2.4 Hydrogen Partial Pressure Effect

We then repeated the reactions using 2 equivalents of hydrogen under stirring. The reactions were consistently faster than their counterparts under only one equivalent of H_2. According to our discussion in 3.2.1, the hydrogenation is always at the first order to the hydrogenation under mass-transfer control or reaction-kinetics control. To prove this, the plots of natural logarithm of alkyne's concentration against time were provided.

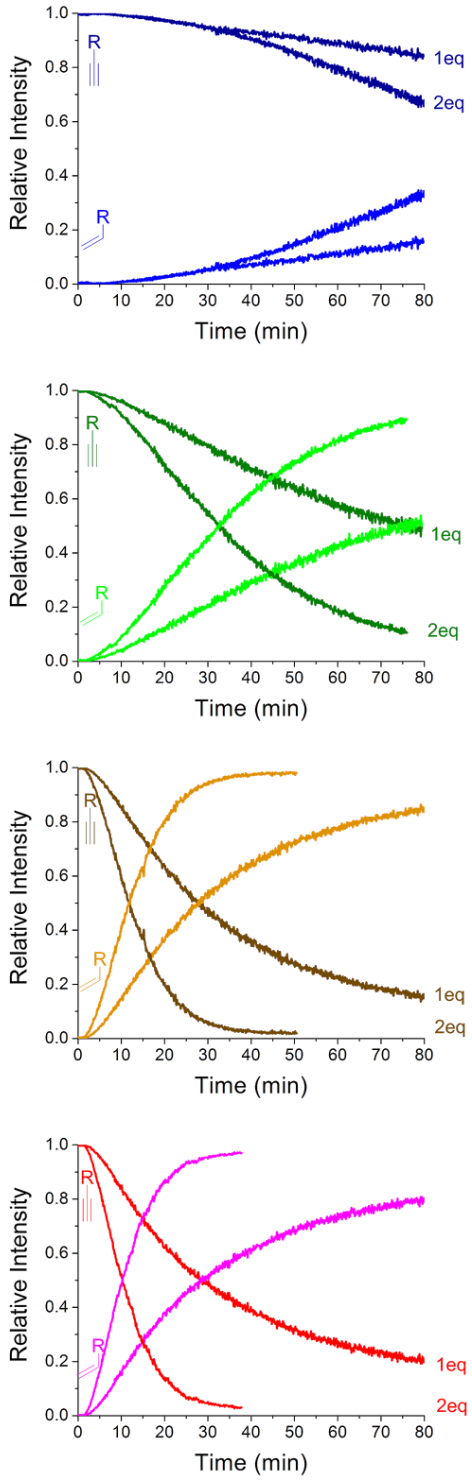

Figure 3.12. 1 eq. vs 2 eq. of H_2 under 10% catalyst loading and stirring

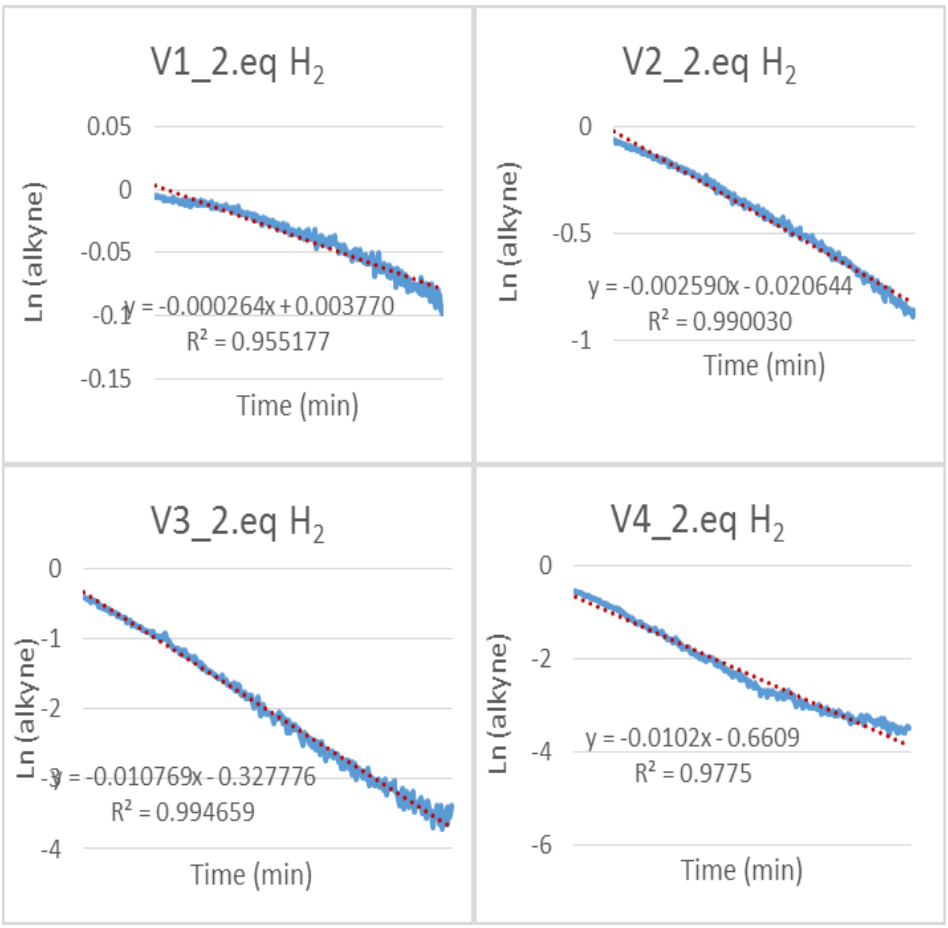

Figure 3.13. The linear relationship between the natural logarithm of alkyne and time

3.2.5 Convection

When the hydrogenation was run under 2 eq. of hydrogen and not stirred, the erratic and complex behaviour of reagents were observed (Figure 3.14). We think this is caused by the convection. The injected hydrogen will float above the solution in the vial and quickly hydrogenate the alkyne near the interface. The hydrogenation products can only move through the solution by convection induced by the exothermic reaction. Also this shows that the sampling method were merely examining a single point of the unstirred solution instead of the average of the whole. And it reveals the complex heterogeneity of the solution.

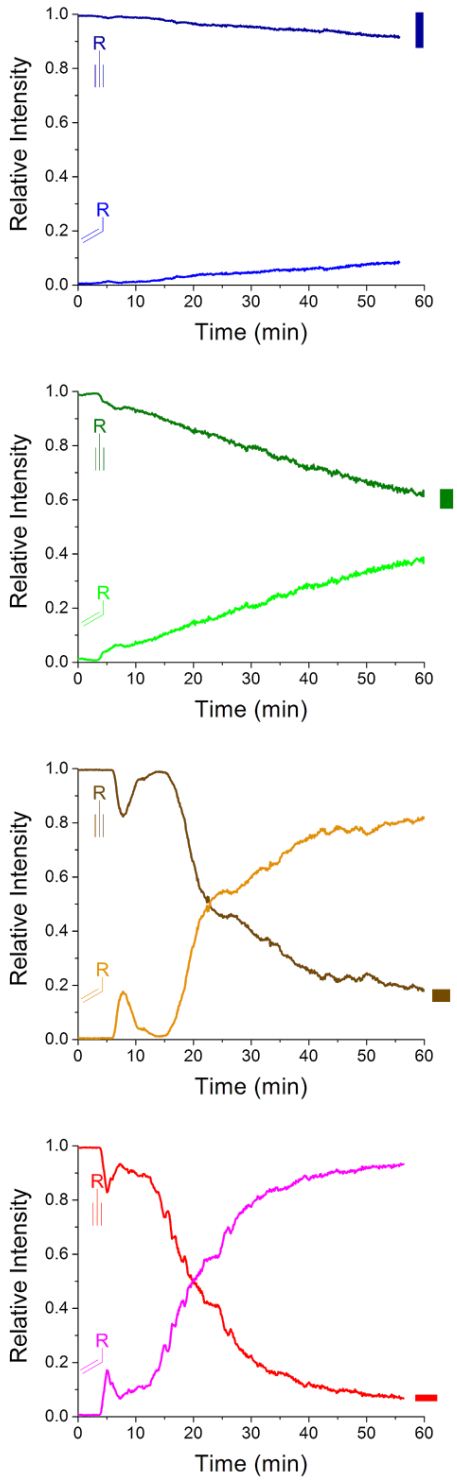

Figure 3.14. Hydrogenation under 2 eq. of hydrogen, 10% and unstirred.

3.3 Conclusion

In the study of reaction mechanism and kinetics, especially when with MS's real-time monitoring, it is important to avoid letting the reaction-rate be controlled by mass transfer. Thus good mixing and large enough contact area are necessary when the other heterogeneous reagent is in low concentration, making sure the reaction is limited by the reaction kinetics rather than the mass-transfer. In our study we find the critical interfacial area, 5.68 cm^{-2}, above which the reaction kinetics would take over as rate determining step. The stirring effect, the other determining factor in mass-transfer, also plays an important role at increasing the reaction rate even though the exact value for contact area when it starts taking over in mass transfer is not resolved in our study.

Also efficient stirring guarantees the sampling is examining the average of the whole complex system instead of a single point. Moreover, under some circumstances mentioned before poorly mixed reaction solution will result in significant convection effect and complicated discrepancy from the ideal behavior. And these are what need to be considered in the future when monitoring reaction in unstirred narrow reaction flasks, like 5 mm NMR tube.

3.4 Experimental

Fluorobenzene was freshly distilled from CaH_2 before use. All reactions were under argon atmosphere. Chemicals and solvents were purchased from Aldrich and used without subsequent purification. The charged alkyne was prepared by a previously published method[82]. The rhodium catalyst, $[Rh(P^cPr_3)_2(FPh)]^+[\ B\{3,5\text{-}(CF_3)_2C_6H_3\}_4]^-$ (P^cPr_3 = triscyclopropylphosphine, PhF = fluorobenzene) was prepared by the method of Goldman et al[83]. All mass spectra were collected by using a Micromass Q-Tof *micro*

mass spectrometer in positive ion mode using pneumatically assisted electrospray ionization: capillary voltage, 3000 V; extraction voltage, 0.5 V; Source temperature, 90°C; desolvation temperature, 180°C; cone gas flow, 100 L/h; desolvation gas flow, 100 L/h; collision voltage, 2 V (for MS experiments); MCP voltage, 2400 V.

A fluorobenzene solution (8.0-9.0 ml) of $[Ph_3P(CH_2)_4C_2H]^+[PF_6]^-$ (3.1 mg, 64.1 μmol was monitored using the PSI-ESI-MS setup. The vial was pressurized to 3 psi using 99.99% purity Argon gas. $[Rh(P^cPr_3)_2(FPh)]^+[BAr^F{}_4]^-$ (0.84 to 1.68 mg, 0.61 to 1.22 μmol, 10% to 20% catalyst loading) was dissolved in 1 to 2 mL of fluorobenzene and injected into the well-stirred vial via a septum. 1.4 ml of H_2 was injected via gas-tight syringe to start the reaction. The solution end of PEEK tubing was protected with a filter to avoid the tube being blocked by any insoluble by-products. Data were processed by normalizing the abundance of each species to the total ion count of all species identified as containing the tag. Data were gained every five seconds. The amount of hydrogen injected was doubled for the two equivalents reaction but no other setup changes were made.

4 Relative Binding Strength, Lability, and Propensity to C-H Activate of a Variety of Phosphine Ligands

Phosphines are among the most common ligands in homogeneous catalyst design as they enjoy remarkable electronic and steric tunability and can impart high regio-/stereo selectivity to the catalyst while remaining as spectator ligands. Synthesis of catalysts with phosphine ligands is generally via substitution and the activation of the catalyst often requires ligand dissociation. In both cases it is imperative to know the relative binding affinities of different ligands. Through the MS/MS studies of a series of systematically synthesized ruthenium complexes with three different phosphine ligands bound to Ru and by comparing the relative abundance of the three products after first fragmentation, it reveals relative binding affinities of different phosphine ligands. Also by monitoring the ligand substitution of positively charged ruthenium complex with MS, insights are gained into the mechanism of this process. An interesting finding in the study is that ligands like triphenylphosphine, usually regarded as the weak binding ligand, is retained even at high collision voltages, leading us to believe that C-H activation occurs at high energies to make the PPh_3 ligand ortho-metallate.

4.1 Introduction

4.1.1 Properties of Phosphine Ligands

The innate softness of phosphorus makes phosphine ligands able to form complexes with all the late transition metals. Also because of its softness, the substituents on the phosphorus have well-established and predictable influence on the electronic and steric properties of the ligand. This is a comparatively well-developed field of study as reviews

on transition metals and phosphine ligands date back to 1970s[84]. Due to the diverse range of substituents, phosphine ligands have a wide range of steric and electronic properties. Below are some representative mono- and bisphosphines:

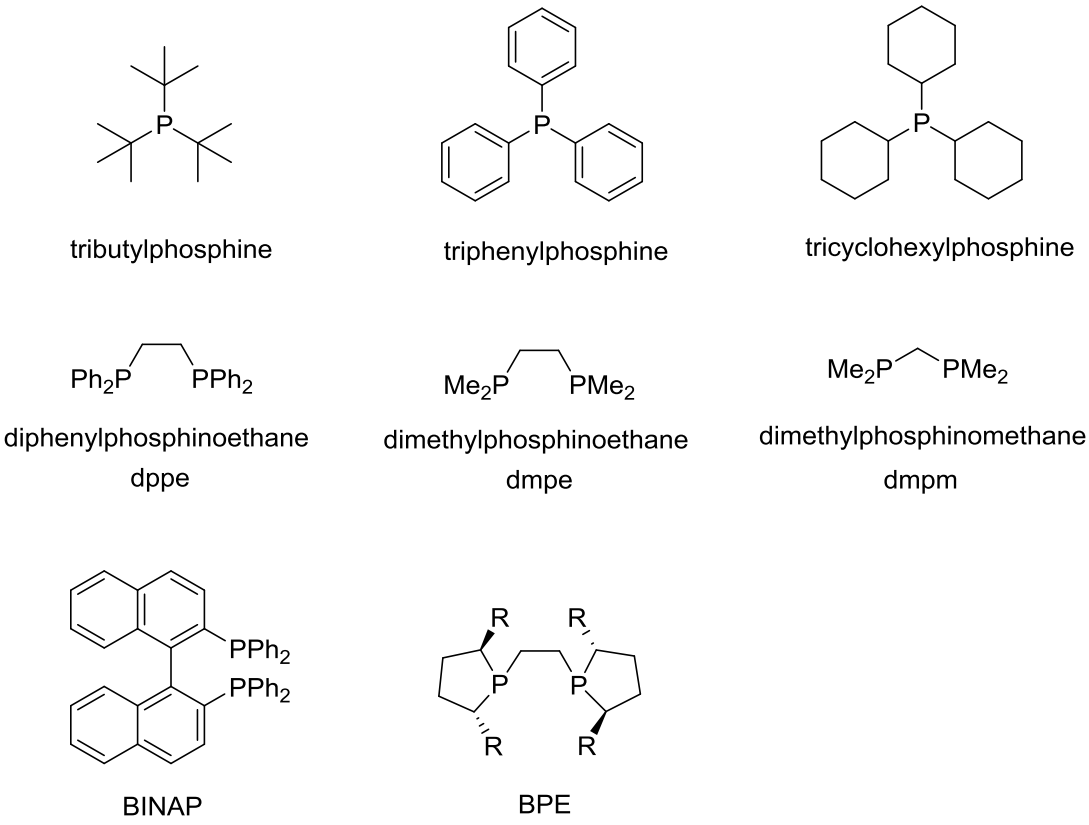

Figure 4.1. Representative phosphine ligands

As late transition metals in low oxidation states are also soft acids, they bind more strongly to the soft phosphorus than to nitrogen ligands. Also, the longer distance between phosphorus and the transition metal due to larger size of the phosphorus makes the steric influence from the substituents in phosphine ligands less critical than their analogous amines. Thus transition metals bind to tertiary phosphines more strongly than to the tertiary amines[85]

At the same time, phosphine ligands are more susceptible to be oxidized by oxygen in the air than amines. Therefore most electron-rich alkylphosphines are air-sensitive while

arylphosphines and phosphites are largely stable under air, especially in the solid state. The more sterically hindered the alkylphosphines, the less air sensitive they are[86].

The energy barrier for inversion at phosphorus in phosphines (29 to 35 kcal/mol) is much higher than that at nitrogen in amines (5.8 kcal/mol)[87]. So unlike amines, phosphines containing three different substituents are optically active and can be stored as enantiomers for a long time, explaining why chiral phosphine ligands are so vastly used in asymmetrical synthesis[88].

Like the CO ligand, phosphines are σ donors and π acceptors. The acceptor orbital is not the mere empty d orbital, but a hybrid one with the vacant 3d orbital and the σ^* orbital from P-R interaction with the latter one dominating[89]. This proposal was supported by structural data from complexes with the same phosphine ligands and geometry but different oxidation states. In complexes with higher oxidation states, the M-P bond was found longer and the P-R bond was found shorter[90]. It is because the transition metal with higher oxidation state has weaker electron back-donating capability to the P-R antibonding orbital.

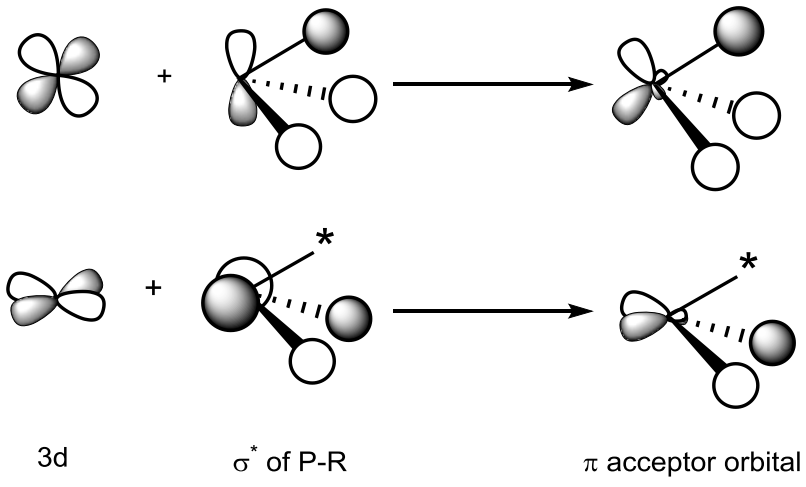

Figure 4.2. Modified version of π acceptance of phosphine ligands

The strength of the electron back-donating between transition metal and phosphine ligands largely depends on the electronegativity of the substituents on phosphorus as it determines the P-R antibonding orbital, σ^*. One computational study in 2007 revealed the relative π-accepting abilities of different phosphines to that of CO(Figure 4.3)[91].

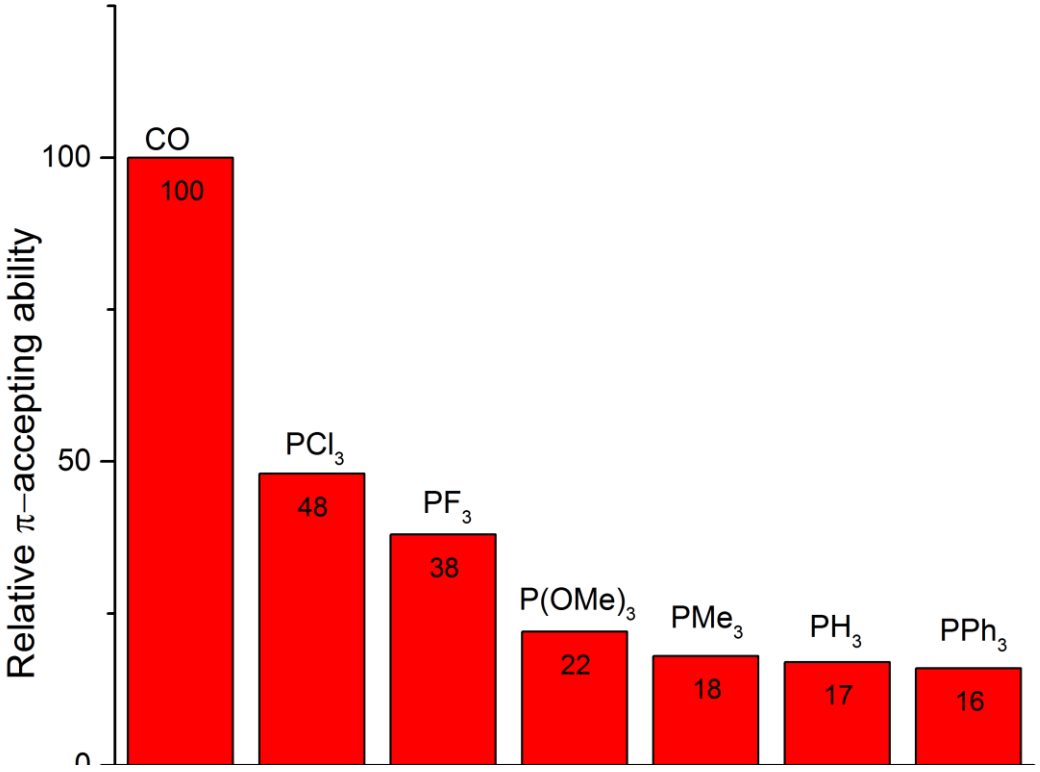

Figure 4.3. Relative π-accepting abilities of different phosphines to that of CO

Another famous approach to reveal electronic properties of phosphine ligands was done in the late 1960s by Dr. Tolman[92]. He measured the frequency of the most distinguishable CO band, v_{CO}, in the infrared spectra of $Ni(CO)_3L$ with different phosphine ligands. The value of v_{CO} reveals the degree of electron back-donating to the CO, which depends on the electron density on the transition metal. Then the electron density is determined by the electron donating ability of the phosphine ligand. In a word, the higher the value of v_{CO}, the weaker the phosphine ligand is at electron donating.

Table 4.1. Values for $Ni(CO)_3L$ with different phosphine ligands*

L	ν_{CO} (cm^{-1})
P^tBu_3	2056
PCy_3	2056
PMe_3	2064
$P(C_6H_4\text{-}4\text{-}OMe)_3$	2066
PPh_3	2069
$P(OMe)_3$	2079
$P(OPh)_3$	2085

*Source from the Tolman, C. A. *Chem. Rev* **1977**, *77*, 313.

Steric properties are also important as the bulkier the ligand, the faster it will dissociate from the metal center. Tolman again contributed to this by bringing up the idea of "cone angle"[84]. The cone angle, represented by θ and as shown by the graph below, is the angle of the cone that encompassed the outermost atoms of the ligand when the phosphorus atom being set at a constant distance away from the transition metal. This definition helped to explain numerous reactivity differences among phosphine ligands, especially before the computational modeling. There are two main limitations of this idea. Firstly, this cone angle is mostly used for symmetric phosphine ligands not the asymmetric ones. Secondly, this idea was based on the assumption that the cone angle of the phosphine ligand is the same as that under its free state, which is not true. The cone angle of the ligand is obviously dependent on its conformation that is variant depending on the complexes.

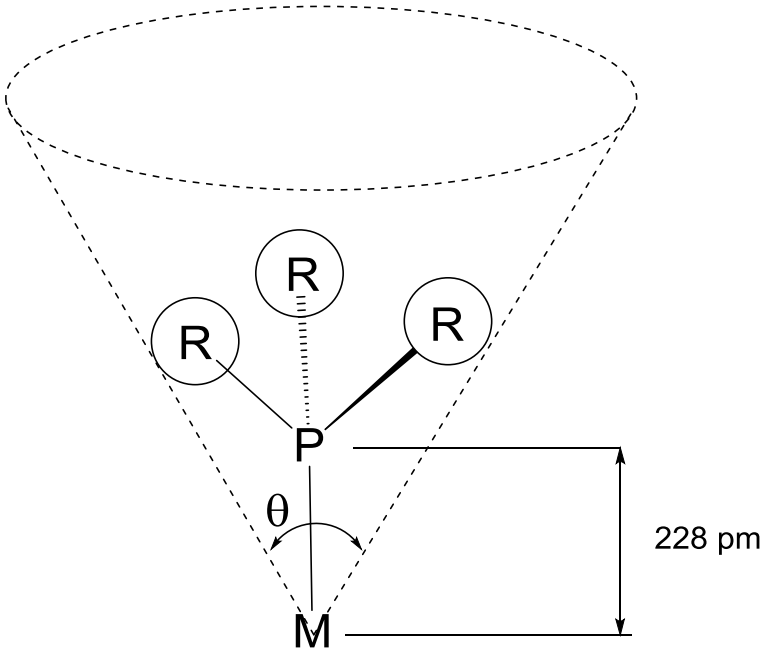

Figure 4.4. Tolman's cone angle

Also the table for common phosphine ligands' cone angle data is provided below:

Table 4.2. Phosphine ligands cone angles[84]

Phosphine ligands	Cone angle (°)
PH_3	87
$P(OMe)_3$	107
PMe_3	118
PMe_2Ph	122
PEt_3	132
PPh_3	145
$P(Bu^t)_3$	182
PCy_3	170
$PHPh_2$	128

4.1.2 Agostic Interactions[93]

Agostic interactions involve the C-H bond of the ligand coordinating to metal in an intramolecular fashion[94]. Agostic complexes are often observed for electrophilic, cationic metal center. The two main agostic interactions are α- and β-agostic interactions, latter of which is the most common one. These two interactions are also considered as intermediates in α-elimination.

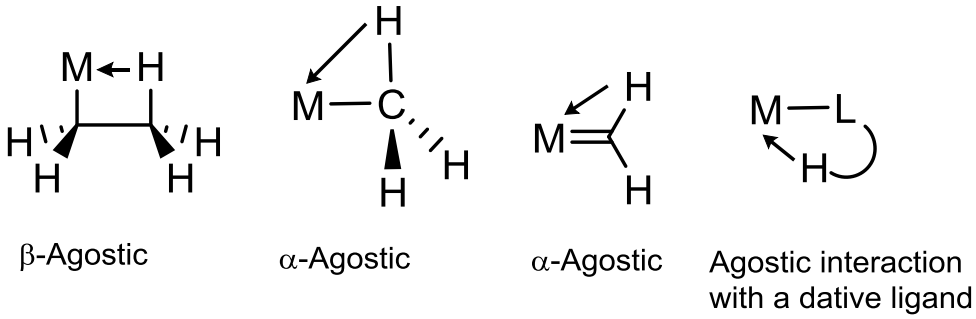

Figure 4.5. Four common agostic interactions

Graph below is the example of phosphine ligand involved in agostic interaction with ruthenium published 50 years ago[94].

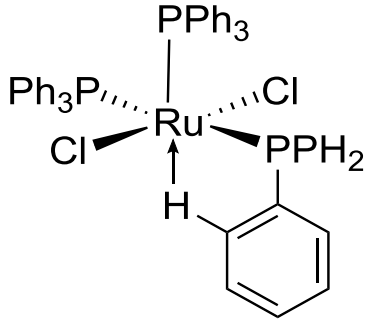

Figure 4.6. Agostic interaction between ruthenium and phosphine ligand

4.1.3 Substitution

Substitution in organometallic chemistry, like the equation below, involves a free ligand replacing a coordinated ligand from the complex[95]. And substitution is so common and important that it is present in almost every synthesis and catalysis cycle.

$$ML_x + L' \rightarrow ML_{x-1}L'$$

There exist typically three mechanisms to explain the substitution process: dissociative **(D)**, associative **(A)** and interchange **(I_A** or **I_D)**. In the associative substitution the first and slowest step is newly incoming ligand trying to bind with the complex, after which the replaced ligand come off. On the other hand, in the dissociative substitution the first and slowest step is the cleavage of the departing ligand. These two mechanisms share a lot of similarities with the S_N1 and S_N2, the nucleophilic substitution mechanisms in organic chemistry.

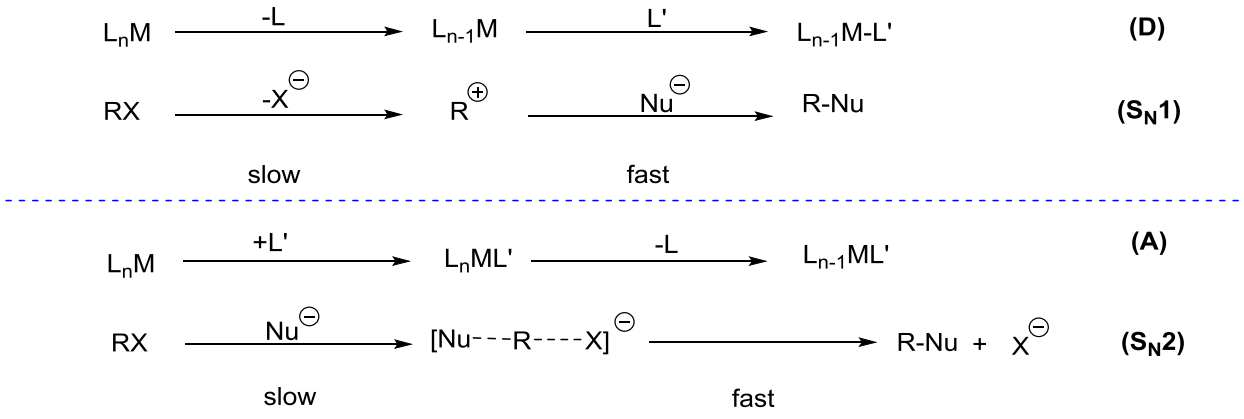

Scheme 4.1. Similarities between dissociative substitution and S_N1, associative substitution and S_N2

The difference between the associative and dissociative substitution is quite obvious, especially the first rate-determining step. Like for the associative mechanism, the coordinatively unsaturated 16-electron complex will coordinate with the free dative ligand at first to form an 18-electron stable complex. And this is the slowest and rate-determining step for associative substitution. Moreover, this process determines the overall substitution rate is at the first order of the incoming ligand. The more basic the entering ligand is, the faster the rate is. Also the reaction rate is not or only slightly

affected by the leaving ligand. To provide a better understanding of the difference between these two mechanisms, a graph listing all the difference in each aspect is below:

	Associative mechanisms	Dissociative mechanisms
Types of complex	16-e$^-$ and 17e$^-$ complexes	18-e$^-$ complexes
Rate law	First order of entering ligand	typically zero order of entering ligand
Electronic effects	Ligand: Favored for more basic entering ligands Metal: Favored for more electrophilic metal centers	Not easily affected by the coming ligand
Effect of departing ligand	Slightly affected by the departing ligand	Strongly dependent on the departing ligand
Steric effects	Favored for sterically accessible metal centers	Favored for sterically hindered metal centers

Figure 4.7. Main difference between associative and dissociative mechanisms of substitution

The two terms “associative substitution” and “dissociative substitution” refer to the states at the extreme in which the intermediate in transition state is predominately formed either by establishing a bond between the transition metal and the coming ligand or by the cleavage of the departing ligand from the metal center. In the situation when both transition states exist, the term “interchange” is used. And when the intermediate is mainly produced by the leaving of the original ligand it is called dissociative interchange, I_D. Or the other way around, when the transition state is mainly produced by the binding between the incoming ligand and the complex, it is called associative interchange, I_A.

The rate law of associative substitution can be described below. According to ^{14}C-labeled experiments, the observed reaction rate consists of two parts[96]. K_1 represents the solvent-assisted pathway. It is common in associative substitution that the solvent joins the reaction process by replacing the departing ligand of the original complex. The second term corresponds to rate constant at the first order of the incoming ligand.

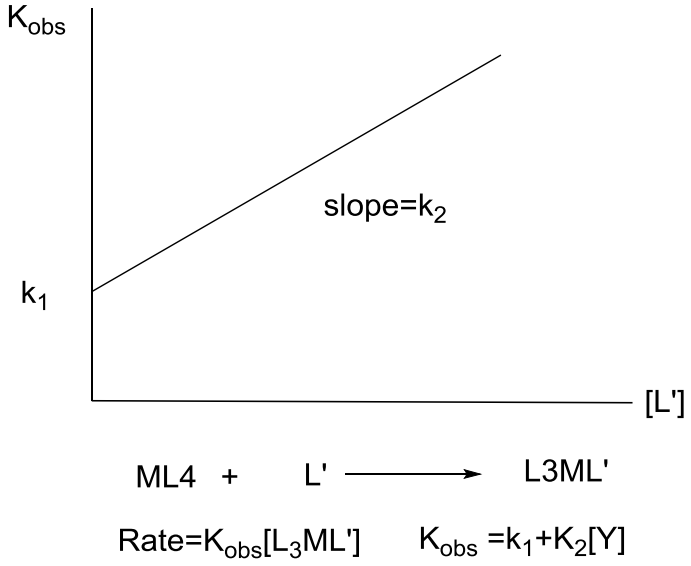

Figure 4.8. Rate law for associative substitution

The rate law of the dissociative substitution is described below. This pathway occurs initially by the cleavage of the departing ligand, which is competing with the re-addition of the departing ligand and finally reaches to equilibrium. Then the coordinatively unsaturated complex can bind with the new incoming ligand competitively with re-addition of departing ligand to the complex. Even though this difference in reaction rate in these two competing process can be small[97], a much higher concentration of the incoming ligand could make the reaction forward faster enough to ignore the reversion of the reaction back to the starting complex. At last, the simplified rate law of dissociative substitution tells us that the rate of the reaction is at the first order of the starting complex

under the circumstance that the concentration of the incoming ligand is a lot higher than the starting complex.

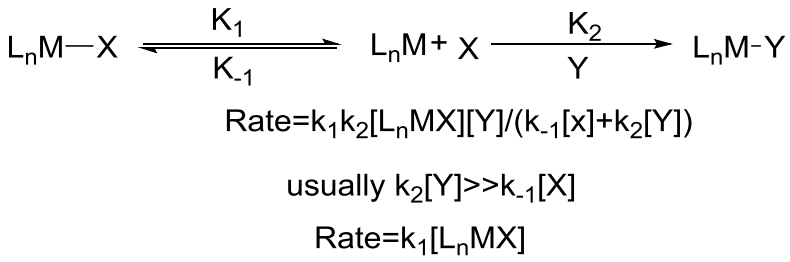

Scheme 4.2. Rate law for dissociative substitution

4.2 Results and Discussion

In this project we divided the experiments into three sections. The first one is studying the substitution reactions by monitoring the behavior of active species after adding new incoming ligands to the ruthenium complex.

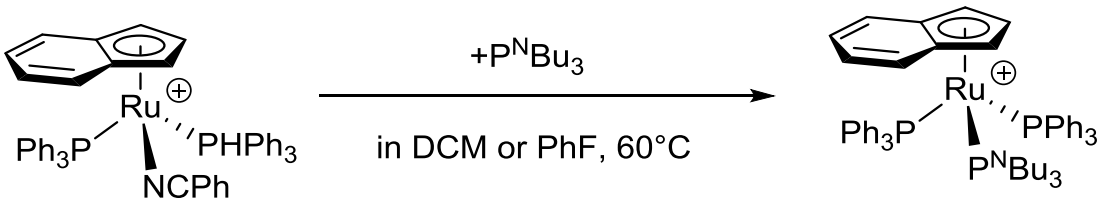

Equation 4.1. The ligand substitution reaction monitored for the first section

Also in the first section by adding two different phosphine ligand in equal amount to the ruthenium complex and comparing the relative intensity of the corresponding products, we can test the overall substituting capability of different phosphine ligands.

The next two sections of this project concern the MS/MS study of ruthenium complex with three or two phosphine ligands. By comparing the relative intensity of the product ions after fragmentation it reveals the relative binding affinity of the different phosphine ligands. Like the graph below there are three different products survived after the first

fragmentation of the ruthenium complex with three different phosphine ligands bound to it, losing one of each phosphine ligand. If the relative intensity of the red complex, losing phosphine ligand A, is the lowest of the three, it means that the ligand A binds to ruthenium most strongly as it is the hardest to lose. And vice versa, if the blue complex is the most abundant among the three, then the leaving ligand C is believed to be the weakest as it is the easiest to lose.

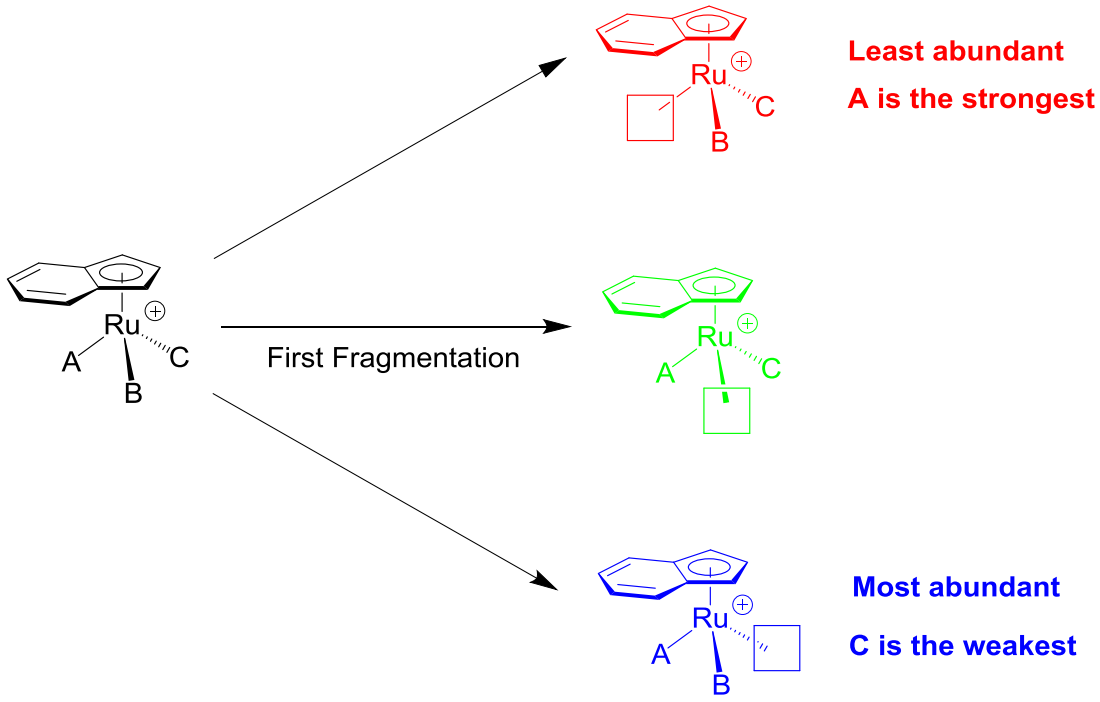

Figure 4.9. By comparing the relative abundance of the products of MS/MS experiments, the relative binding affinity of different phosphine ligands can be easily revealed.

The difference between the second and third section is that the former one studies the electron-saturated ruthenium complex with three phosphine ligands. However, in the third section we increased the cone voltage in the source of the mass spectrometer to dissociate one ligand from the ruthenium complex to pre-activate it prior to further analysis by MS/MS.

4.2.1 Competitive Substitution Mechanism between Two Phosphine Ligands

In the $[(indenyl)Ru(PPh_3)_2(PhCN)]^+$ dichloromethane solution, 10 equivalents of diphenylphosphine and diethylphosphine were added. The substitution process of these two phosphine ligands replacing the labile benzonitrile was finished within 10 minutes. And the relative intensities of the products, one with the PPh_2H replacing the benzonitrile and the other with the PEt_2H, are 0.40 and 0.58 respectively. It proves that the diethylphosphine is a better substituting ligand to the ruthenium complex than diphenylphosphine. It can be explained by the better σ-donating capability of the diethylphosphine. From the steric effect's point of view, the diphenylphosphine is bulkier than the diethylphosphine. Therefore it is harder for the diphenylphosphine to insert into the already crowded ruthenium complex with 2 triphenylphosphine ligands bound to it.

Another point to mention here is the appearance of the complex at *m/z* 782. It is assigned as the ruthenium complex with the acetonitrile replacing the benzonitrile. And this contamination is believed to happen during the preparation of the stock solution in the glove box or from the cross-contamination from previous users of the instrument, as it is such a common solvent used in the group. At the same time the MS is so sensitive that even trace amounts of acetonitrile in the sample can be detected.

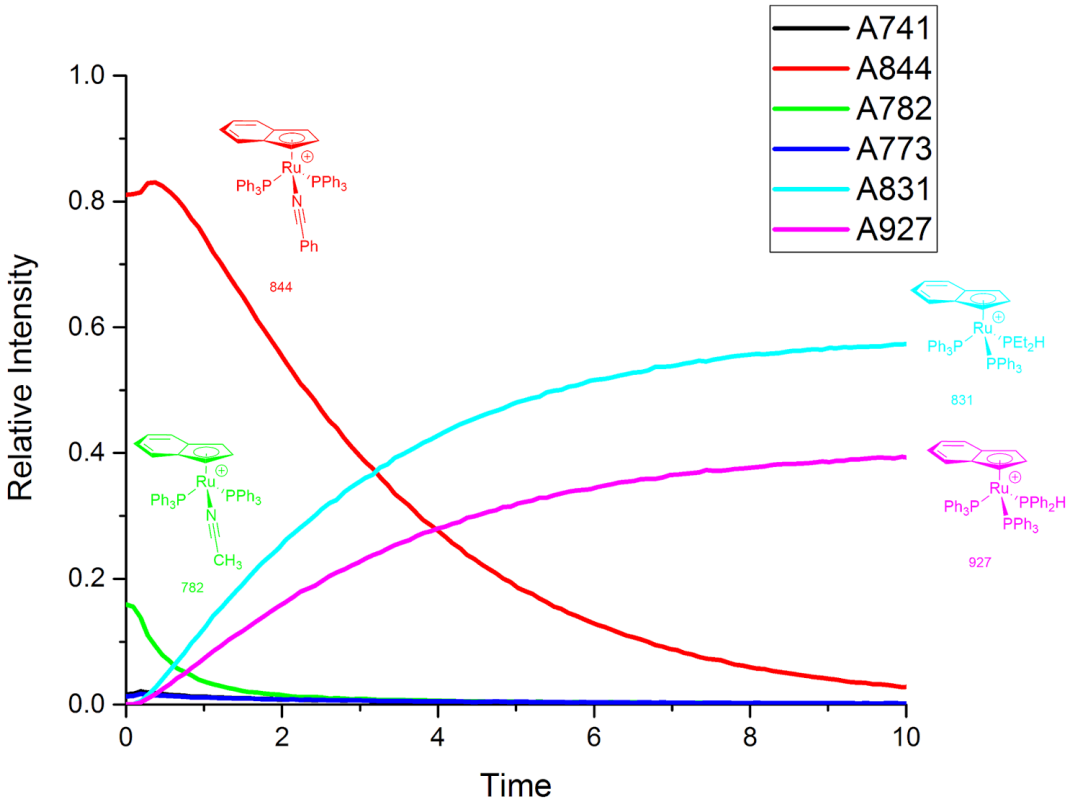

Figure 4.10. Substitution of ruthenium complex with PPh_2H and PEt_2H in 1:10:10 ratio. Average of 2 trials.

We then increased the amounts of the phosphine ligands from 10 equivalents to 100 equivalents to the ruthenium complex. When comparing the two graphs in 10 eq. and 100 eq. of phosphine ligands, there is no big difference. The substitution process still takes 10 minutes to go equilibrium and the relative intensity of both products are the same.

The independence of the reaction rate on the amount of the incoming ligands shows that the rate-determining step is the dissociation of the leaving ligand instead of the association the incoming ligand. The difference in relative intensity of those two products results from the different association rate of the two phosphine ligands to the ruthenium complex, which is a lot faster than the dissociation step. Overall, it shows that the mechanism of the substitution is dissociative at the first stage.

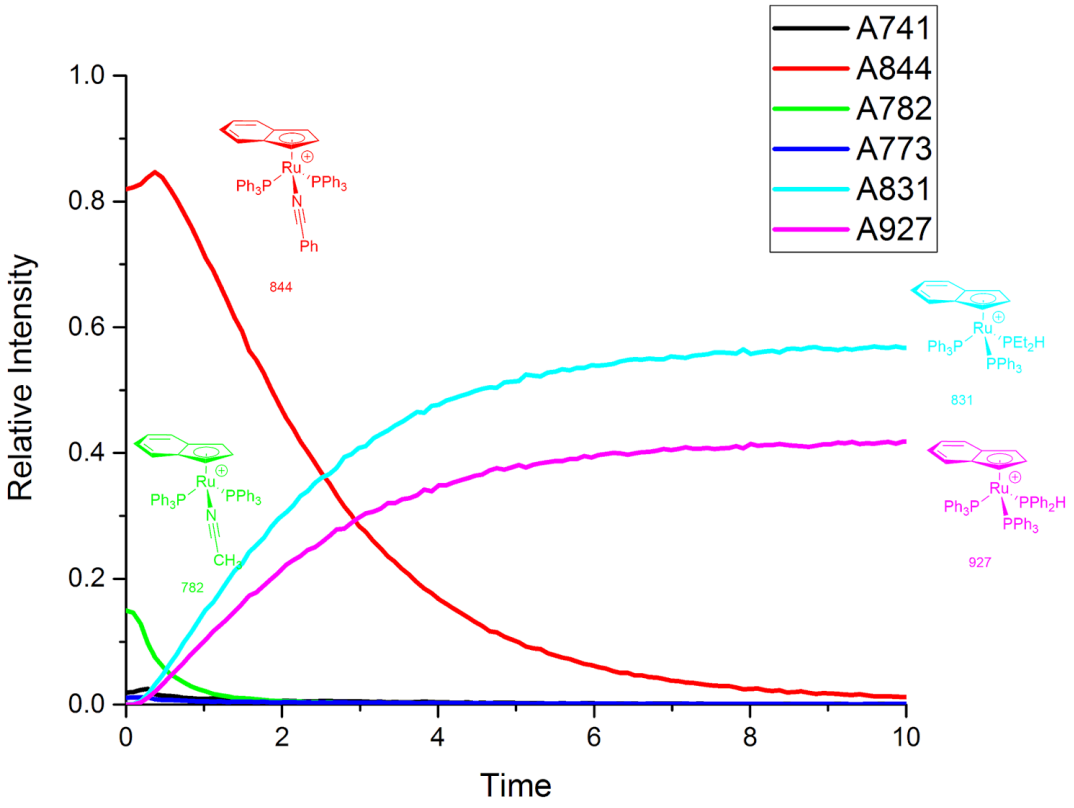

Figure 4.11. Substitution of ruthenium complex with PPh_2H and PEt_2H in 1:100:100 ratio. Average of 2 trials.

Based on the findings above we proposed a competitive dissociative substitution mechanism for the reaction adding two phosphine ligands to the ruthenium complex solution. Like the mechanism below, the first and slowest step is the benzonitrile dissociating from the ruthenium center. Then the two incoming phosphines will take up the vacant spot at different rate depending on the respective ligand's electric and steric properties, which results in the constant ratio of relative abundance between the two respective complexes.

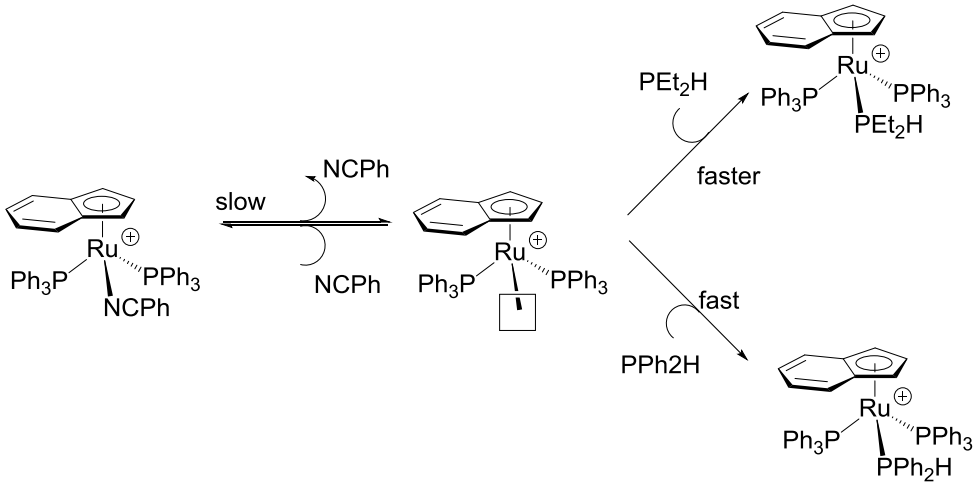

Scheme 4.3. Proposed dissociative mechanism for the competing ligand substitution

Later on we tested another two phosphine ligands, dicyclohexylphosphine and diphenylphosphine, in 10 equivalent amount to the ruthenium complex. As the graph below, the relative intensities of the two products, one with the diphenylphosphine replacing the benzonitrile and the other with the dicyclohexylphosphine, are 0.94 and 0.05. This big difference in relative intensity demonstrate an important role the steric effect plays here. Despite its strong electron-donating ability, the dicyclohexylphosphine is so bulky that it makes the ruthenium complex too sterically hindered to accommodate the PCy_2H.

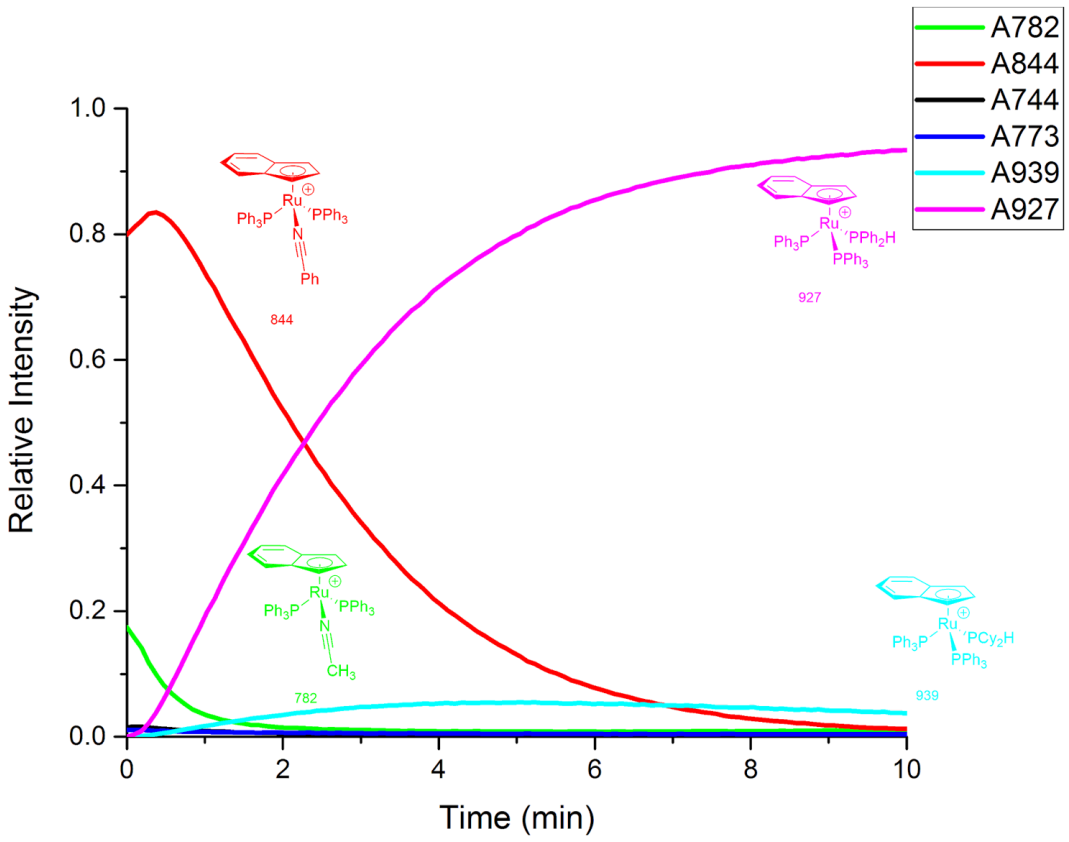

Figure 4.12. Substitution of ruthenium complex with PPh_2H and PCy_2H in 1:10:10 ratio. Average of 2 trials.

Overall, the three experiments above present the relative substituting ability of the three different secondary phosphine ligands. It is PEt_2H > PPh_2H >> PCy_2H to the ratio 27: 18: 1.

COPASI Modeling

To test this competitive dissociative substitution mechanism, we used COPASI, a biochemical network and dynamic analysis software, to model and simulate the process. Firstly, we plugged-in all the components (reagents, products, kinetic rates of the reaction) of our proposed reaction in the rigid biochemical compartments. Then the task of *Parameter Estimation* was employed to find out the best fit reaction rate for each step.

When comparing the estimated reaction rate constant of these two substitution steps, the same ratio of 3:2 between diethylphosphine and diphenylphosphine is observed again. It just confirms our proposal that in this competing dissociative substitution mechanism the relative abundance of the products is dependent on the rate of the phosphine taking up the vacant spot.

Thus the relative abundance of the products or the estimated rate constant can quantitatively reveal the competence of each phosphine ligand in substituting the leaving ligand from ruthenium complex.

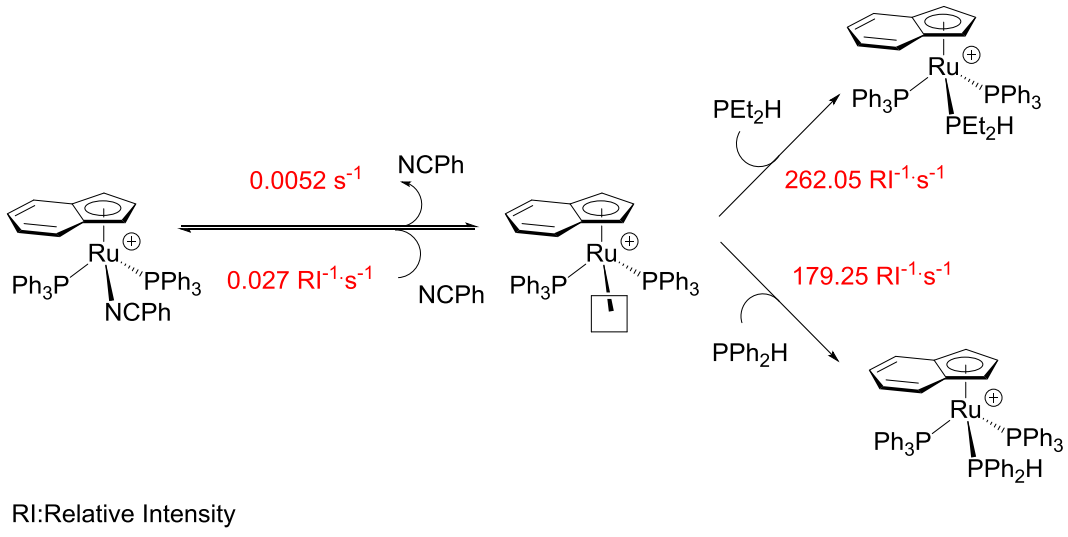

Figure 4.13. Results from the *Parameter Estimation*. The breakdown of the proposed competing dissociative substitution mechanism between PEt_2H and PPh_2H. The reaction rate constant for each step is highlighted in red.

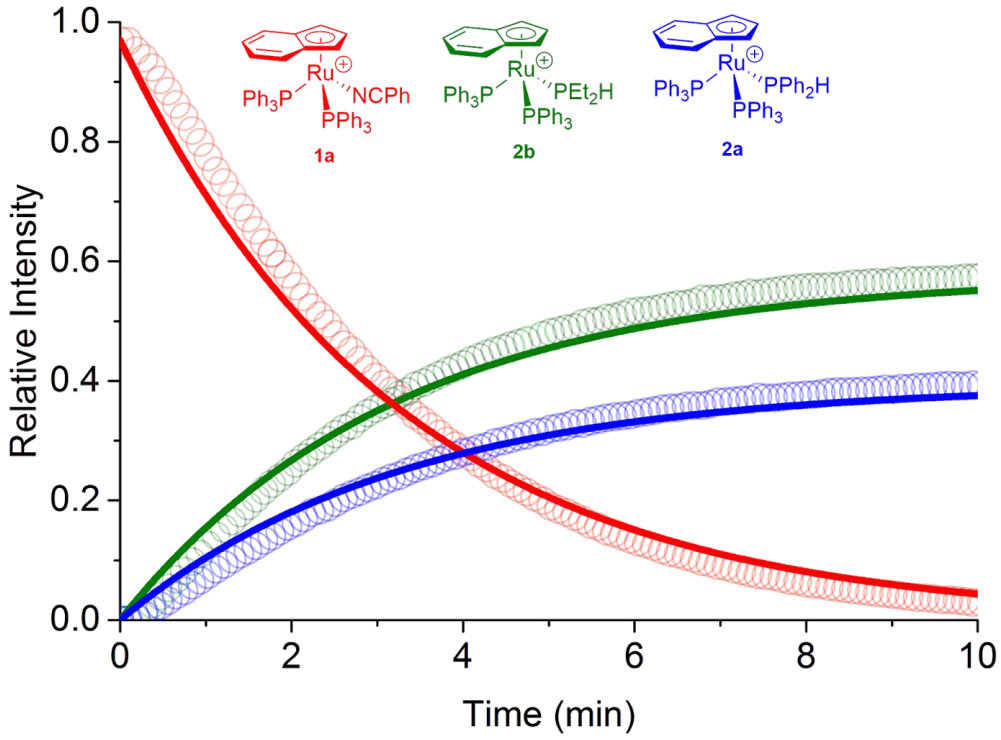

Figure 4.14. Experimental (circles) and simulated (lines) for the competiting substitution reaction PPh_2H (10 equivalents) and PEt_2H (10 equivalents). Parameter estimation conducted using COPASI.

To test the proposed mechanism again and the utility of this simulation, the same parameters were used to simulate the process with 100 equivalents of each incoming phosphine ligands. Again it fits well and supports our mechanism.

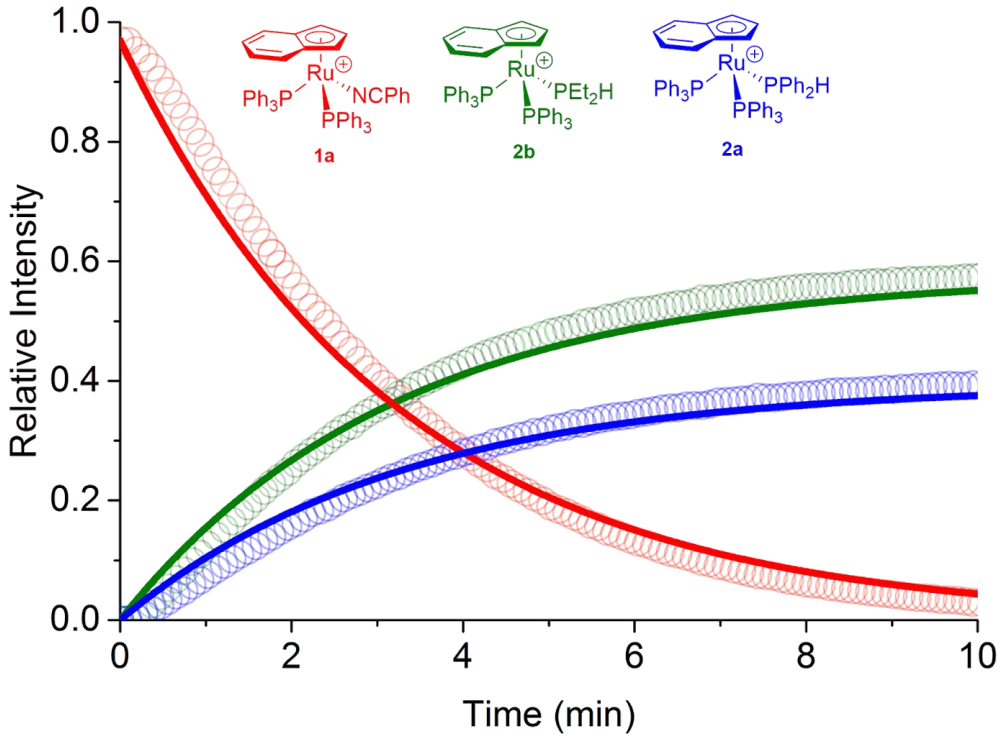

Figure 4.15. Experimental (circles) and simulated (lines) for the competiting substitution reaction PPh_2H (100 equivalents) and PEt_2H (100 equivalents). Parameter estimation conducted using COPASI.

The same procedure was conducted to simulate and model the competing substitution reaction between the ruthenium complexes with the PPh_2H and PCy_2H (10 equivalents each). From the estimated rate constant of the two substitution step we can tell the substitution competence between dicyclohexylphosphine and diphenylphosphine is 0.0026 to 0.046 or 1:18 when normalised to 1.

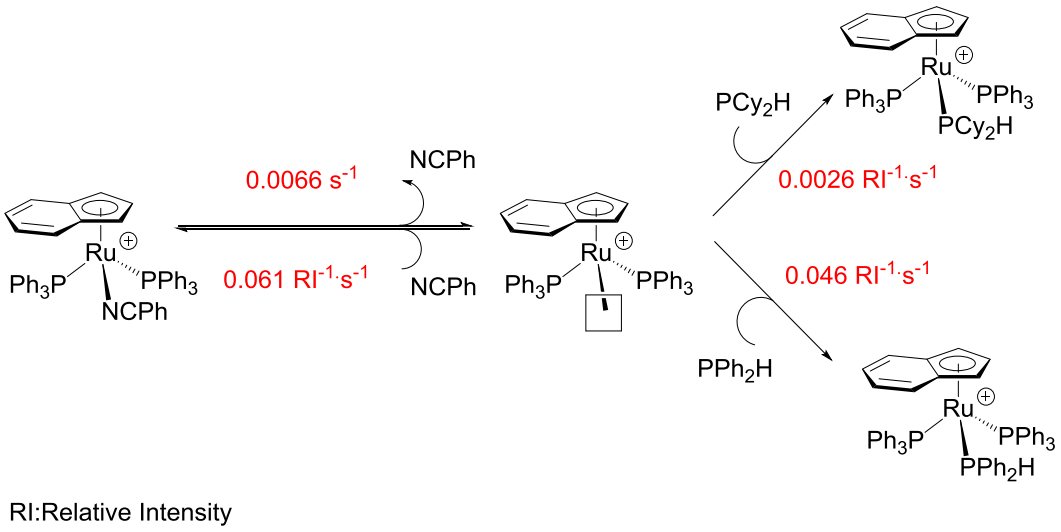

Figure 4.16. The breakdown of the proposed competing dissociative substitution mechanism between PCy_2H and PPh_2H. The reaction rate constant for each step is highlighted in red.

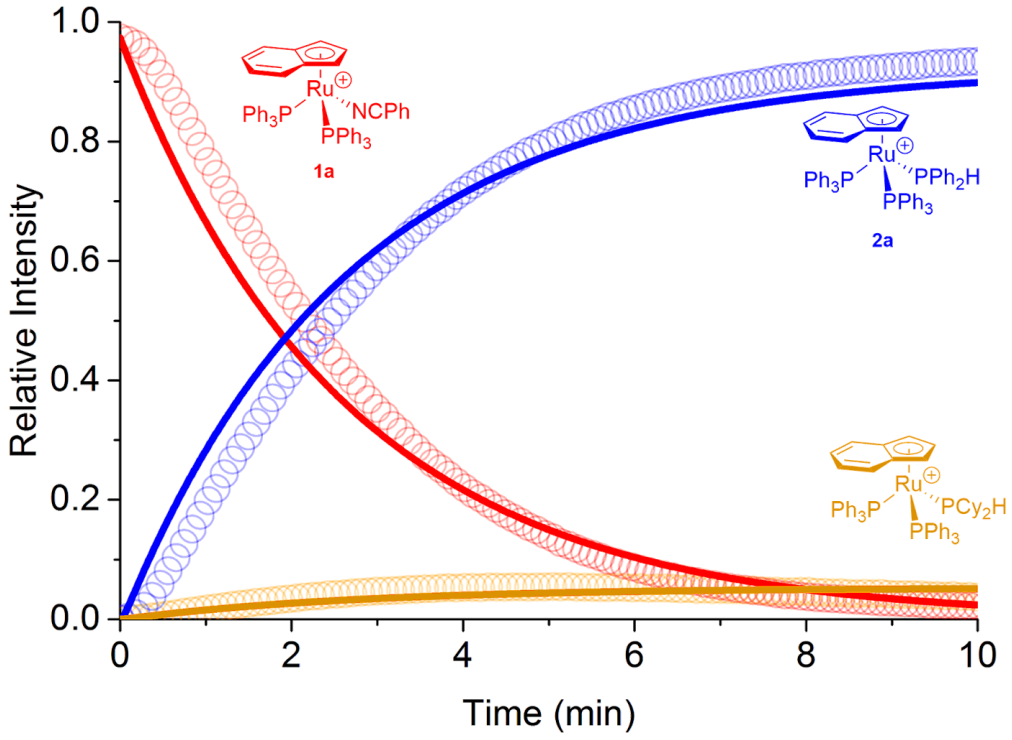

Figure 4.17. Experimental (circles) and simulated (lines) for the competiting substitution reaction PPh_2H (10 equivalents) and PEt_2H (10 equivalents). Parameter estimation conducted using COPASI.

In conclusion, from the competing substitution reaction between two phosphine ligands, we can easily tell the substitution competence of phosphine ligand by simply comparing the relative abundance of respective products or the relative estimated rate constant of respective substitution steps. And the ratio of relative substitution competence of the three phosphine ligands tested above is PEt_2H: PPh_2H: PCy_2H=27:18:1.

4.2.2 Competitive Substitution Mechanism in Adding Single Phosphine Ligand

In daily organometallic synthesis a single phosphine is always added and usually the desired first or second substitution product cannot be achieved. To explore the substitution mechanism more deeply, we focused on the single tri-n-butylphosphine reacting with the ruthenium complex rather than two phosphine ligands competing with each other. The choice of the tri-n-butylphosphine is based on its compatible electron-donating ability and steric bulkiness.

Substitution reaction in the dichloromethane solution

Adding the tri-n-butylphosphine in different amounts (10eq, 50eq and 100eq) separately to the ruthenium complex in DCM solution results in similar behavior in both reagent and products. It further proves the dissociative substitution mentioned above. However there are two interesting findings that lead us to propose a more complex mechanism for the single phosphine ligand substitution situation.

Firstly the expected product (*m/z* 943), the ruthenium complex with only one tri-n-butylphosphine replacing the benzonitrile, is shown to be only an intermediate in the whole reaction. It is formed at the very beginning and will soon be consumed. Also at a larger scale, the secondary substitution product (m/z 883), the one with two tri-n-butylphosphines replacing both the benzonitrile and a triphenylphosphine, is formed over

the reaction. This means that it is thermodynamically favored for the better substituting phosphine ligand (higher electron-density and lower steric hindrance) to replace all the unfavored ones as long as there is enough incoming ligands.

Secondly, the appearance of the ruthenium complex with the incoming P^NBu_3 replacing one triphenylphosphine (*m/z* 784) instead of the benzonitrile is out of our expectation. Initially we thought it the product from the first substitution, which is counterintuitive as benzonitrile is a lot more labile than the triphenylphosphine. Thus it could only be the product from the other parallel reactions such as secondary substitution.

However, when running this substitution in dichloromethane we found the linear increase of the ruthenium complex at *m/z* 967. According to this linear behavior we can be reasonably sure it is a decomposition product. The isotope pattern matches with the empirical formula for $[(\text{indenyl})Ru(PBu_3)_2(PPh_3)(CH_2Cl_2)]^+$. But the ion was insufficiently abundant for MS/MS studies, so we cannot comment on possible structures.

Another problematic issue brought up by using dichloromethane as solvent is that we could not get meaningful information from the 10 equivalents experiments. The unknown impurities got increasingly obvious when we scaled down to only use 10 equivalents of phosphine ligand to the ruthenium complex. It is a quite common issue for mass spectrometer users whose sample is already in a scale from mM to nM. Even traces amount of impurities can distort the behavior of active species in catalysis especially when you are scaling down your experiment but the impurity in the solvent remained the same.

All of these led us to use fluorobenzene as the solvent.

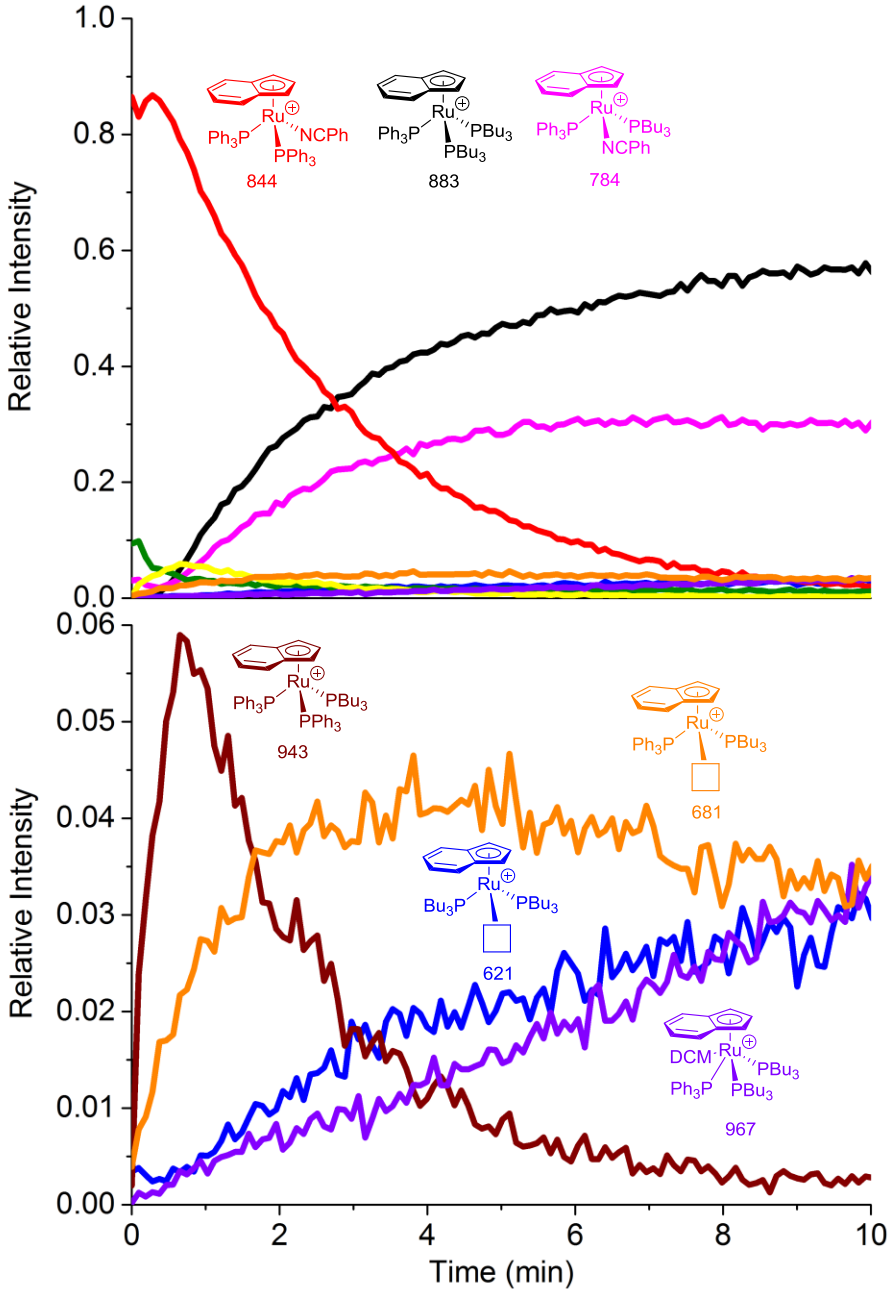

Figure 4.18. 100 eq. of tri-n-butylphosphine substitution in DCM

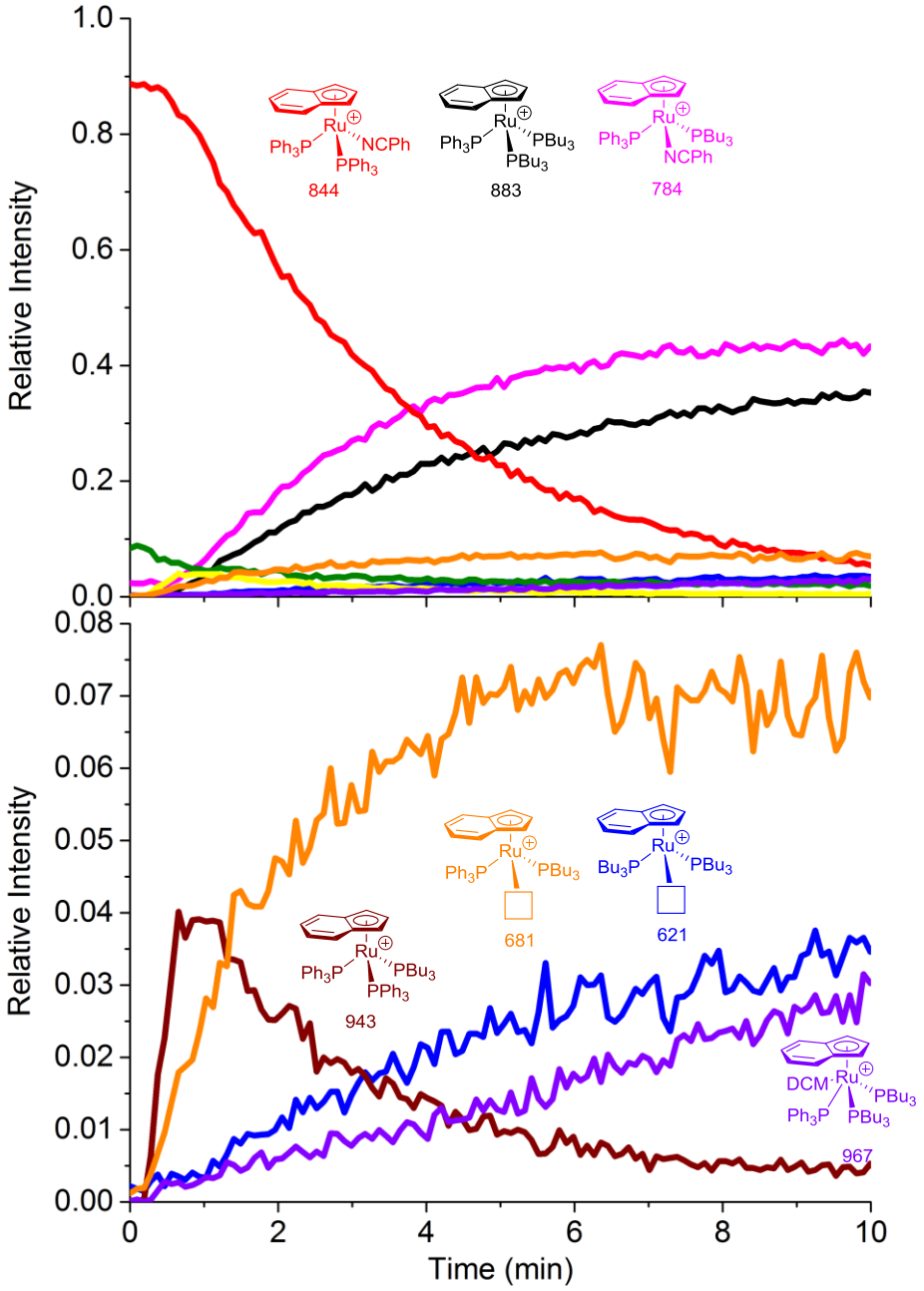

Figure 4.19. 50 eq. of tri-n-butylphosphine substitution in DCM

Summing up the findings mentioned above, we can still propose the mechanism for the tri-n-butylphosphine substitution below. The first step is the slow dissociation of the labile benzonitrile, after which the incoming ligand, tri-n-butylphosphine, will soon take up the vacancy in the complex. The next step involves the slow dissociation of the

triphenylphosphine from the first substitution product. Here the reason why the triphenylphosphine will dissociate is because of its higher steric hindrance and poor electron-donating ability. Then as there exists both benzonitrile and tri-n-butylphosphine in solution, a competing substitution occurs. As these two ligands each enjoy one advantage (benzonitrile has smaller steric hindrance and tri-n-butylphosphine is a better donor).

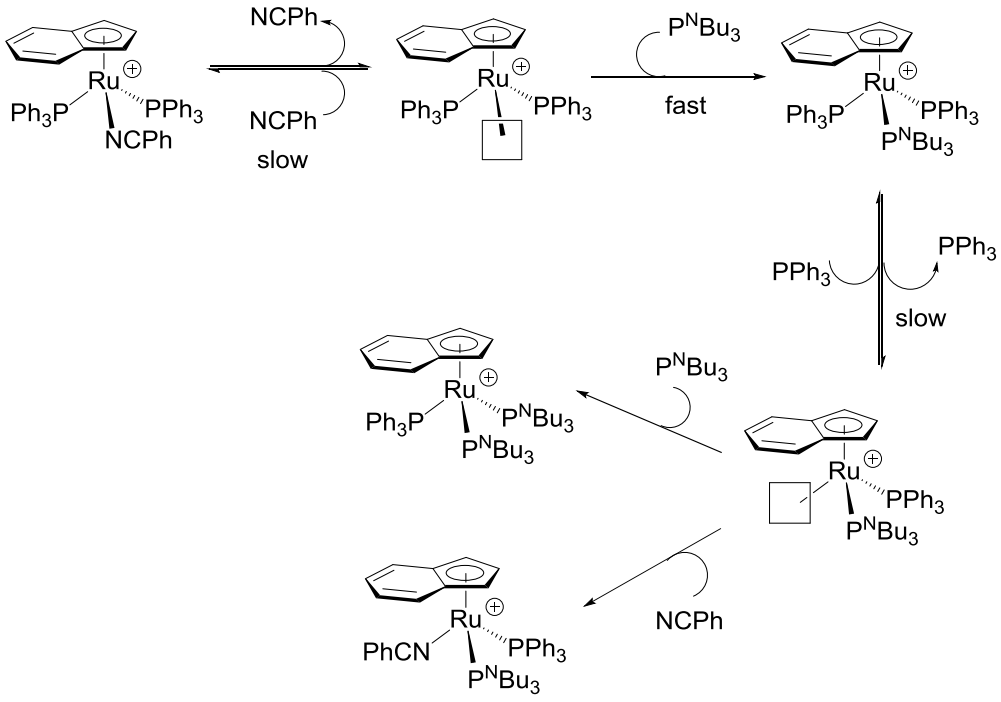

Scheme 4.4. Proposed mechanism for tri-n-butylphosphine substitution

Substitution reaction in the fluorobenzene solution with better results

As mentioned before to avoid the complication brought by the usage of DCM and to test the utility of this mechanism, we ran the tri-n-butylphosphine substitution in 100, 50 and 10 equivalents in fluorobenzene solution. Compared with the ones in DCM solution, a similar but clearer trend lines of all species are observed with neither impurities nor decomposition products.

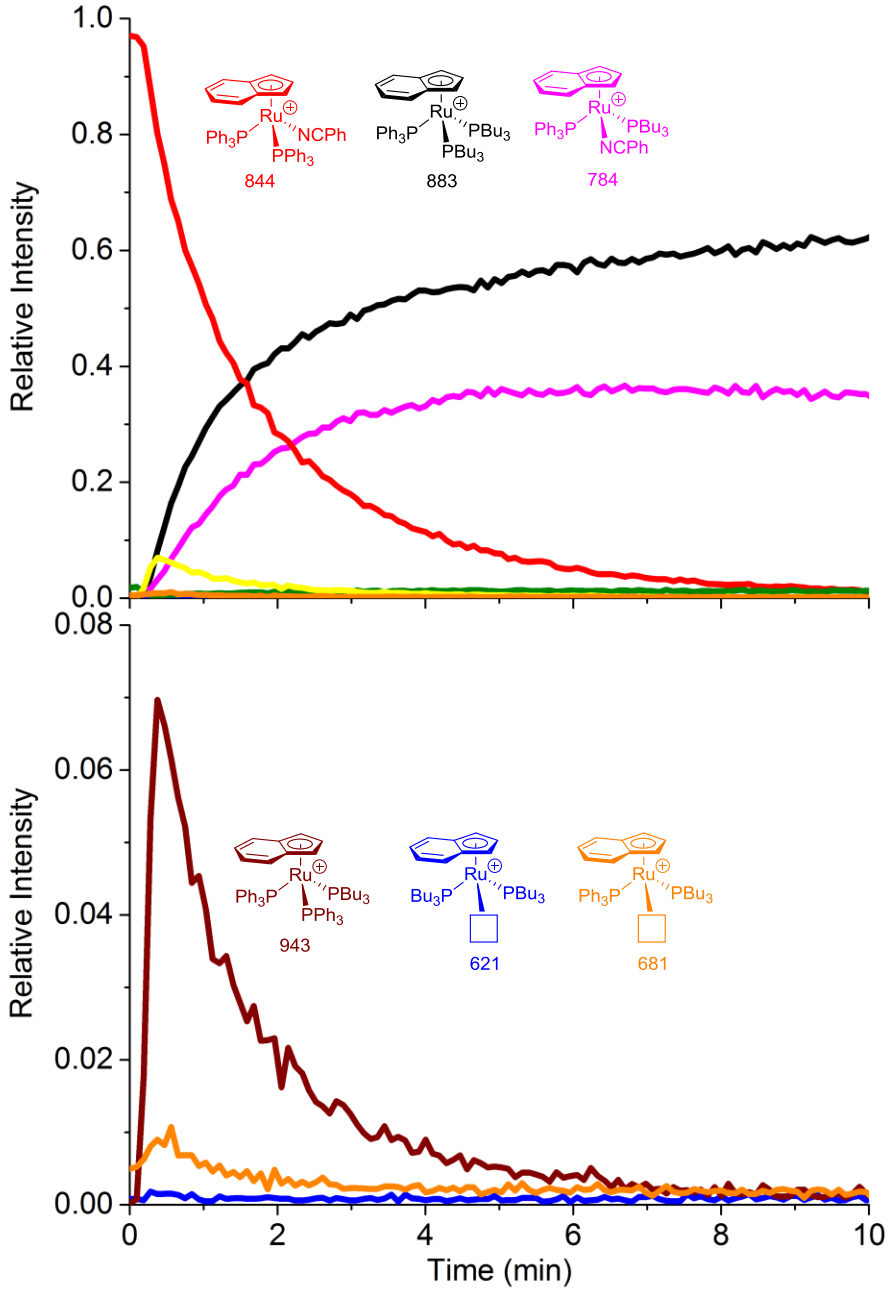

Figure 4.20. 100 eq. of tri-n-butylphosphine substitution in PhF

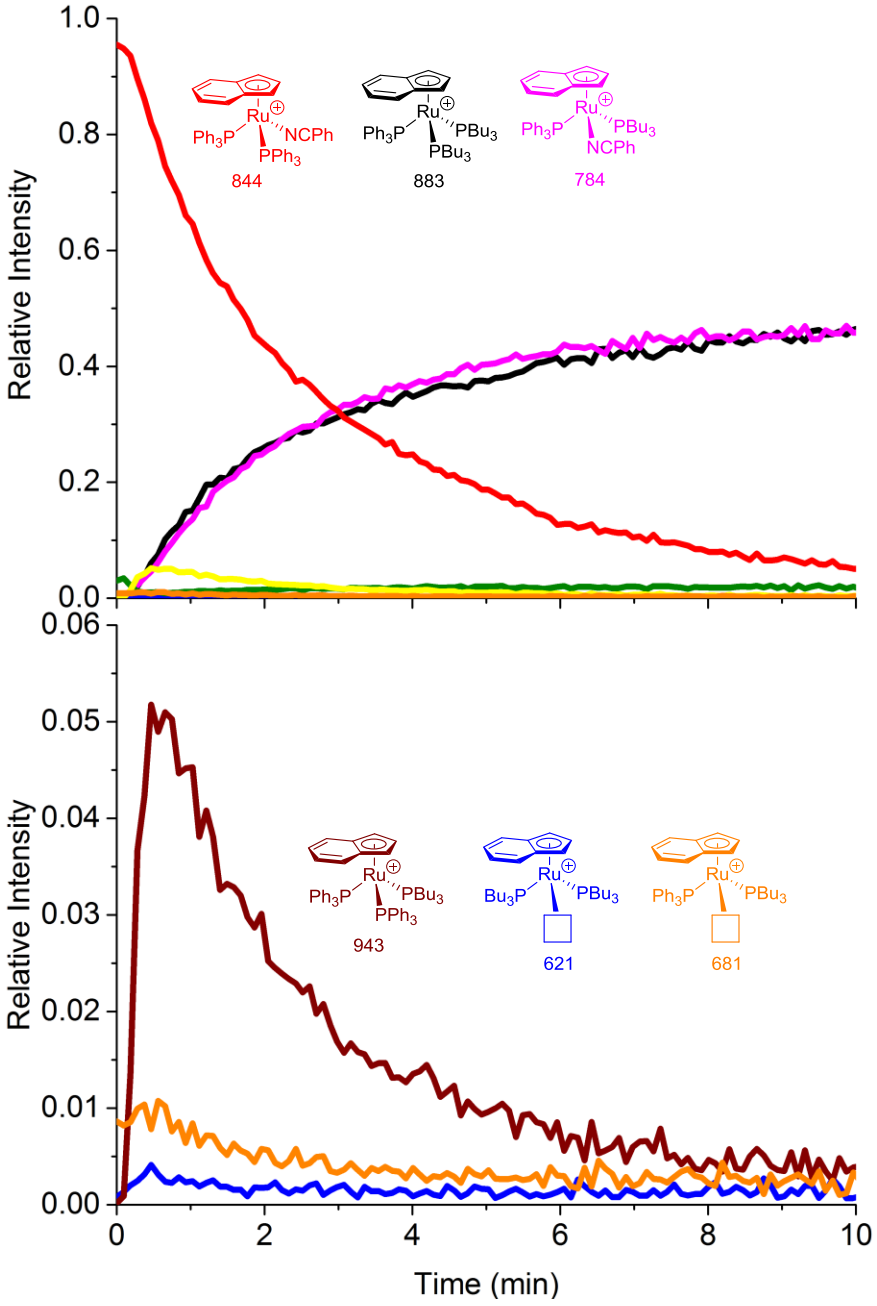

Figure 4.21. 50 eq. of tri-n-butylphosphine substitution in PhF

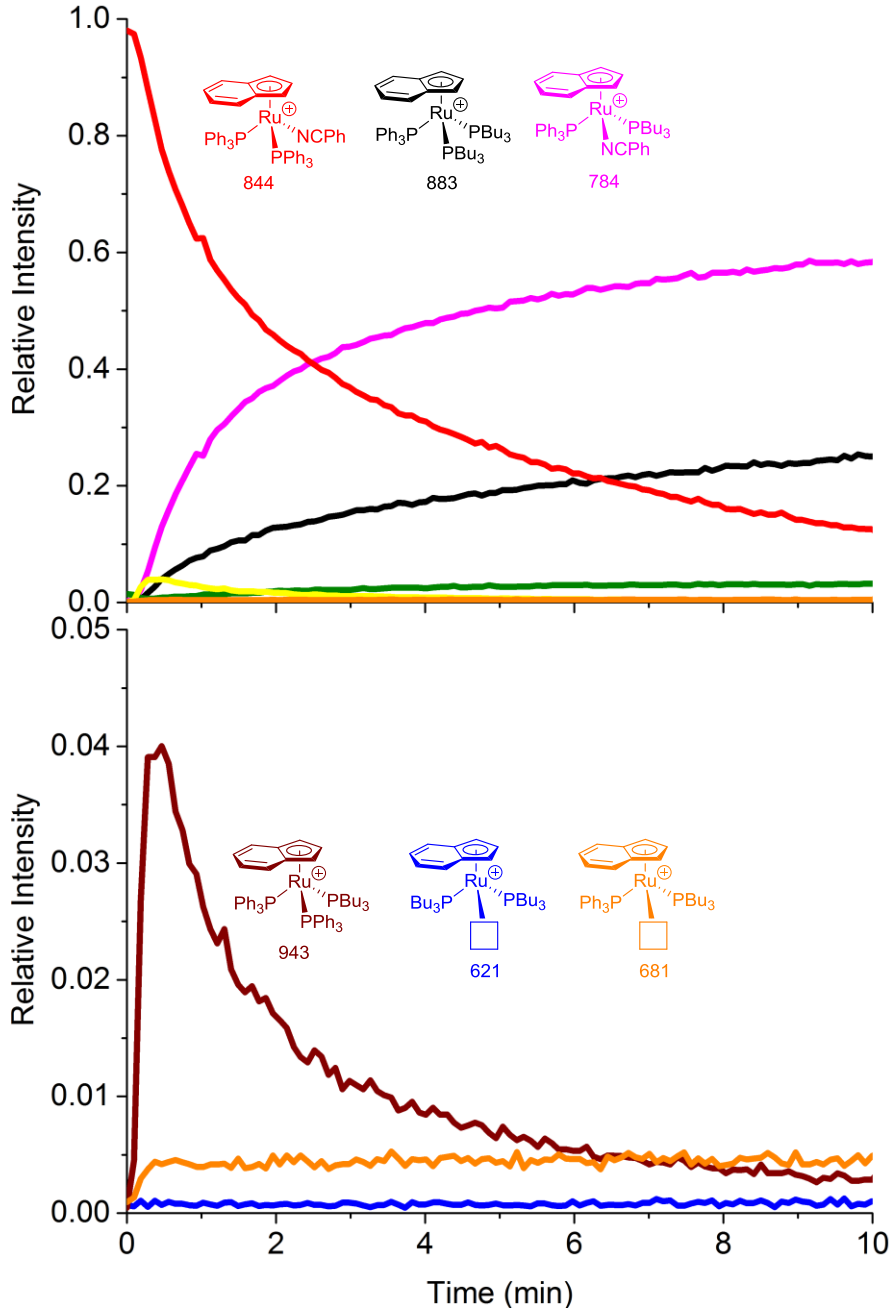

Figure 4.22. 10 eq. of tri-n-butylphosphine substitution in PhF

Another notable finding is the unexpectedly low abundance of the second substitution product even though large amount of the incoming ligand was added (around 60% under 100 equivalents let alone those less than that). It is because benzonitrile is a very competitive ligand in the secondary substitution (see Scheme 4.4), competing with tri-n-

butylphosphine. And most importantly in this case the steric influence should play a more important role as the ruthenium complex is already crowded with 2 trialkylphosphines before accommodating the incoming one. Thus if the amount of tri-n-butylphosphine added to the ruthenium complex was only one equivalent (benzonitrile: tri-n-butylphosphine = 1:1), the relative intensity of the secondary substitution product would even be lower than 20% (the relative intensity of product under 10 equivalents of tri-n-butylphosphine).

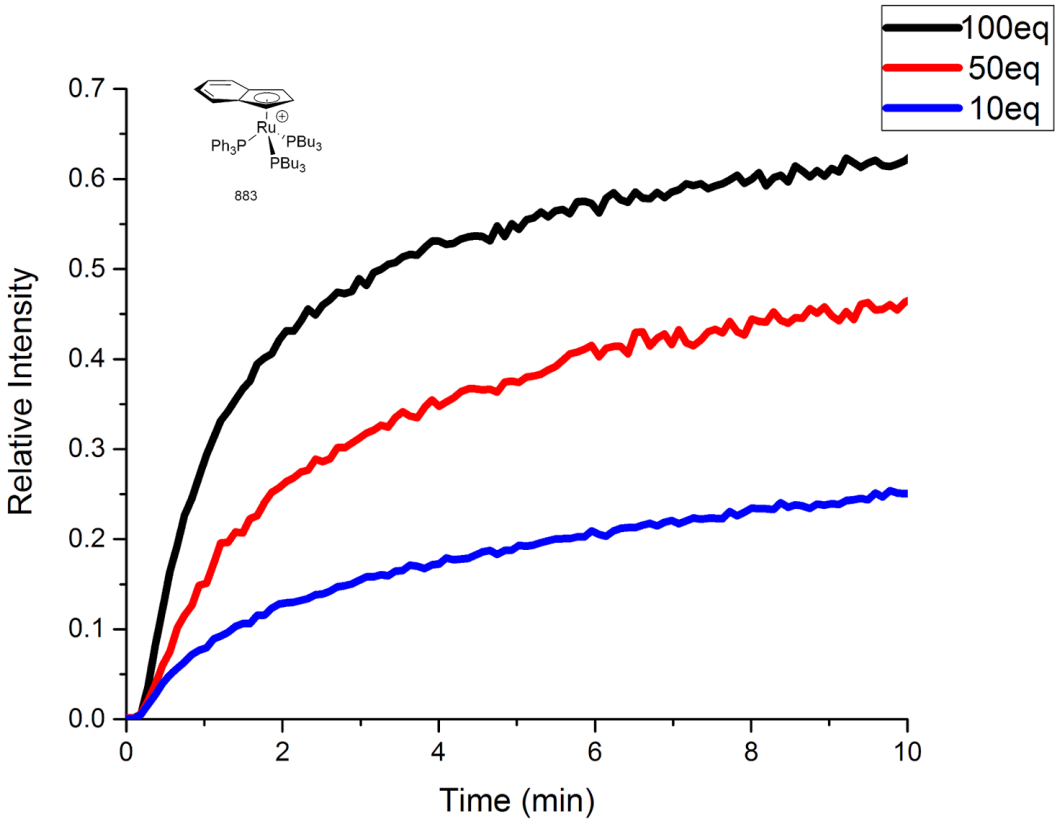

Figure 4.23. Comparing the influence of increasing the concentration of incoming ligand on the relative intensity of the secondary product.

COPASI modeling

The substitution reaction between 100, 50 and 10 equivalents of tri-n-butylphosphine and the ruthenium complex was all run under the *Parameter Estimation* to find out the reaction rate constant for each step of the proposed mechanism. The average of the three was used to make the result to fit all three experimental data as well as possible. The results were highlighted in red.

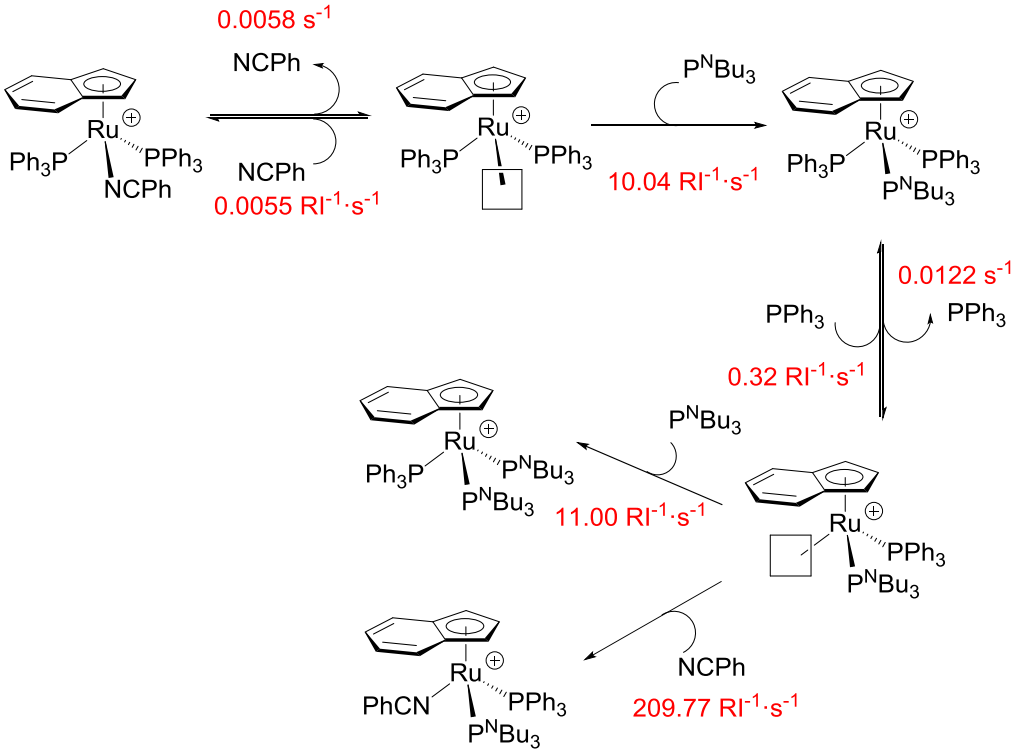

Figure 4.24. Result from the *Parameter Estimation*. The breakdown of the proposed dissociative substitution mechanism between the ruthenium complex and P^NBu_3. The reaction rate constant for each step is highlighted in red.

The experimental data and simulation for all three experiments were shown in the figures below. It is not hard to tell that the simulation fits well in both reactions with100 and 50 equivalents of tri-n-butylphosphine. However in the case of 10 equivalents of added

phosphine obvious variance was seen. It can be explained by the same problematic issues discussed earlier which will happen when scaling down the experiment.

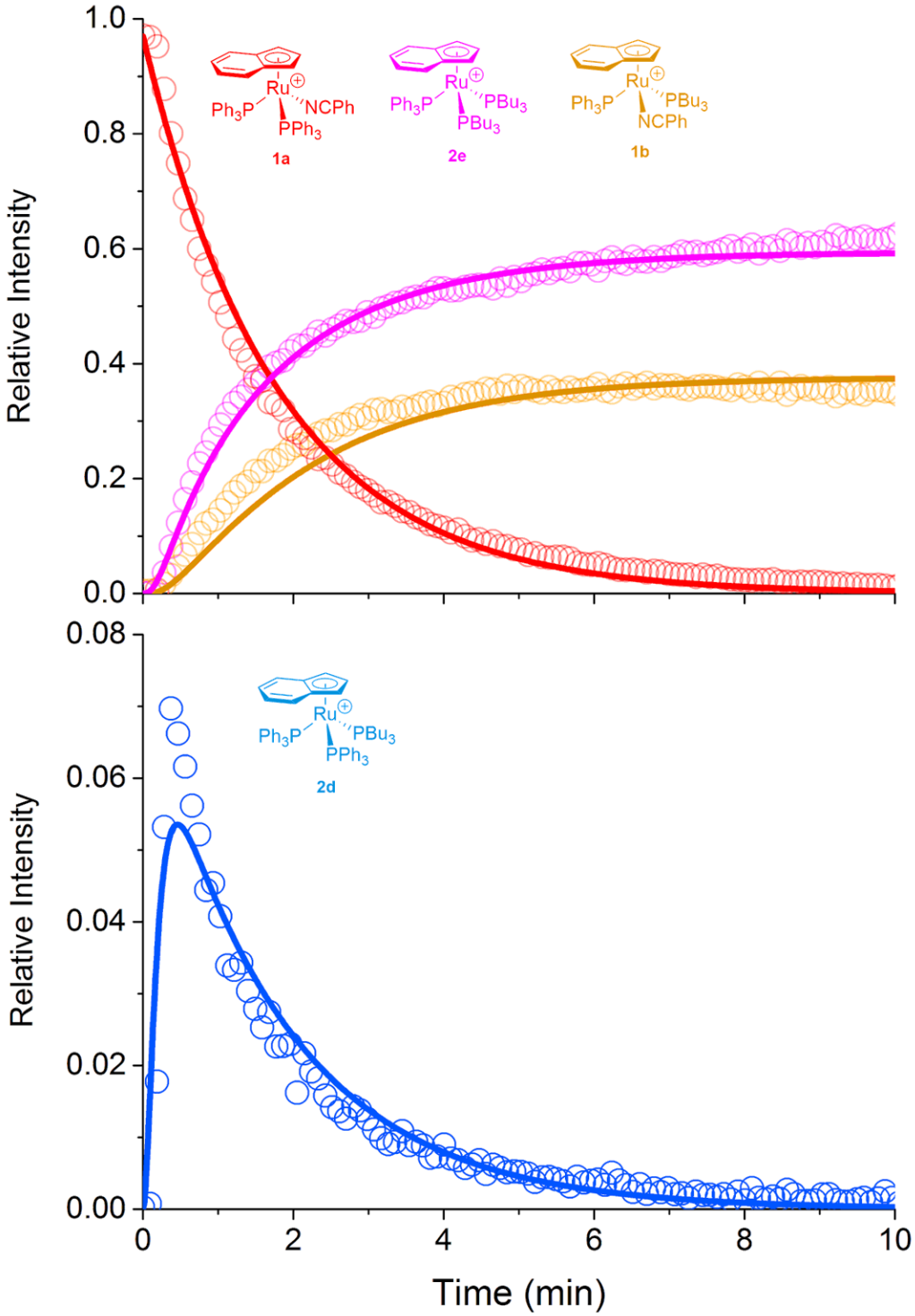

Figure 4.25. Experimental (circles) and simulated (lines) for the dissociative substitution reaction with 100 equivalents of tri-n-butylphosphine ligand. Parameter estimation conducted using COPASI.

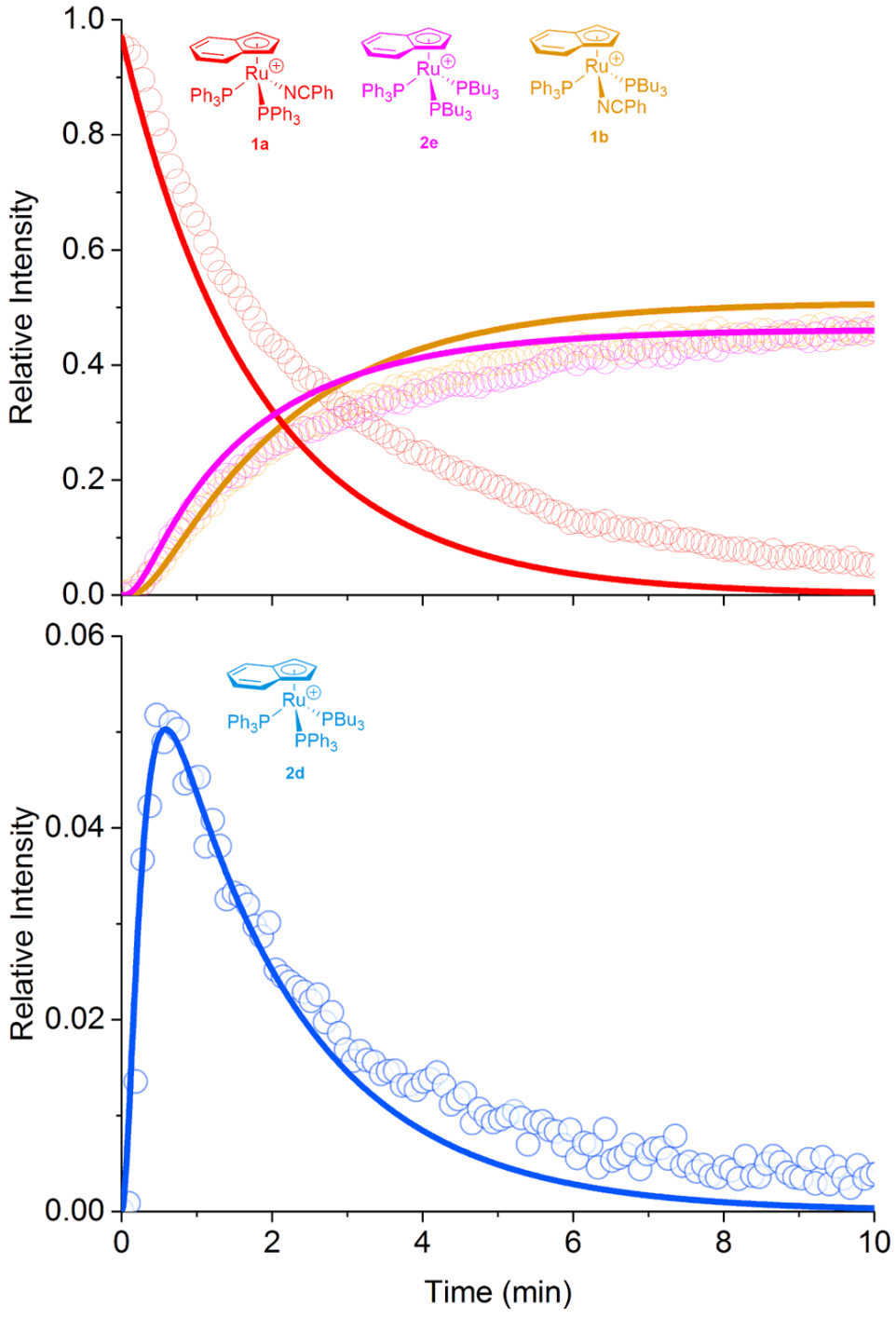

Figure 4.26. Experimental (circles) and simulated (lines) for the dissociative substitution reaction with 50 equivalents of tri-n-butylphosphine ligand. Parameter estimation conducted using COPASI.

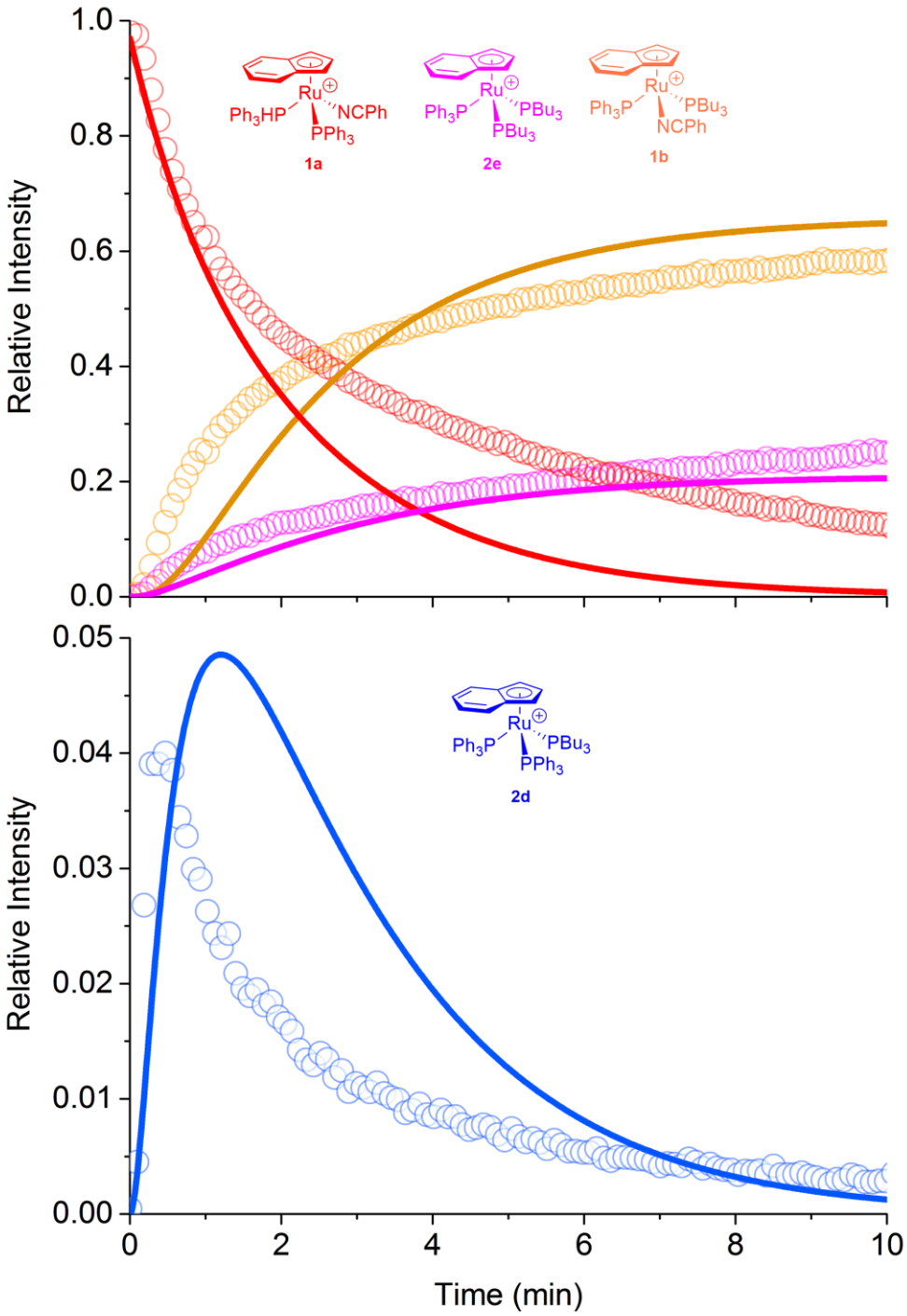

Figure 4.27. Experimental (circles) and simulated (lines) for the dissociative substitution reaction with 10 equivalents of tri-n-butylphosphine ligand. Parameter estimation conducted using COPASI.

To conclude this section, in this study we proposed a more complex dissociative substitution mechanism when only one phosphine ligand was added in ruthenium complex solution which involves both second substitution and original leaving ligand re-substituting back to the metal center. This mechanism helps to answer the problems like the first substitution product is lost in synthesis (like the complex **2d** in our study which is the first substitution product) and unexpected product like **2e** (which is explained in page 84). It reveals the competing substitution between the original leaving ligand and the desired phosphines added. The leaving ligand benzonitrile can be very competitive to the tri-n-butylphosphine in the second substitution (19:1 according to the ratio between the respective rate constants from Figure 4.24). It is what organometallic synthesists have to consider when choosing their starting materials as the original leaving ligand may re-substituting back due do its electric or steric advantage in second substitution.

4.2.3 MS/MS Experiments on $[LRuP_3]^+$

In this section we systematically made ruthenium complexes with three different phosphine ligands bound to them by substitution. Under the MS/MS function of the mass spectrometer, we programmed the system to increase the collision voltage every 10.12 seconds. In the mass spectrometer the ruthenium will collide with the collision gas, argon, and dissociate. It is called collision-induced-dissociation (CID).

Due to a large mass range of complexes were tested and to avoid the influence of the difference in mass, the mass normalized collision voltage is used as below[98]:

$$E_0 = E_{exp} \times m_{argon}/(m_{argon} + m_A)$$

Where the E_0 is the mass normalized collision voltage, E_{exp} is the collision voltage recorded in the experiment, m_{argon} is the molecular weight of the argon and the m_A is the molecular weight of the analyte ion.

The first example is the ruthenium with one triphenylphosphine, one diethylphosphine and one diphenylphosphine. After increasing the mass normalised collision voltage to the range of 0.5 to 1 volt (blue square in Figure 4.28) where is not influenced by the second fragmentation, the three fragmentation products each losing one phosphine ligand appeared. To get meaningful quantitative date about relative binding affinity of the phosphine ligands the influence of the second fragmentation has to be avoided as it affects and complicates the abundance of the first fragmentation products.

Guided by the logic mentioned before that the relative binding affinity of the leaving phosphine ligands can be determined by the relative abundance of the respective first fragmentation products, the order of binding strength PEt2H>PPh_2H≈PPh_3 is achieved. To have the quantitative comparison of binding strength of those phosphine ligands, the reciprocal of the slope of the trend line was used (how much energy was needed to increase every one percent of the first fragmentation product). Thus the relative binding affinity of PEt_2H:PPh_2H:PPh_3=4.66:1.1:1. This result suits well with the electric and steric properties of the phosphine ligands as being more electron donating and less bulky help to increase the binding affinity.

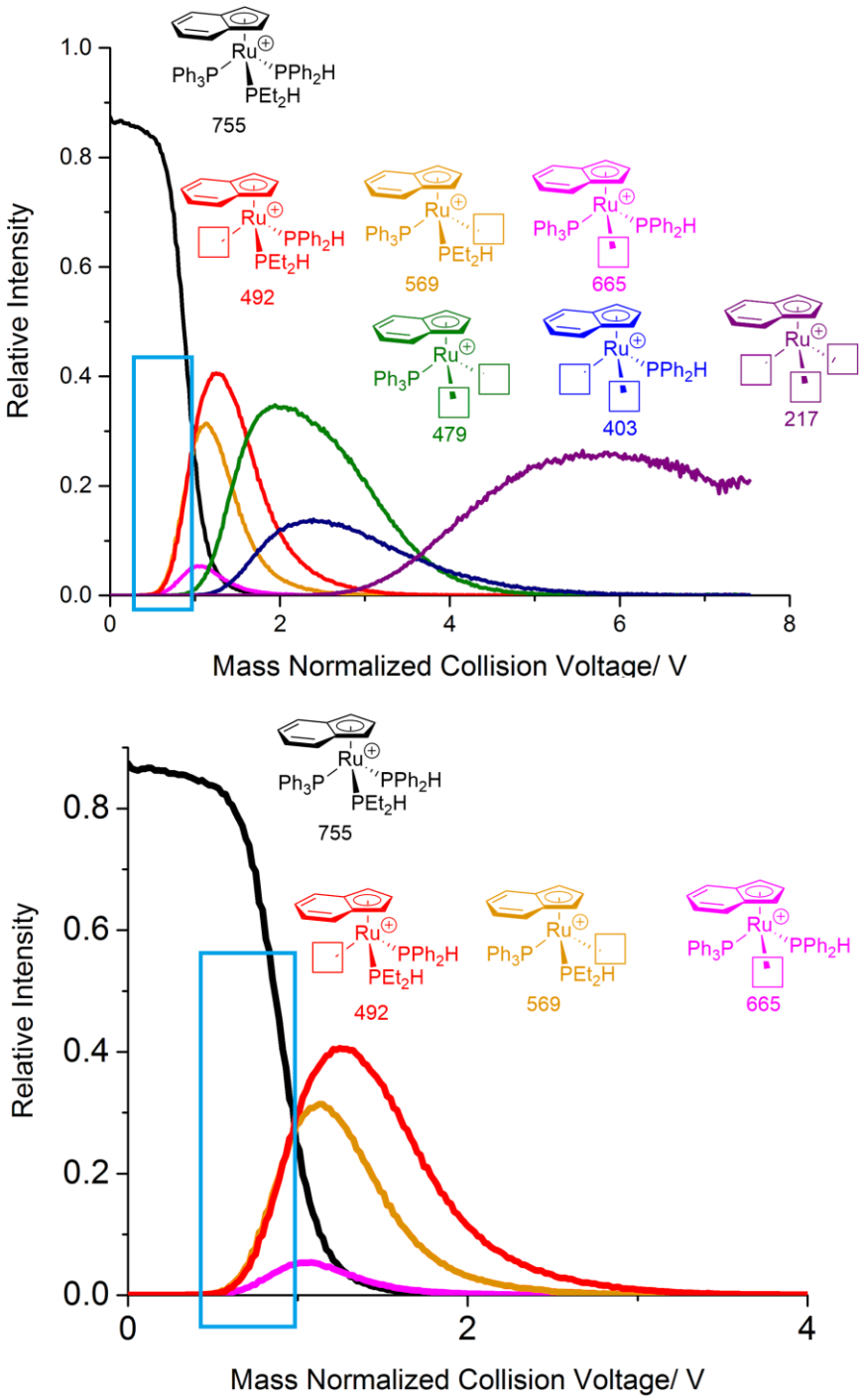

Figure 4.28. MS/MS of Ru(indenyl)(PPh_3)(PPh_2H)(PEt_2H). Full range of the MS/MS data with both first and second fragmentation products (above). In the blue square the influence of the second fragmentation can be ignored. In the figure below (below) is the zoom-in version with only trend lines of first fragmentation products. In the blue square is the region where second fragmentation can be ignored.

The MS/MS study on the $[Ru(indenyl)(PPh_3)(PPh_2H)(PCy_2H)]^+$ reveals the binding order of the three phosphine ligands as below: $PPh_2H \approx PCy_2H > PPh_3$.The same process was carried out to get the binding affinity order quantitatively as $PPh_2H:PCy_2H:PPh_3=1.61:1.90:1$. The slightly stronger binding affinity of PCy_2H than PPh_2H may be because the electric property plays a more important role here in determining binding strength. And the different binding affinity ratio between PPh_2H and PPh_3 (1.61 instead of 1.1 in the last example) reveals that this binding comparison is case-dependent. The binding affinity of the same phosphine ligand can change accordingly to its ambient chemical environment (the other binding ligands, transition metal, etc.). Thus the order of all four phosphine ligands above can be drawn like $PEt_2H > PCy_2H > PPh_2H > PPh_3$, but not quantitatively.

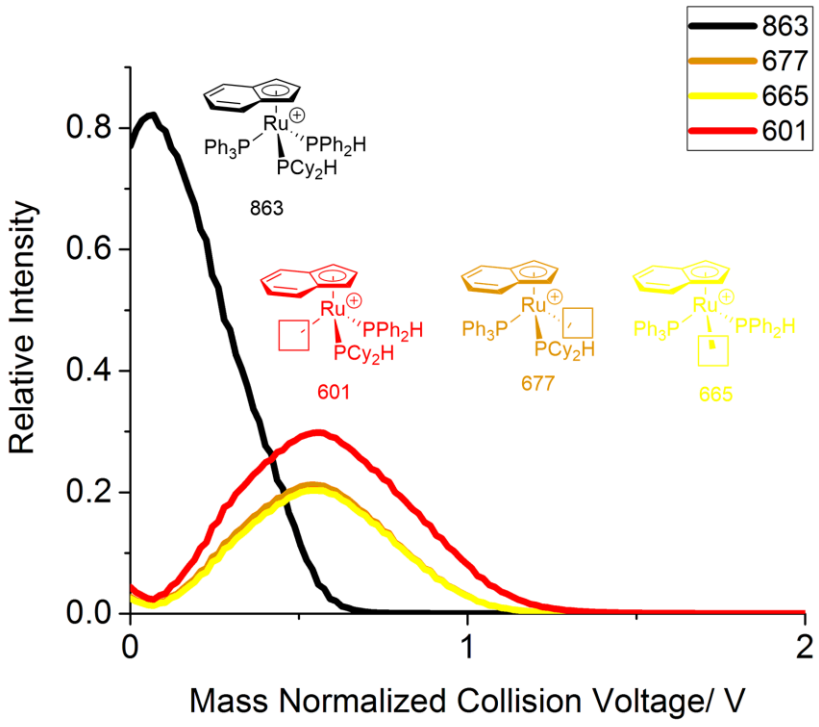

Figure 4.29. MS/MS of $Ru(indenyl)(PPh_3)(PPh_2H)(PCy_2H)$

Then the MS/MS study on the $[Ru(indenyl)(PPh_3)_2(PEt_2H)]^+$ provided an interesting finding. The first fragmentation is overwhelmingly losing the weak binding ligand, PPh_3. However, in the second fragmentation the ruthenium did not lose the PPh_3 again but the PEt_2H, which is supposed to be a way stronger as a binding ligand.

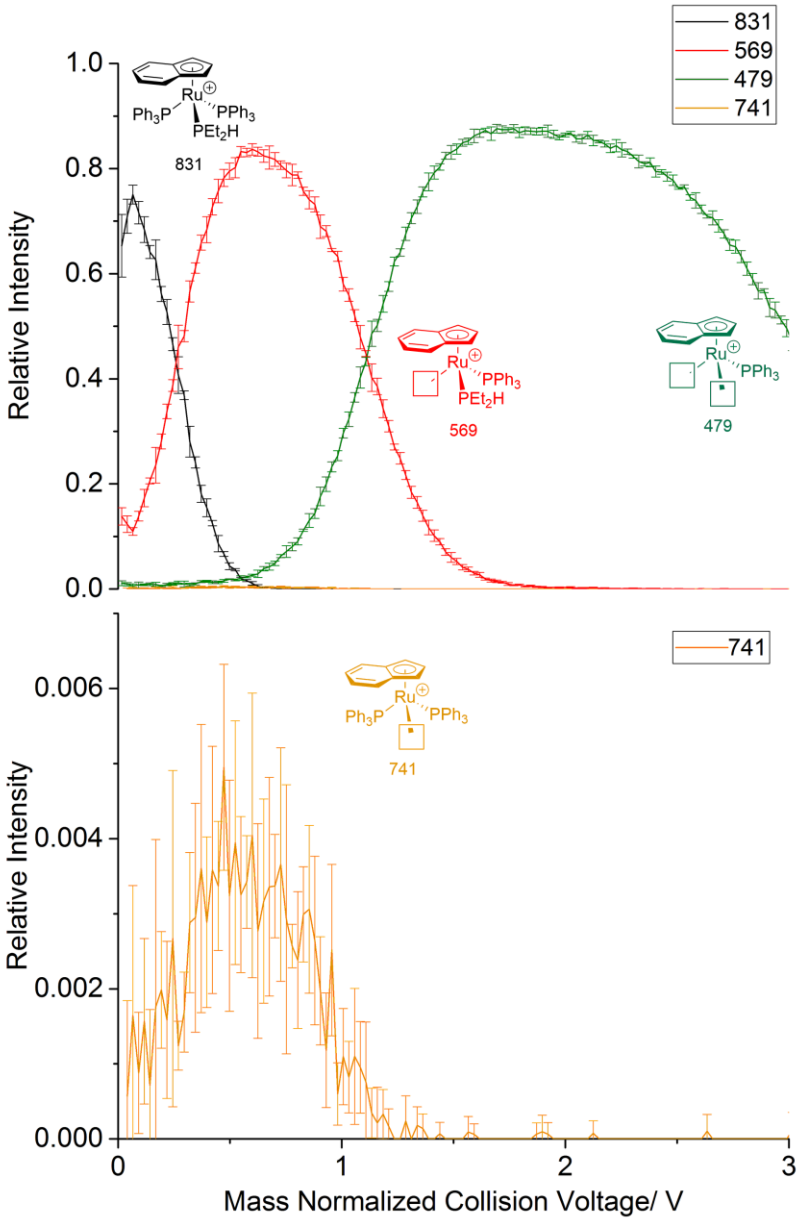

Figure 4.30. Average of 5 trials for MS/MS of (indenyl)$Ru(PPh_3)_2(PEt_2H)$

The reason behind this phenomenon, according to our belief, is the agostic interaction between the triphenylphosphine ligand and the ruthenium. As after the first fragmentation and losing a dative ligand, the remaining ruthenium complex is in an electron-poor and activated state. To accommodate this electron deficiency at the metal center, the ortho-hydrogen on the benzene in triphenylphosphine can be activated can coordinate to the ruthenium in a chelating manner (ortho-metallation. This makes the triphenylphosphine a bidentate ligand and greatly increases its binding strength to the metal center.

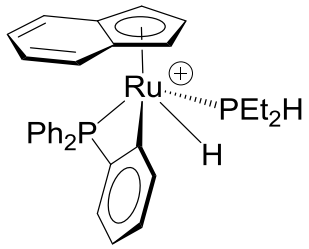

Figure 4.31. C-H activation of triphenylphosphine in activated ruthenium complex to provide extra electron to the metal center, which at the same time increases the binding strength of the ligand.

To test this we have run the MS/MS of the other ruthenium species with two triphenylphosphine ligands like the two graphs below. In both cases, the leaving of triphenylphosphine will dominate in the first fragmentation due to its both bulkiness and poor electron-donating capability. However, after increasing the mass normalized collision voltage to around 1.5V the triphenylphosphine is no longer that easy to be removed from the ruthenium center. Actually, the leaving of triphenylphosphine in the second fragmentation process is minimal compared to that of the others.

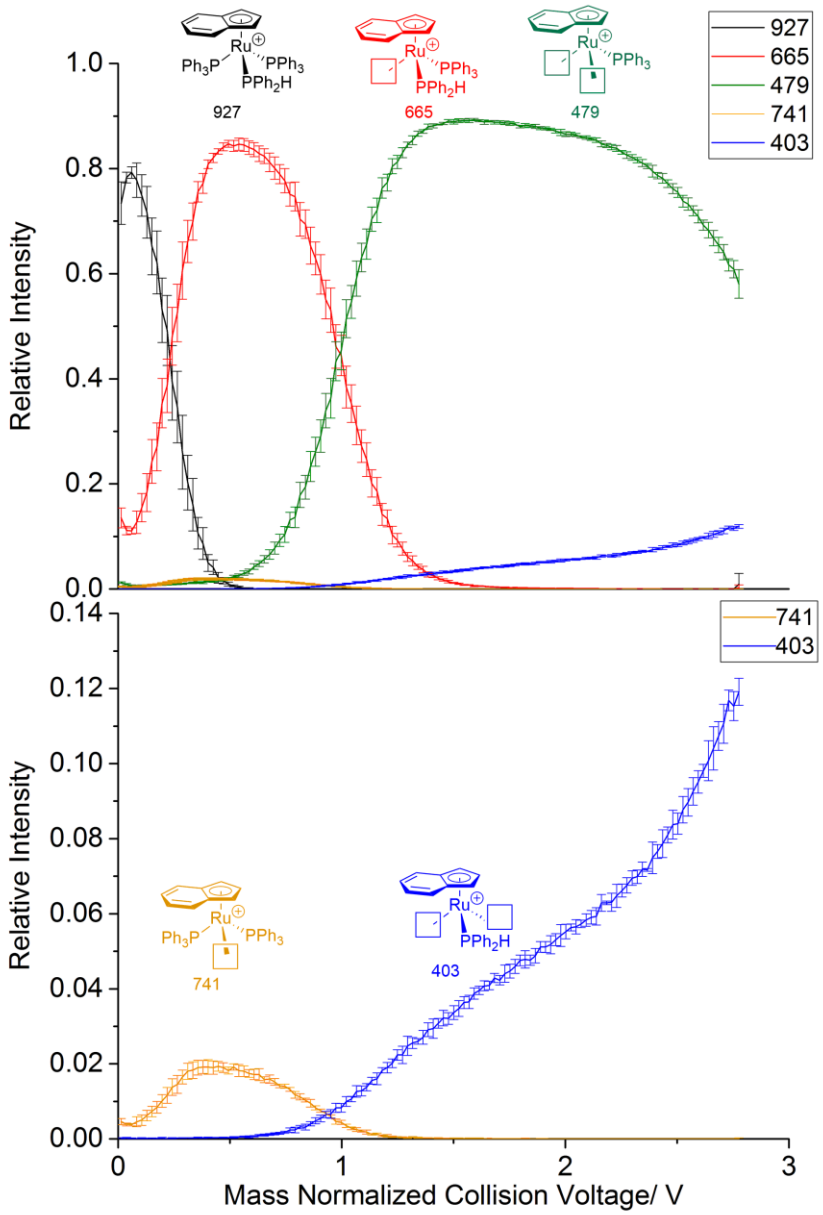

Figure 4.32. Average of 5 trials for MS/MS of (indenyl)Ru(PPh_3)$_2$(PPh_2H). When the mass normalized collision voltage increased to 0.5 V, the first fragmentation products reached to their peaks. And the red complex which lost the triphenylphosphine is dominant. Then when the mass normalized collision voltage increased to about 1.5 V, the products of the secondary reached to their heights and this time the complex losing diphenylphosphine dominated. This again proves that the binding affinity of triphenylphosphine is greatly enhanced in the energy activated ruthenium complex.

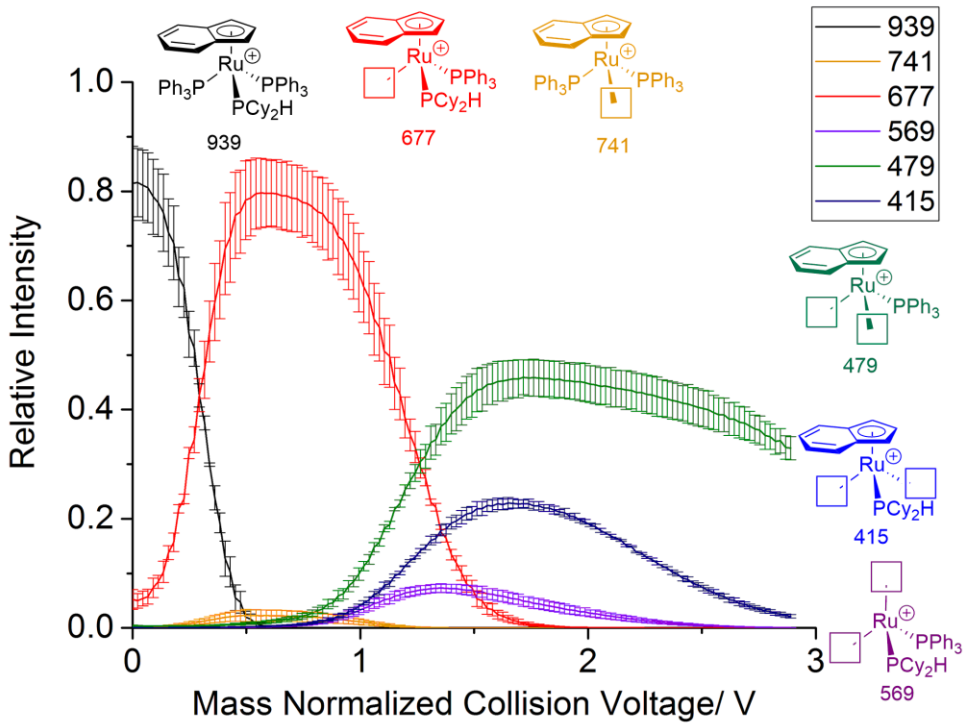

Figure 4.33. Average of 5 trials for MS/MS of (indenyl)Ru(PPh_3)$_2$(PCy_2H). The first fragmentation products, (indenyl)Ru(PPh_3)$_2$ and (indenyl)Ru(PPh_3)(PCy_2H), appeared at their peaks under about 0.5 V of mass normalized collision voltage. Still the triphenylphosphine is easy to be knocked off. What is interesting in this MS/MS study is the detecting of the other first fragmentation product which loses the indenyl at a much higher collision voltage range than that of normal first fragmentation. Then in the second fragmentation, again the product losing dicyclohexylphosphine accounts more.

In this section a couple of ruthenium complexes with only triphenylphosphine and the other two identical phosphine ligands were also tested under MS/MS like the two graphs listed below. The findings of these two experiments just further confirms our conclusion above of this section:

1) The relative binding affinity of different phosphine ligands can be achieved quantitatively by the reciprocals of the trend lines of first fragmentation product within the region without interference of second fragmentation. However this is dependent on the ambient chemical environment of the ligand, thus the value may

vary. But the order can still be drawn as PEt_2H> PCy_2H> PPh_2H> PPh_3, even though not quantitatively.

2) In the second fragmentation duo to ortho-metallation the binding affinity of triphenylphosphine is greatly enhanced.

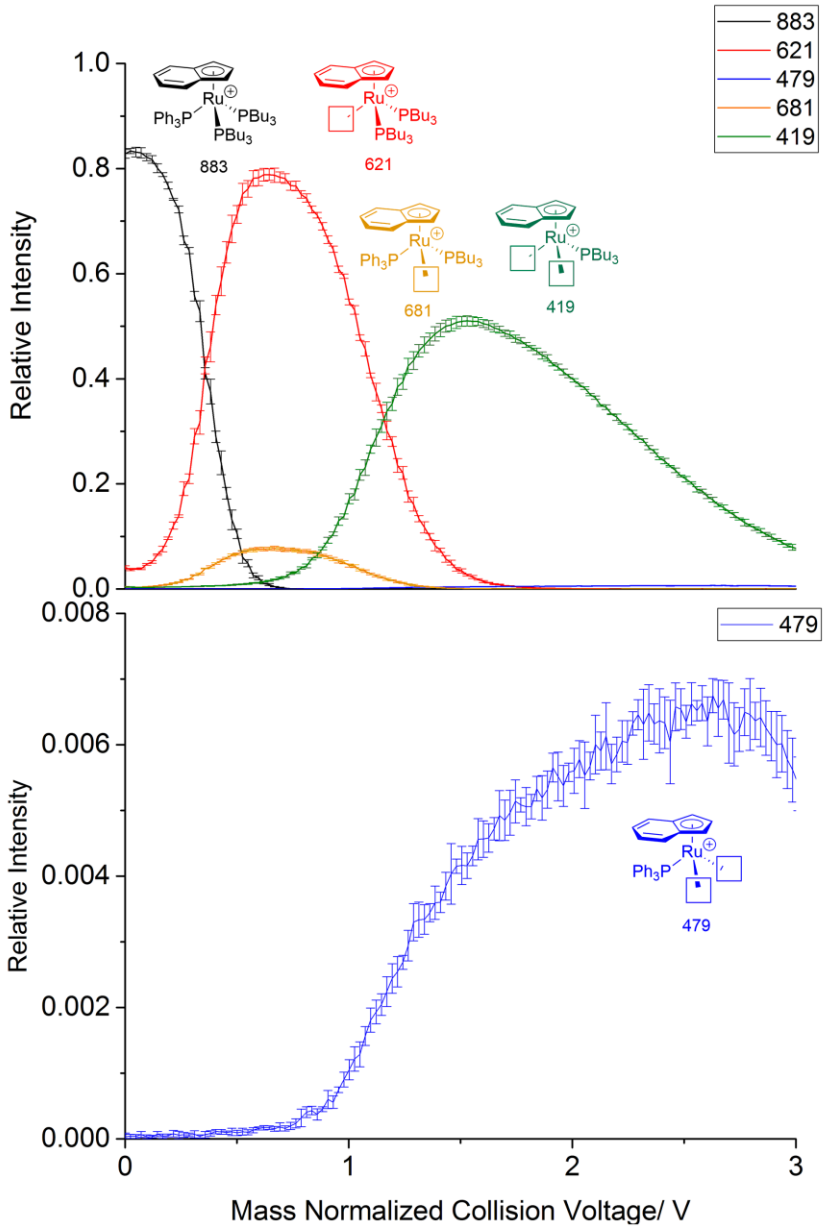

Figure 4.34. Average of 5 trials for MS/MS of (indenyl)Ru(PPh_3)(PBu_3)$_2$. The first fragmentation products of the Ru(PPh_3)(PBu_3)$_2$ reached their peaks at about 0.6 V of mass normalized collision voltage. During this process most of the triphenylphosphine dissociated from the ruthenium which explains the minor intensity of triphenylphosphine in the second fragmentation.

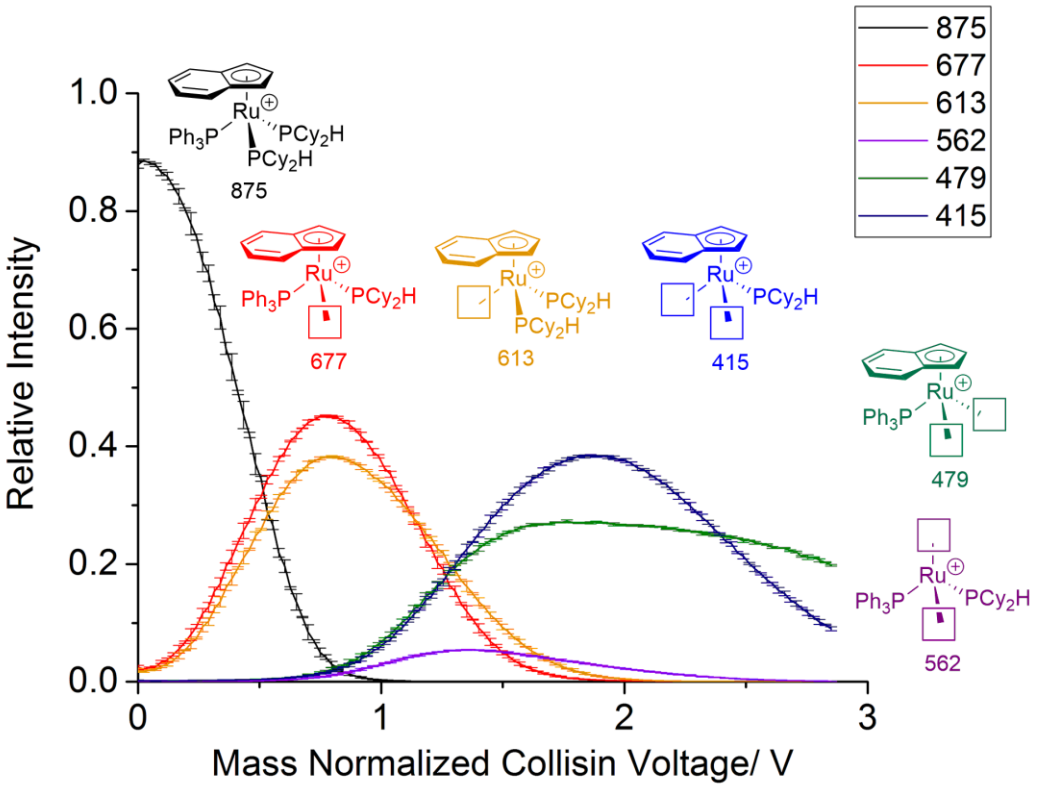

Figure 4.35. Average of 5 trials for MS/MS of (indenyl)Ru(PPh_3)(PCy_2H)$_2$. The MS/MS on ruthenium complex with dicyclohexylphosphine is always interesting with appearance of the first fragmentation product losing indenyl when the mass normalized collision voltage increased to about 1.5 V. And duo to the bulkiness in all three phosphine ligands, the steric hindrance plays an important role here. The similar relative intensity of the two first fragmentation products reveals the binding strength between triphenylphosphine and dicyclohexylphosphine.

4.2.4 MS/MS Experiments on $[LRuP_1P_2]^+$

According to the findings from the last section, the ligand dissociation of phosphine ligand does not follow strictly as predicted merely by binding strength of free phosphine ligands when the complex is energetically activated. To delve deeper in this phenomenon, in the third section of the project we initiated the MS/MS on the already energy-activated $[LRuP_1P_2]^+$ by increasing the cone voltage.

The first one we have done is the activated ruthenium complex with one triphenylphosphine and one diphenylphosphine. As the mass normalized collision voltage increases, the product with triphenylphosphine bound to it predominates. And according to our discussion before there is an ortho-metallation for ruthenium complex with tri-/diphenylphosphine ligand. However triphenylphosphine ligand is more prone to ortho-metallate to the metal duo to the two following reasons. Firstly, there are more ortho-hydrogens (12) in triphenylphosphine than that in diphenylphosphine (4). Secondly, the bulkier triphenylphosphine ligand can have ortho-hydrogen closer to the metal center.

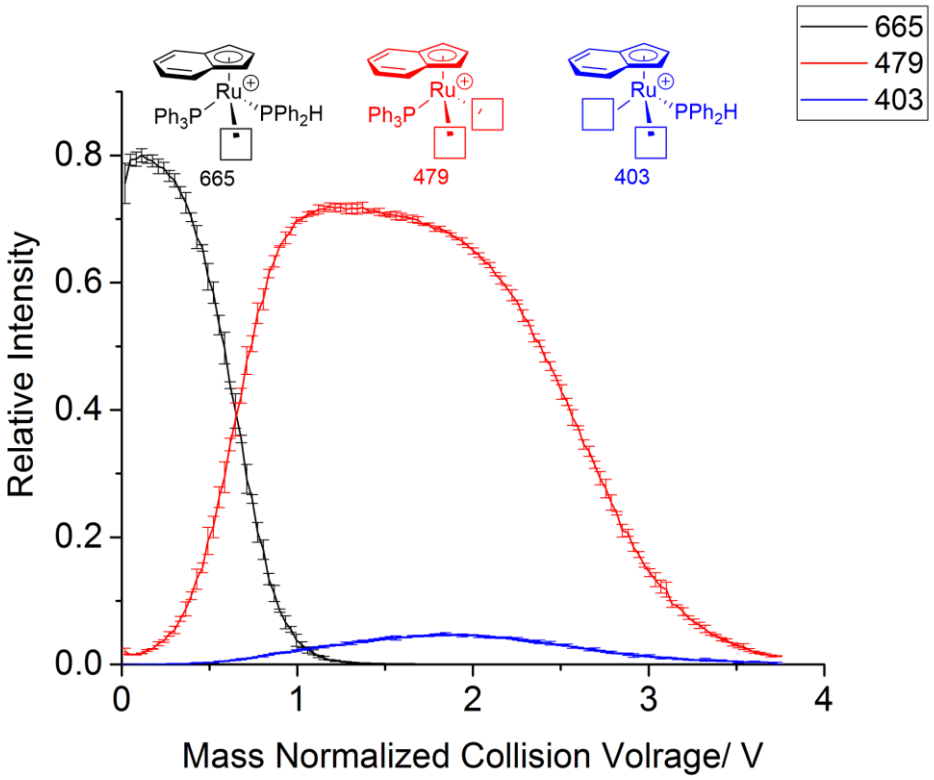

Figure 4.36. Average of 5 trials for MS/MS of (indenyl)Ru(PPh_3)(PPh_2H).

The MS/MS study on activated ruthenium with one triphenylphosphine and one dicyclohexylphosphine ligand reveals the relative binding affinities of the three ligands. The more abundant the fragmentation product, the weaker the leaving phosphine ligand

is. Thus the binding strength order is indenyl > PPh_3 > PCy_2H. Indenyl, a η^5 ligand, is still the stronger ligand than the bidentate triphenylphosphine under energy-activated situation.

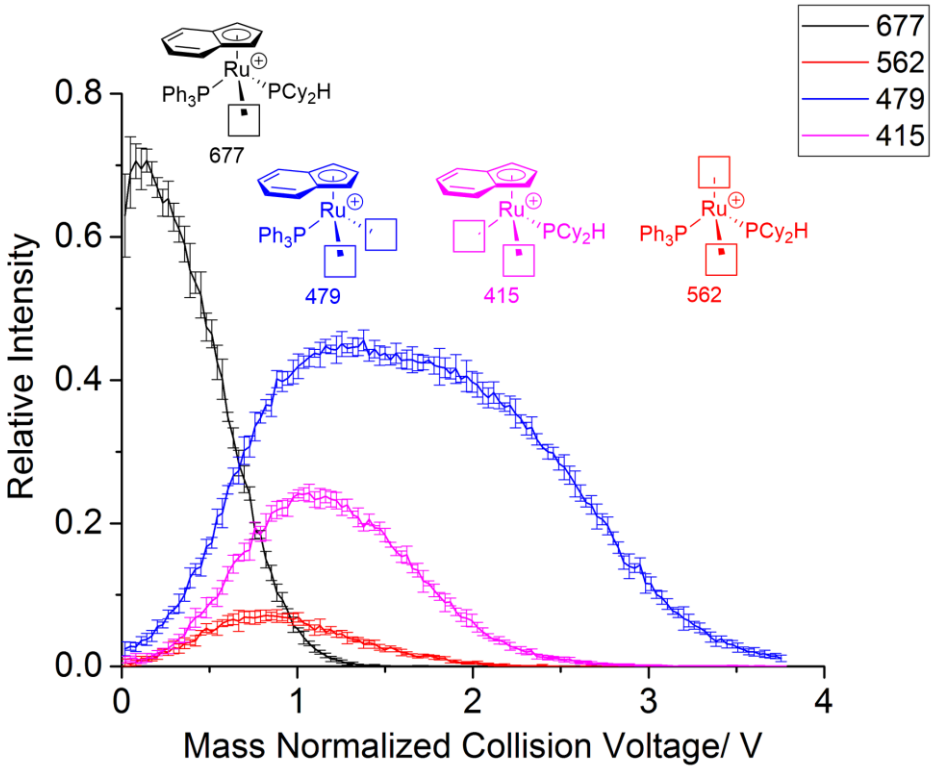

Figure 4.37. Average of 5 trials for MS/MS of (indenyl)Ru(PPh_3)(PCy_2H).

The same is the MS/MS study of ruthenium complex with one diethylphosphine and one triphenylphosphine ligand. The originally strongest binding phosphine ligand, diethylphosphine, is almost only one ninetieth as strong as the bidentate triphenylphosphine under energy-activated condition according to the relative abundance of the respective products. From this perspective it reveals how greatly the binding affinity of the triphenylphosphine has been enhanced by ortho-metallation.

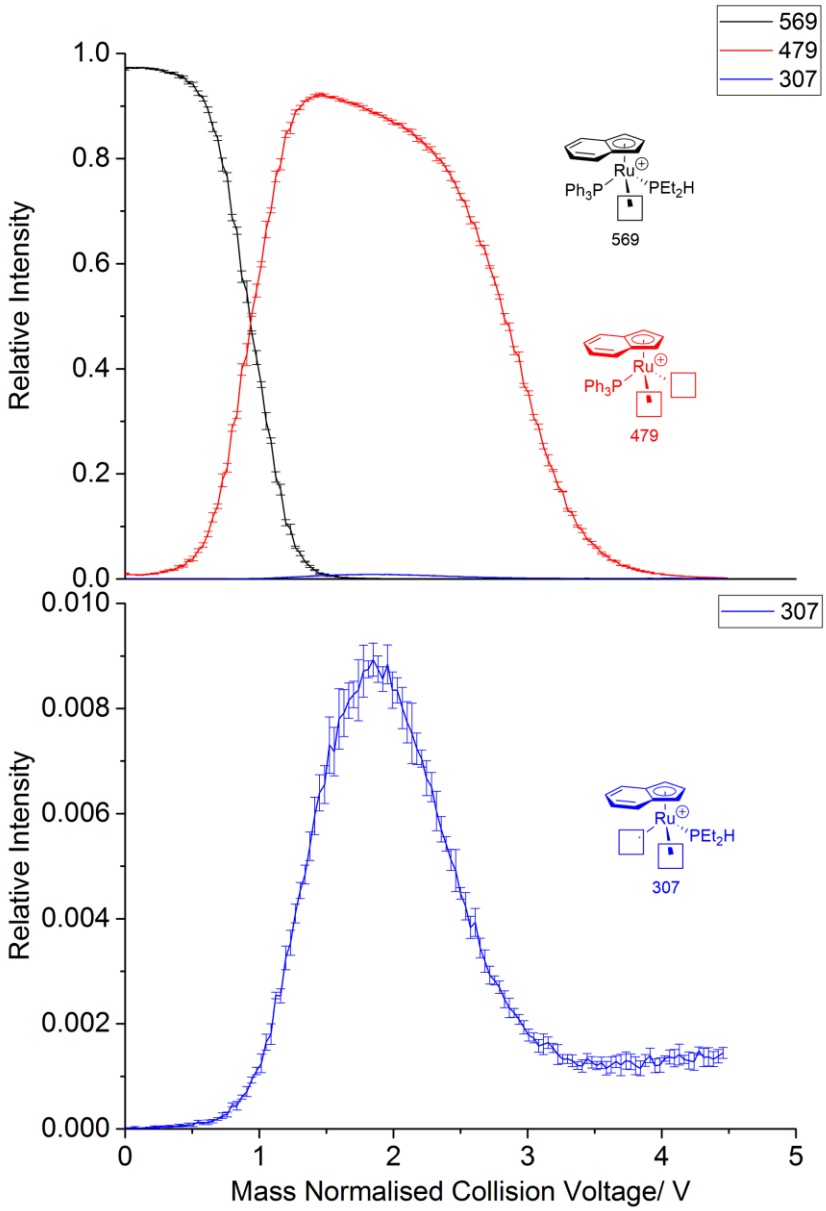

Figure 4.38. Average of 5 trials for MS/MS of (indenyl)Ru(PPh_3)(PEt_2H).

To conclude the findings in this section, we find:

1) Compared to diphenylphosphine and dicyclohexylphosphine, triphenylphosphine is more prone to ortho-metallate to the ruthenium center to increase its binding affinity.

2) The binding affinity of the η^5 indenyl is still way stronger than the bidentate triphenylphosphine under energy activated condition.
3) Under the energy activated condition the binding affinity of the triphenylphosphine is about 90 times stronger than that of diethylphosphine, which is originally the strongest one in the last section.

4.3 Conclusion

ESI-MS is a powerful facility to study organometallic reactions with charged species as it can monitoring multiple species simultaneously. In the reactions with two phosphine ligands added to the ruthenium complex solution the competitive dissociative substitution mechanism is proposed, which is confirmed by the COPASI modeling. And the relative substituting competence of phosphine ligands can be achieved by the relative abundance of respective products or the estimated rate constant of respective substitution steps like this PEt_2H: PPh_2H: PCy_2H=27:18:1.

In the reaction involves only one phosphine ligand a more complex mechanism is proposed, which helps to explain the missing first substitution products and unexpected product with the leaving ligand re-substituted back the metal center. It is mainly because of the competing substitution mechanism between the originally leaving ligand and the incoming ligand. Like in the section benzonitrile is very competitive to the tri-n-butylphosphine in second substitution. Even 100 equivalents of added phosphine only resulted in about 60 percent of second substitution products. All of these have to be considered by organometallic synthesists.

Also under the MS/MS studies of a series of ruthenium complexes with different phosphine ligands, the relative binding affinity can be revealed. Even though exact

quantitative binding affinity varies with various chemical environment, the order binding affinities studied can still be achieved like PEt_2H> PCy_2H> PPh_2H> PPh_3.

An interesting finding in the study is that under energy activated condition the triphenylphosphine's binding affinity is greatly enhanced in an ortho-metallation manner, about 90 times stronger than that of diethylphosphine. Even so, it is still weaker than the indenyl as a binding ligand.

4.4 Experimental

DCM and fluorobenzene were freshly distilled from P_2O_5 before use. All phosphine ligands were purchased from Strem Chemicals Inc. without further treatment. The starting ruthenium complex was synthesized by Roman Belli. All the chemicals and reactions were kept and run under inert gas atmosphere. All the mass spectra were collected with Micromass Q-Tof Mirco mass spectrometer in positive ion mode. The parameters were determined as below: capillary voltage, 2800 V; sample cone voltage, 10.0 V; extraction cone voltage, 1.0 V; desolvation temperature, 160 °C; source temperature, 60 °C; cone gas flow, 0 L/h; desolvation gas flow, 40 L/h; MCP voltage, 2700 V; collision voltage (MS study), 2 V; collision voltage (MS/MS study), programed by ***Autohotkey*** to increase the 1 V every 10.12 seconds from 0 to 100 V.

ESI-MS Reaction Monitoring Using Pressurized Sample Infusion

10.5ml dichloromethane (or fluorobenzene) solution of $[Ru(PPh_3)_2(NCPh)]^+[B(C_6F_5)_4]^-$ (0.2 mg, 0.131 μmol) was monitored using the pressurized sample infusion electrospray

ionization mass spectrometry (PSI-ESI-MS) setup. The Schlenk flask was pressurized to 3 psi using 99.999% purity argon gas. To start the reaction, 0.5ml dichloromethane (or

fluorobenzene) solution of 10eq, 50eq or 100eq of phosphine ligands was injected. Detailed data are as below: diphenylphosphine (100eq, 36μl; 10eq, 3.6μl); diethylphosphine (100eq, 18 μl ; 10eq, 1.8 μl); dicyclohexylphosphine (100eq, 39 μl ; 10eq, 3.9 μl); tri-n-butylphosphine (100eq, 3.3 μl ; 50eq, 1.65 μl ; 10eq, 0.33 μl).

MS/MS Study on $[LRuP_3]^+$ and $[LRuP_2]^+$

5ml dichloromethane solution of $[Ru(PPh_3)_2(NCPh)]^+[B(C_6F_5)_4]^-$ (2mg, 1.31 μmol) was reacted with 10eq of phosphine ligands to make designed ruthenium complexes. Detailed data are as below: diphenylphosphine (36μl); diethylphosphine (18μl); dicyclohexylphosphine (39μl) and tri-n-butylphosphine (3.3μl). The MS/MS data were collected by increasing the collision voltage 1 V every 10.12 seconds controlled by the ***Autohotkey***.

For the MS/MS study of the energy activated ruthenium complex, the sample cone voltage was increased to 25 or 30 V to dissociate the weakest bound phosphine ligand in the desolvation process in the source. Then the same procedure was followed as mention above.

Simulation and Modeling

In COPASI *Parameter Estimation*, the Genetic Algorithm method was used. Detailed operation please refer to the User Manual applied to COPASI 4.8 (Build 35). Here just provides you an example on simulating the tri-n-butylphosphine substitution process.

At first the proposed mechanism should be ready with the name for each step and chemical (here the molecular weight is used).

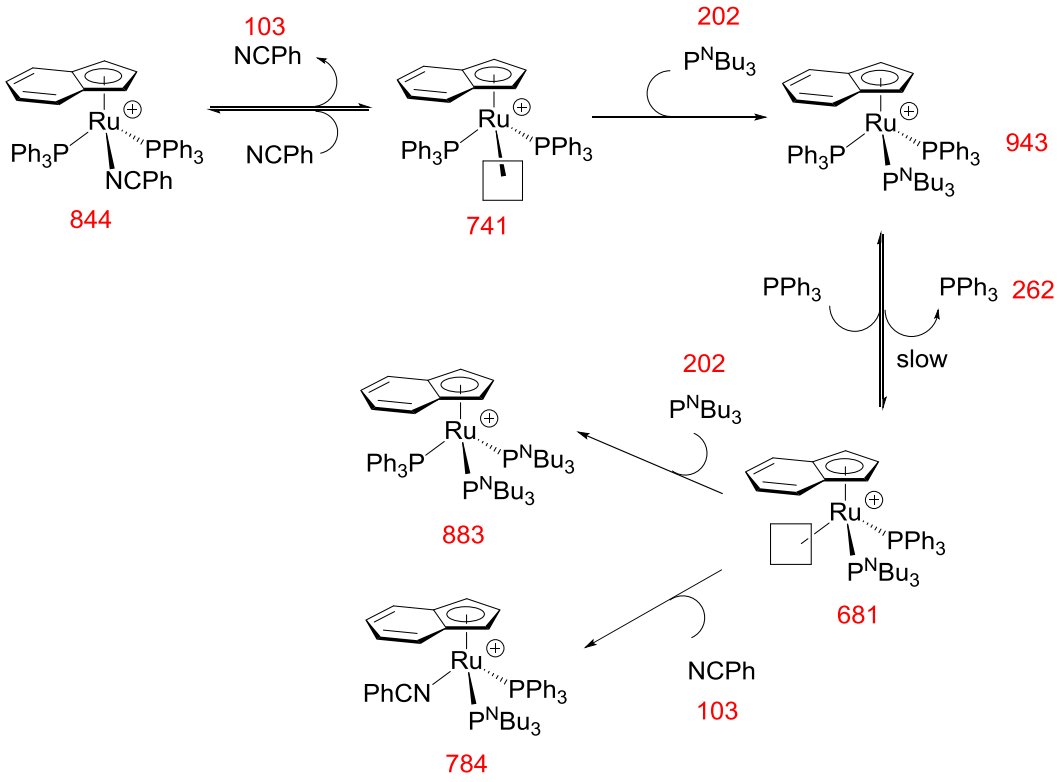

Figure 4.39. Proposed mechanism tested by COPASI

Then all the information of the mechanism above was input to the species and reactions of the biochemical section in the model. For the initial concentrations of the species, their relative intensities were used instead of the actual concentration (to make the comparing between the estimation and experimental results more obvious). And all the species have to be input even if some of them may not be visible to the MS.

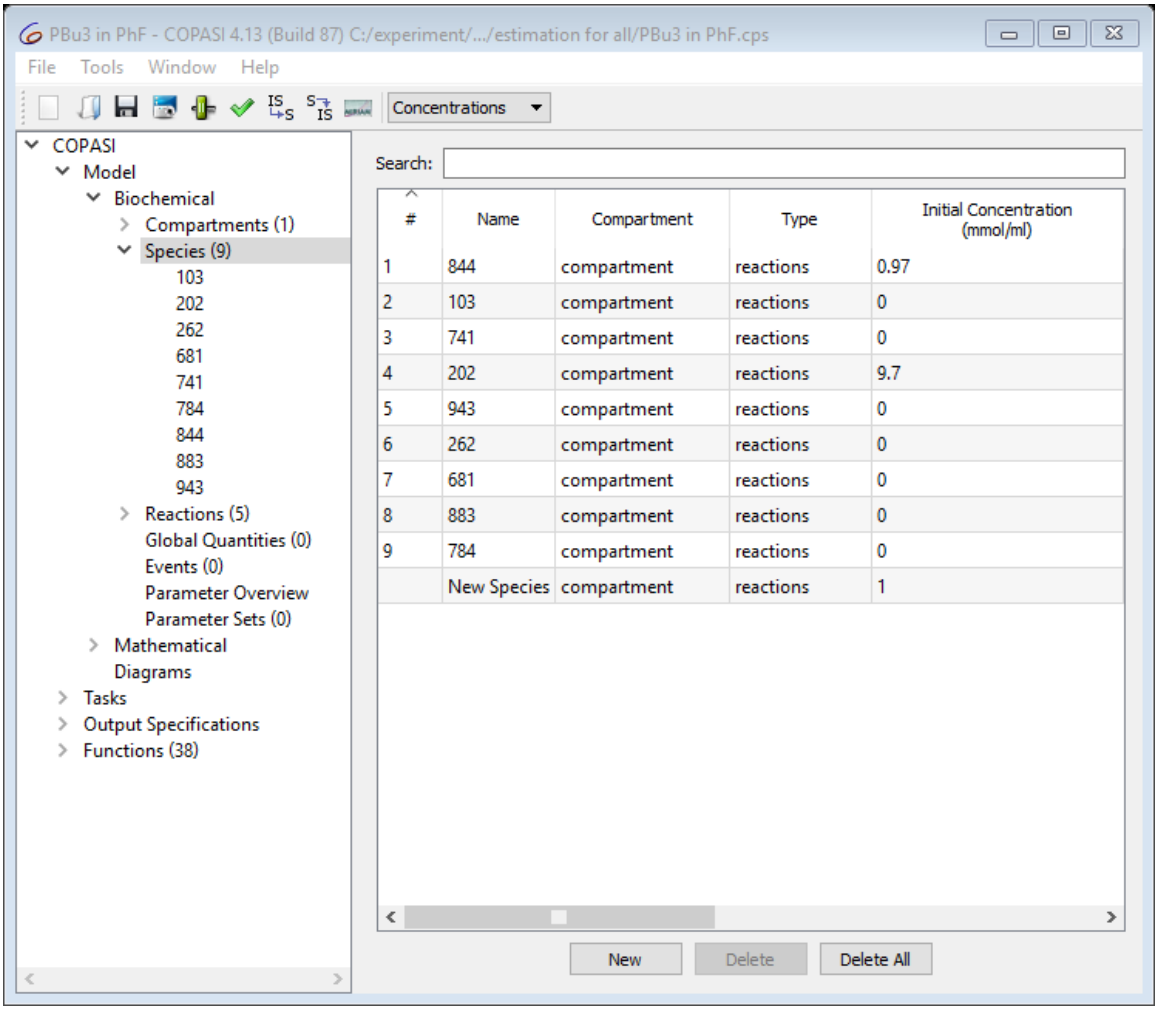

Figure 4.40. Screenshot of COPASI window for species.

Then the second step is the input of all reactions involved in the mechanism. All the reagents and products have to be in double quotes to be recognized by the software. And to represent the reversible reaction the equal sign is used. For the irreversible reaction the sign “->” is used.

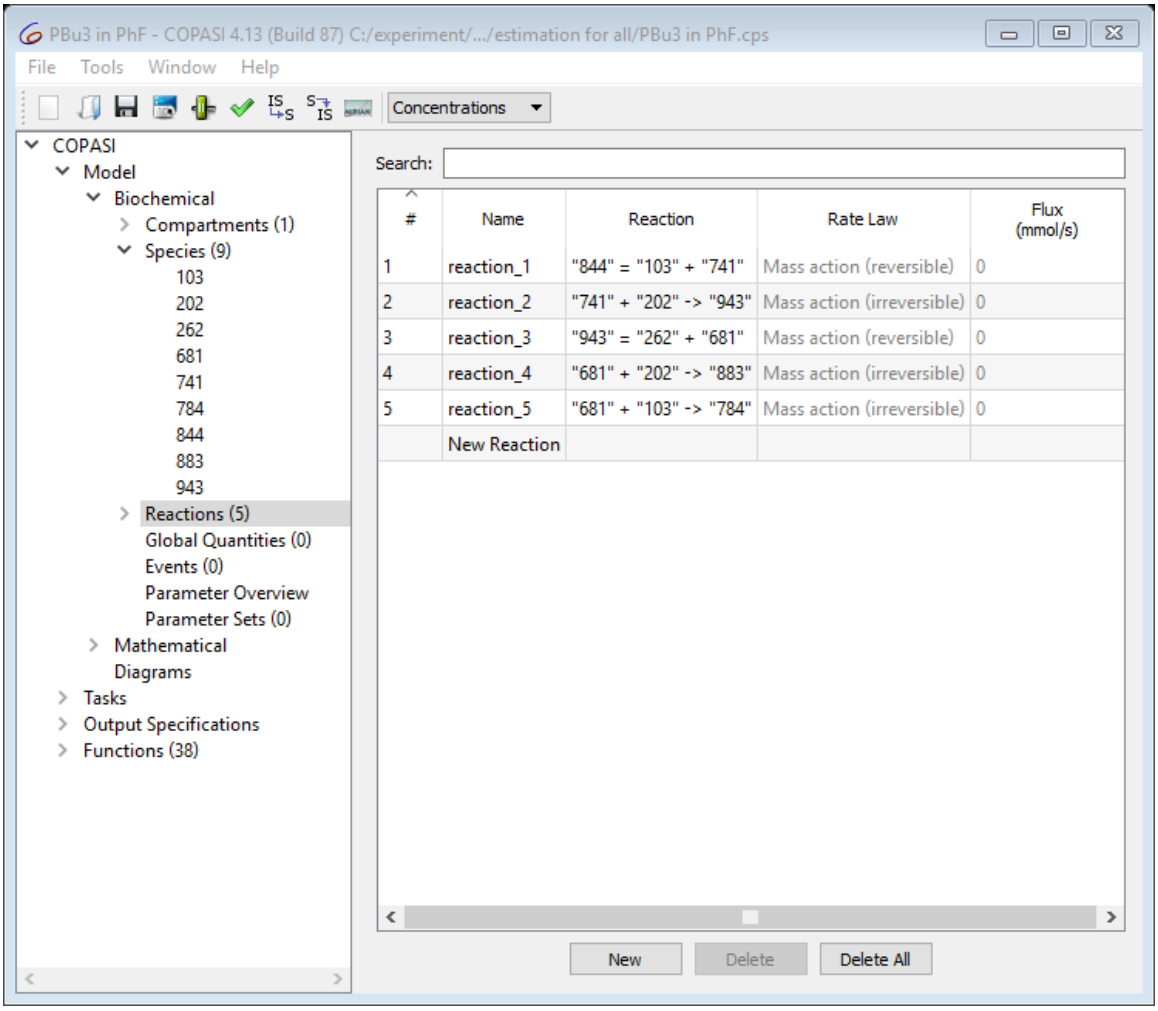

Figure 4.41. Screenshot of COPASI window for reactions.

To set the reaction rate constant for each step, double click each reaction to edit further details. Because we were going to use the Parameter Estimation later to get the accurate ones, here we just guessed 0.1 for slow steps and 10 for fast steps.

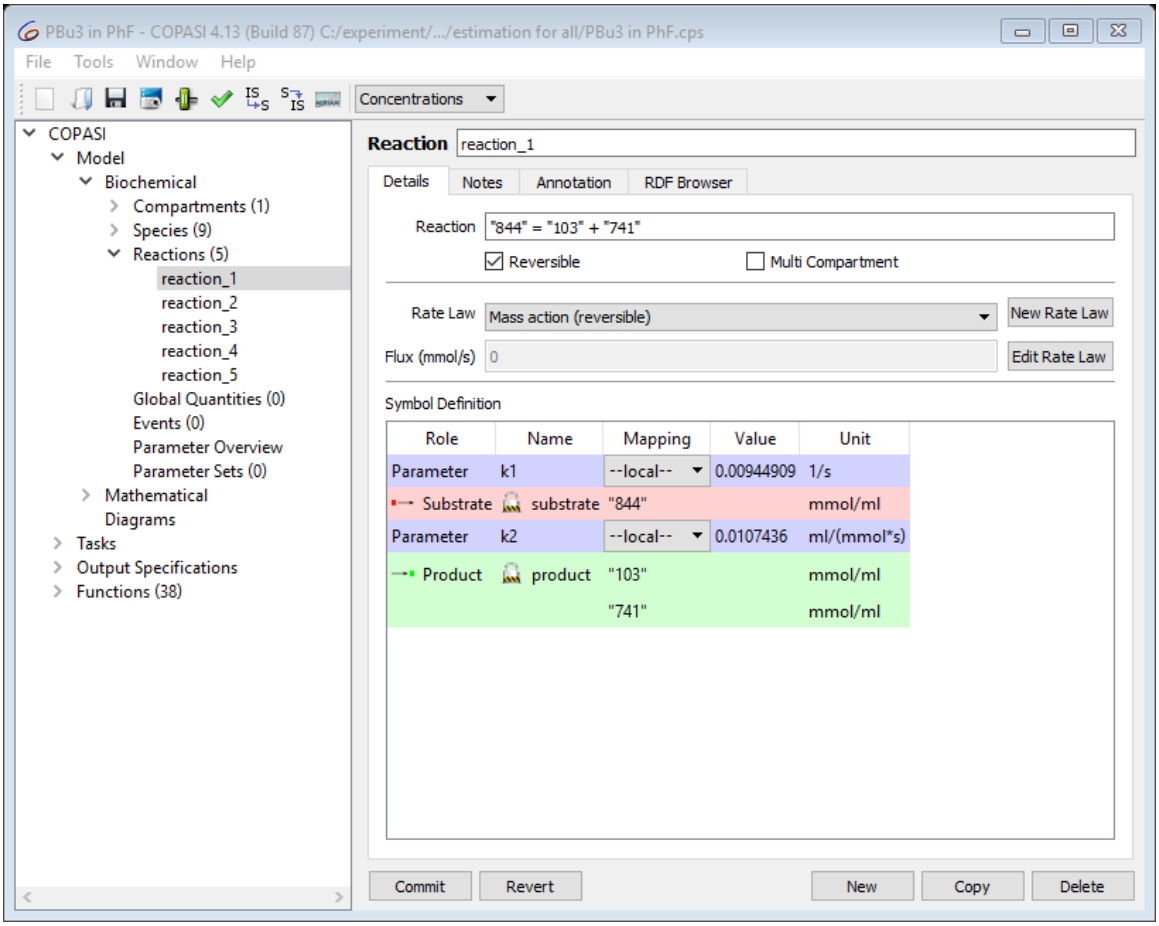

Figure 4.42. Screenshot of COPASI window for reaction details.

After introduced your experimental data, Parameter Estimation was used to find best match for the reaction rates for each step. To set the boundary for the COPASI to work, usually +/- 500% was used. And the estimation method was Genetic Algorithm.

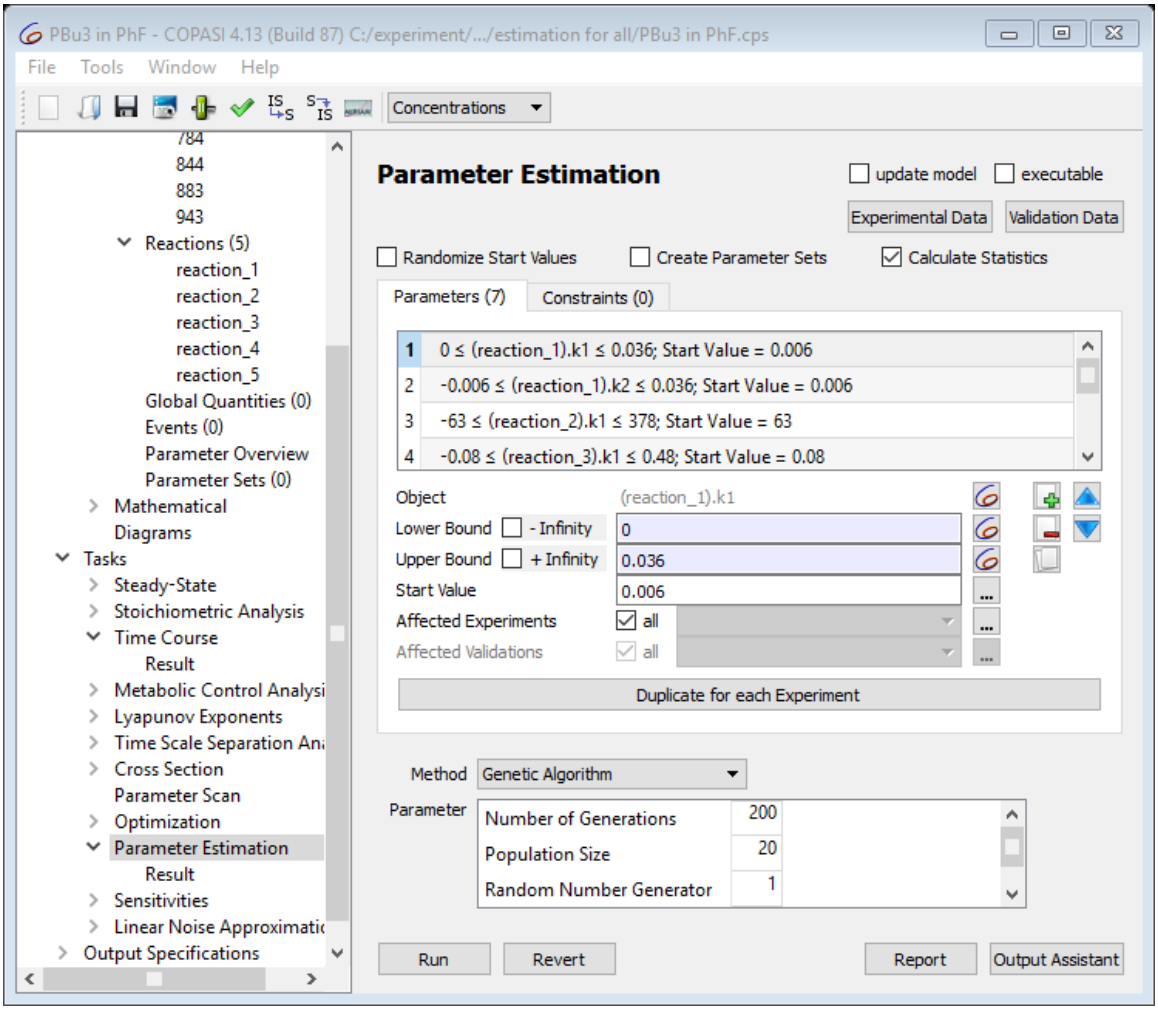

Figure 4.43. Screenshot of COPASI window for Parameter Estimation.

After getting the Parameter Estimation, the results were pasted back to reaction rate sections. Then the simulation can be done with the Time Course function of COPASI. As our reaction can be complete within 10 minutes the duration was set at 600 seconds with 1 second interval.

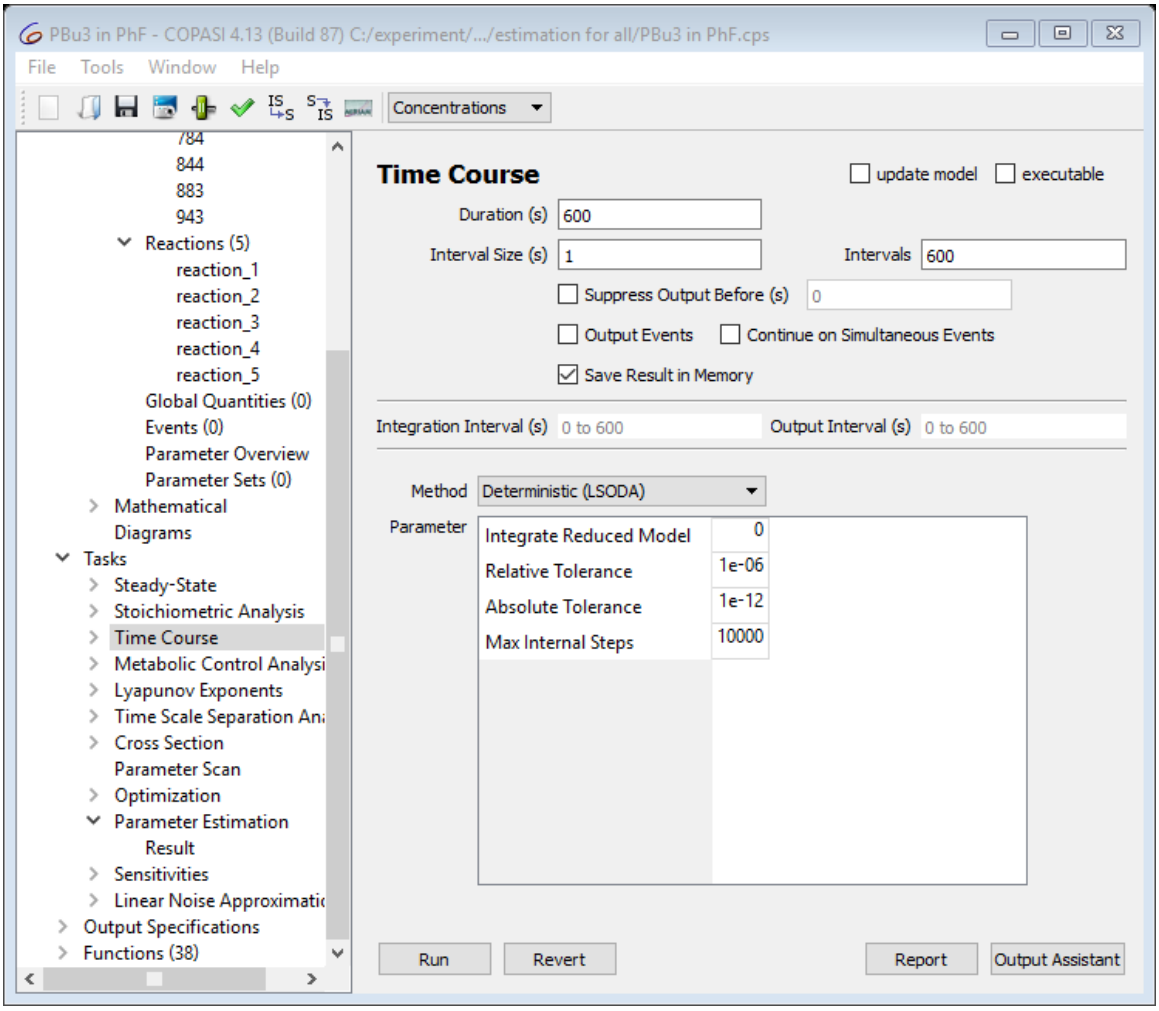

Figure 4.44. Screenshot of COPASI window for Time Course.

Bibliography

(1) Zeise, W. C. *Ann. Phys. Chem.* **1831**, *21*, 497.
(2) Duward .F. Shriver; Peter Atkins; Langford, C. H. *Inorganic Chemistry*; W.H. Freeman and Company, 1994.
(3) Astruc, D. *Organometallic Chemistry and Catalysis*; Springer Berlin Heidelberg, 2007.
(4) B. Cornils; W. A. Herrmann; Rasch, M. *Angew. Chem. Int. Ed.* **1994**, 2144.
(5) W. Reppe.; Schweckendiek, W. *Liebigs Ann. Chem* **1948**, *560*, 104.
(6) Woodward., R. B. *Pure Appl. Chem* **1968**, *17*, 519.
(7) Cotton, F. A. *Inorg. Chem* **2002**, 643.
(8) Astruc, D. *New Journal of Chemistry* **2005**, 42.
(9) Seechurn, C. C. C. J.; Kitching, M. O.; Colacot, T. J.; Snieckus, V. *Angewandte Chemie. Intl. Ed* **2012**, *51*, 5062.
(10) Crabtree, R. H. *The Organometallic Chemistry of the Transition Metals*; JOHN WILEY & SONS, INC., 2001.
(11) Anastas, P. T.; Zimmerman, J. B. *Env. Sci. Tech* **2003**, *37*, 94A.
(12) Henderson, W.; McIndoe, J. S. *Mass Spectrometry of Inorganic and Organometallic Compounds: Tools-Techniques-Tips*; Wiley-Interscience, 2005.
(13) Knof, D. A. *Phys. Chem* **2011**, 21050.
(14) Asbury, G. R.; Herbert H. Hill, J. *Anal. Chem* **2000**, *73*, 580.
(15) Danielle M. Chisholm; Allen G. Oliver; McIndoe, J. S. *Dalton Trans* **2010**, 364.
(16) Dole, M.; Mack, L. L.; Hines, R. L.; Mobley, R. C.; Ferguson, L. D.; Alice, M. B. *J. Chem. Phys* **1968**, 2240.
(17) Yamashita, M.; Fenn, J. B. *J. Phys. Chem* **1984**, 4451.
(18) Iribarne, J. V.; Thomson, B. A. *J. Chem. Phys* **1976**, 2287.
(19) Guilhaus, M.; Mlynski, V.; Selby, D. *Rapid Commun. Mass Spectrom* **1997**, 951.
(20) Stephens, W. E. *Phys. Rev.* **1946**, 691.
(21) Alikhanov, S. G. *Sov. Phys* **1957**, 452.
(22) Jennings, K. R. *Int. J. Mass. Spectrom* **2000**, 479.
(23) Griffiths, P. R.; De Haseth, J. A. *Fourier Transform Infrared Spectrometry*; Wiley, 2007.
(24) Michelson, A.; Morley, E. *American Journal of Science* **1887**, *34*, 333.
(25) Smith, B. C. *Fundamentals of Fourier Transform Infraed Spectroscopy*; Second Edition ed.; CRC Press, 2011.
(26) Chaplin, A. B.; Hooper, J. F.; Weller, A. S.; Willis, M. C. *J. Am. Chem. Soc* **2012**, 4885.
(27) Luo, J.; Oliver, A. G.; McIndoe, J. S. *Dalton Transactions* **2013**, 11312.
(28) Lee, E. D.; Mueck, W.; Henion, J. D.; Covey, T. R. *J. Am. Chem. Soc* **1989**, *13*, 4600.
(29) Swensen, J. S.; Xiao, Y.; Ferguson, B. S.; Lubin, A. A.; Lai, R. Y.; Heeger, A. J.; Plaxco, K. W.; Soh, H. T. *J. Am. Chem. Soc* **2009**, *12*, 4262.
(30) Karsai, A.; Muller, S.; Platz, S.; Hauser, M.-T. *Biotechniques* **2002**, *4*, 790.

(31) George, G. A.; P.Cole-Clarke; John, N. S.; G.Friend *Journal of Applied Polymer Science* **1991**, *42*, 643.
(32) Petucci, C.; Diffendal, J.; Kaufman, D.; Mekonnen, B.; Terefenko, G.; Musselman, B. *Anal. Chem* **2007**, *13*, 5064.
(33) Gard, E.; Mayer, J. E.; Morrical, B. D.; Dienes, T.; Ferenson, D. P.; Prather, K. A. *Anal. Chem* **1997**, *20*, 4083.
(34) Kebarle, P.; Tang, L. *Anal. Chem* **1993**, *65*, 972A.
(35) Tang, K.; Page, J. S.; Smith, R. D. *J Am Soc Mass Spectrom* **2004**, *15*, 1416.
(36) Willis, M. C. *Chem. Res* **2010**, *110*, 725.
(37) Sakai., K.; Ide., J.; Oda., O.; Nakamura, N. *Tetrahedron Lett.* **197**, 1287.
(38) Vora., K. P.; Lochow., C. F.; Miller, R. G. *J. Organomet. Chem.* **1980**, *192*, 257.
(39) Vora., K. P.; Lochow., C. F.; Miller, R. G. *Synth. Commun.* **1983**, *13*, 99.
(40) Marder., T. B.; Roe., D. C.; D.Milestein *Organometallics* **1988**, *7*, 1451.
(41) Suggs, J. W. *J. Am. Chem. Soc.* **1978**, *100*, 640.
(42) Lee., H.; Lee., C.; Bull, H. *Korean Chem. Soc* **1995**, *16*, 66.
(43) Willis., M. C.; Randell., H. E.; Beswick, P. J. *Angew. Chem. Int. Ed.* **2004**, *43*, 340.
(44) Moxham., G. L.; Randell-Sly., H. E.; Brayshaw., S. K.; Woodward., R. L.; Weller., A. S.; Willis, M. C. *Angew. Chem. Int. Ed.* **2006**, *45*, 7618.
(45) Tanaka., K.; Shibata., Y.; Suda., T.; Hagiwara., Y.; Hirano, M. *Org. Lett.* **2007**, *9*, 1215.
(46) Roy., A. H.; Lenges., C. P.; Brookhart, M. J. *J. Am. Chem. Soc.* **2007**, *129*, 2082.
(47) Jun., C. H.; Lee., D. Y.; Lee., H.; Hong, J. B. *Angew. Chem. Int. Ed.* **2000**, *39*, 3070.
(48) Jun., C. H.; Huh., C. W.; Na, S. J. *Angew. Chem. Int. Ed.* **1998**, *37*, 145.
(49) Jun., C. H.; Chung., K. Y.; Hong, J. B. *Org. Lett.* **2001**, *3*, 785.
(50) Blackmond, D. G. *Angew. Chem. Int. Ed.* **2005**, 4302.
(51) Hartwig, J. *Organotransition Metal Chemistry: from Bonding to Catalysis*; University Science Books, 2010.
(52) James, B. R. *Homogeneous Hydrogenation*; John Wiley & Sons Canada, Limited, 1973.
(53) Calvin.M *J. Am. Chem. Soc* **1939**, *61*, 2230.
(54) Jardine, F. H.; Osborn, J. A.; G.Wilkinson; F.Young, J. *Chem. Ind. (London)* **1965**, 560.
(55) D.Evans; A.Osborn, J.; Jardine, F. H.; Wilkinson, G. *Nature* **1965**, 1203.
(56) Halpern.J.; Okamoto.T.; Zakhariev.A. *J. Mol. Catal* **1977**, *2*, 65.
(57) Horner.L; Siegel.H; Buthe.H *Angew. Chem., Int. Ed. Engl* **1968**, *7*, 942.
(58) Knowles, W. S.; J.Sabacky, M. *J. Chem. Soc., Chem. Commun* **1968**, 1445.
(59) P., D. T.; B., K. H. *J. Chem. Soc., Chem. Commun* **1971**, 481.
(60) Inoguchi.K.; Sakuraba.S.; Achiwa.K *Synlett* **199**, 169.
(61) Chan.A; Halpern.J *J. Am. Chem. Soc* **1980**, *102*, 838.
(62) R.R.Schrock.; J.A.Osborn. *J. Am. Chem. Soc* **1976**, *98*, 2143.
(63) Schrock., R. R.; Osborn., J. A. *J. Chem. Soc., Chem. Commun* **1970**, 567.
(64) J.Halpern *Inorg. Chim. Acta* **1981**, *50*, 11.
(65) D, G. J.; Imamoto.T; Hoge.G.; Kouchi.M; Takahashi.H *J. Am. Chem. Soc* **2008**, *130*, 2560.

(66) O'Connor. C., Y. G., Evans. D., Wilkinson. G. J. *J. Chem. Soc., Chem. Commun* **1968**, 420.
(67) Miyahita. A., Y. A., Takaya. H., Totiumi. K., Ito. T., Souchi. T., Noyori. R. *J. Am. Chem. Soc.* **1980**, *102*, 7932.
(68) Saito. T.; Yokozawa. T.; Ishizaki. T.; Moroi. T.; Sayo. N.; Miura. T.; H, K. *Adv. Synth. Catal* **2001**, *343*, 264.
(69) Dotta.P.; Kumar.P.G.A.; Pregosin.P.S.; Albinati.A.; RIzzato.S *Organometallics* **2004**, *23*, 2295.
(70) Zhang. X. Y.; Mashima. K.; Koyano. K.; Sayo. N.; Kumobayashi. H.; Akutagawa. S.; H., T. *Tetrahedron Lett.* **1991**, *32*, 7283.
(71) Burk.M; Feaster.J.F; Nugent.W.A; Harlow.R.L *J. Am. Chem. Soc.* **1993**, *115*, 10125.
(72) Anantharaman, N.; Meera., K. M.; Begum, S. *Mass Transfer: Theory and Practice*; PHI Learning Pvt. Ltd, 2011.
(73) Cussler, E. L. *Diffusion: Mass Transfer in Fluid Systems*; illustrated, reprint, revised ed.; Cambridge University Press, 2009.
(74) Incropera, F. P.; DeWitt, D. P.; 3rd ed.; John Wiley & Sons, 1990.
(75) Nicola.J.F.; Robert.M.; Scott.M *Dalton Trans* **2006**, 4570.
(76) Evans.C., H. W. *Inorg. Chim. Acta.* **1999**, *294*, 183.
(77) Gimbert. Y., L. D., Milet. A., Fournier. F., Greene. A. E., Tabet. J. C. *Org. Lett.* **2003**, *5*, 4073.
(78) Decker, C.; Henderson, W.; Nicholson, B. K. *J. Chem. Soc., Dalton Trans* **1999**, 3507.
(79) Chisdholm., D. M.; McIndoe, J. S. *Dalton Trans* **2008**, 3933.
(80) Farrer, N. J.; Vikse, K. L.; McDonald, R.; J.S.McIndoe *Eur. J. Inorg. Chem* **2012**, 733.
(81) Luo, J.; Theron, R.; Sewell, L.; Hooper, T.; Weller, A.; Oliver, A.; McIndoe, J. *Organometallics* **2015**, 3021.
(82) Luo.J.; Oliver.A.G.; McIndoe.S. *Dalton Trans* **2013**, *42(31)*, 11312.
(83) Kun.W.; Martin.E.G.; Thomas.J.E.; Alan.S.Goldman. *Journal of Organometallic Chemistry* **1996**, *518*, 55.
(84) Tolman, C. A. *Chem. Rev* **1977**, *77*, 313.
(85) Pearson, R. G. *J. Am. Chem. Soc* **1963**, *85*, 3533.
(86) Wolfe, J. P.; Tomori, H.; Sadighi, J. P.; Yin, J.; Buchwald, S. L. *J. Org. Chem* **2000**, *65*, 1158.
(87) Kolmel, C.; Ochsenfeld, C.; Ahlrichs, R. *Theor. Chim. Acta* **1991**, *82*, 271.
(88) Juge, S.; Stephan, M.; Laffitte, J. A.; Genet, J. P. *Tetrahedron Lett.* **1990**, *31*, 6357.
(89) Giordan, J. C.; Moore, J. H.; Tossell, J. A. *Acc. Chem. Res* **1986**, *19*, 281.
(90) Dunne, B. J.; Morris, R. B.; Orphen, A. G. *J. Chem. Soc., Dalton Trans.* **1991**, 653.
(91) Leyssens, T.; Peeters, D.; Orphen, A. G.; Harvey, J. N. *Organometallics* **2007**, *26*, 2637.
(92) Mastryukova, T. A.; Kabachnik, M. J. *Chem. Rev* **1969**, *38*, 795.
(93) Brookhart, M.; Green, M. L. *J. Organomet. Chem* **1983**, *250*, 395.
(94) Placa, J. P. L.; Ibers, J. A. *Inorg. Chem.* **1965**, *4*, 778.

(95) Richens, D. T. *Chem. Rev* **2005**, *105*, 1961.
(96) Odell, A. L.; Raethel, H. A. *J. Chem. Soc., Chem. Commun* **1968**, 1323.
(97) Hyde, C. L.; Darensbourg, D. J. *Inorg. Chem.* **1973**, *12*, 1286.
(98) Pike, S. D.; Pernik, I.; Theron, R.; McIndoe, J. S. *Journal of Organometallic Chemistry* **2015**, *784*, 75.